TECHNICAL UNIVERSITY OF CRETE

SCHOOL OF ELECTRICAL & COMPUTER ENGINEERING

DIPLOMA THESIS

Optimal operation of large Electric Power Systems with HVDC interconnections

Konstantinos Goumagias

Committee

Supervisor: Kanellos Fotios, Associate Professor

Committee Member: Kalaitzakis Kostas, Professor

Committee Member: Koutroulis Eftychios, Associate Professor

Chania, 2019

ΠΟΛΥΤΕΧΝΕΙΟ ΚΡΗΤΗΣ

ΣΧΟΛΗ ΗΛΕΚΤΡΟΛΟΓΩΝ ΜΗΧΑΝΙΚΩΝ & ΜΗΧΑΝΙΚΩΝ ΥΠΟΛΟΓΙΣΤΩΝ

ΔΙΠΛΩΜΑΤΙΚΗ ΕΡΓΑΣΙΑ

Βέλτιστη λειτουργία μεγάλων Συστημάτων Ηλεκτρικής Ενέργειας με διασυνδέσεις συνεχούς ρεύματος

Κωνσταντίνος Γουμάγιας

Επιτροπή

Επιβλέπων: Κανέλλος Φώτιος, Αναπληρωτής Καθηγητής

Μέλος Επιτροπής: Καλαϊτζάκης Κώστας, Καθηγητής

Μέλος Επιτροπής : Κουτρούλης Ευτύχιος, Αναπληρωτής Καθηγητής

Χανιά, 2019

Abstract

HVDC systems constitute a well-established technology used for massive electric power transmission over long distances. The term stands for High Voltage Direct Current, indicating the utilization of Direct Current (DC) as a substitute to Alternate Current (AC) in cases where the latter would prove highly problematic. The underwhelming performance of HVAC due to its high transmission losses and the significant operating cost make HVDC systems stand out in numerous applications. Moreover, in a world where the integration of renewables to the power grid becomes of utmost priority, HVDC is gradually gaining more ground in the collective attempt of the energy production decarbonisation.

Under these circumstances, HVDC systems have become a growing trend for interconnecting regional or national electrical grids in order to form a larger unified network with enhanced stability and increased efficiency. Large interregional grids give to their individual subsystems the ability to conduct power transactions with the purpose of efficiently distributing the power generated across the wider system, which is the center of this work.

The main aspect of this thesis is the optimization of large electric power systems, consisting of subsystems that do not possess information about the operating state of each other. The individual systems are interconnected by utilizing HVDC transmission lines, which allow them to exchange power in the attempt to achieve the global minimum operating cost. First, a reference is made to the properties, benefits and weaknesses of HVDC technology, along with its role in the today's world. We present the fundamental technologies behind its operation while providing a glimpse of their characteristics. Additionally, we give an overview of the power flow (PF) and optimal power flow (OPF) analysis, in the context of Matpower, a simulation tool that was used extensively throughout our research. Then, we proceed to the thorough description of the algorithm that carries out the optimization, and the objective function that was based on the idea of the linearization of system operation cost. Finally, we showcase the performance of our approach alongside the baseline results by Matpower's optimal power flow function. Experimental evaluation was performed for small and large system case studies, where our algorithm's accuracy and performance were further examined.

Abstract in Greek

Τα συστήματα HVDC αποτελούν μια ευρέως καθιερωμένη τεχνολογία για τη μαζική μετάδοση ηλεκτρικής ισχύς σε μεγάλες αποστάσεις. Ο όρος αναφέρεται στα συστήματα Υψηλής Τάσης Συνεχούς Ρεύματος, υποδεικνύοντας τη χρησιμοποίηση του συνεχούς ρεύματος (DC) ως αντικαταστάτη του εναλλασόμενου ρεύματος (AC) σε περιπτώσεις που το τελευταίο θα αποδεικνυόταν ιδιαίτερα προβληματικό. Η μικρή απόδοση του HVAC λόγω των υψηλών απωλειών μεταφοράς και του σημαντικού λειτουργικού κόστους κάνουν τα συστήματα HVDC να ξεχωρίζουν σε πολλές εφαρμογές. Επιπρόσθετα, σε ένα κόσμο όπου η διείσδηση των ανανεώσιμων πηγών ενέργειας στο δίκτυο είναι υψίστης προτεραιότητας, το HVDC κερδιζει σταδιακά περισσότερο έδαφος στη συλλογική προσπάθεια για μείωση των εκπομπών αερίων ρύπων από την παραγωγή ενέργειας.

Κάτω από αυτές τις συνθήκες, τα συστήματα HVDC γίνονται όλο και πιο δημοφιλή για τη διασύνδεση περιφερειακών ή εθνικών ηλεκτρικών δικτύων για το σχηματιμό ενός μεγαλύτερου, ενωποιημένου δικτύου με ενισχυμένη ευστάθεια και αυξημένη αποδοτικότητα. Τα μεγάλα διαπεριφερειακά συστήματα δίνουν στα επιμέρους υποσυστήματα τη δυνατότητα να διεξάγουν συναλλαγές ισχύος με στόχο την αποτελεσματική κατανομή της παραγόμενης ισχύς στο ευρύτερο σύστημα, το οποίο είναι και το κέντρο γύρω από το οποίο αναπτύσσεται η παρούσα η εργασία.

Στο πλαίσιο αυτό, η κύρια πτυχή της εργασίας είναι η βελτιστοποίηση μεγάλων συστημάτων ηλεκτρικής ενέργειας, αποτελούμενων από υποσυστήματα που δεν διαθέτουν πληροφορία το ένα για την κατάσταση λειτουργίας του άλλου. Τα επιμέρους συστήματα είναι διασυνδεδεμένα αξιοποιώντας γραμμές μεταφοράς HVDC, που τους επιτρέπουν την ανταλλαγή ισχύος για την επίτευξη του ολικού ελάχιστου κόστους λειτουργίας. Πρώτα, γίνεται αναφορά στις ιδιότητες, τα οφέλη και τις αδυναμίες της τεχνολογίας HVDC, και στο ρόλο της στη σημερινή πραγματικότητα. Παρουσιάζουμε τις θεμελιώδεις τεχνολογίες πίσω από τη λειτουργία της ενώ ρίχνουμε μια συνοπτική ματιά στα χαρακτηριστικά τους. Επιπλέον, δίνουμε μια σφαιρική εικόνα της ανάλυσης ροής ισχύος (PF) και βέλτιστης ροής ισχύος (OPF) στα πλαίσια του Matpower, ενός εργαλείου προσομοίωσης που χρησιμοποιείται εκτεταμένα σε όλη την έκταση της έρευνας μας. Έπειτα, προχωράμε στην αναλυτική περιγραφή του αλγορίθμου που φέρνει εις πέρας τη βελτιστοποίηση, και της αντικειμενικής συνάρτησης ελαχιστοποίησης που βασίζεται στη γραμμικοποίηση των συνάρτησεων κόστους λειτουργίας των επιμέρους συστημάτων. Τέλος, παρουσιάζουμε την απόδοση της προσέγγισης μας σε σχέση με τα ενδεικτικά αποτελέσματα της συνάρτησης βέλτιστης ροής ισχύος του Matpower. Πραγματοποιήθηκε πειραματική αξιολόγηση για περιπτώσεις μικρών και μεγάλων συστημάτων όπου η ακρίβεια και η απόδοση του αλγορίθμου μας εξετάστηκαν περαιτέρω.

Acknowledgements

Firstly, I would like to express my utmost appreciation and gratitude towards my supervisor, Professor Fotios Kanellos, for his support and guidance throughout the whole final year of my studies. He introduced me to a field that I was unfamiliar with, and inspired my interest and excitement about the subject of this thesis. I would also like to deeply thank the two members of the committee, Professors Konstantinos Kalaitzakis and Eftychios Koutroulis.

I can't be grateful enough to all the people who accompanied me all these years. I wish to especially thank my mother Helen, my father Vasilis and my brother Ilias, for generously providing me with the strength and motivation to pursue a respectable degree on a subject that always fascinated me. Their unconditional trust and support kept fueling my efforts along the way.

It would be impossible not to thank and express my sincere gratitude to my close friends Dimitris, Michalis and Mike from the bottom of my heart, for their support in every aspect of my student life, which they made truly unique and meaningful. Also, my childhood's invaluable friends, George and Thodoris.

Finally, I would like to thank Penny from the bottom of my heart for her invaluable support. She stood by my side with patience and understanding in both good and bad times.

Contents

Chapter 1: Introduction

The aim of the first chapter is to provide a thorough description of HVDC technology. It presents an overview of the trends in the field of electricity distribution networks and the place of the technology in this rapidly changing environment. Also, a brief reference to the roots of HVDC is made, along with a summary of its properties and the applications it has in the modern world.

1.1. HVDC Technology Overview

The term HVDC stands for High Voltage Direct Current and constitutes a well-established technology utilized for massive transmission of electric power over long distances, with great efficiency. After more than a century in which High Voltage Alternate Current systems (HVAC) have been the backbone of electricity distribution, HVDC came to cover the deficiencies of the former and provide feasible alternatives in cases that traditional AC would fail.

HVDC stands out for its capability of transmitting vast amounts of power over long distances using DC current, a field that AC suffers due to its high transmission losses. This property makes a huge difference in applications that require the interconnection of remote areas to the power grid, while it also makes possible the exchange of power between national electrical grids. The increasing integration of RES, such as photovoltaics and offshore wind farms into the electrical grid, poses a serious challenge that also proves HVAC insufficient. Many of those cases require reliable subsea interconnections, a field in which HVDC systems excel (Pierri, Binder, Hemdan, & Kurrat, 2017).

Today renewables in Europe are gaining substantially more ground than ever before, as the Union has set an ambitious course for total decarbonization of the power production in the future, in order to minimize CO_2 emissions. Just in the second quarter 2018, hydro assets produced 109.2TWh, which made them the main source of renewable energy. Wind farms followed with 71.6TWh. In total, renewables produced 252.8TWh, more than the 224.8TWh of power generated from fossil fuels in the same quarter. Figure 1.2 shows the portion of Europe's energy map that renewables had taken over early in 2019. Clearly, renewables constitute a significant part of the european energy production, and tend to substitute conventional fuel types. This would not be possible without the development of HVDC technology.(Gordon, 2019).

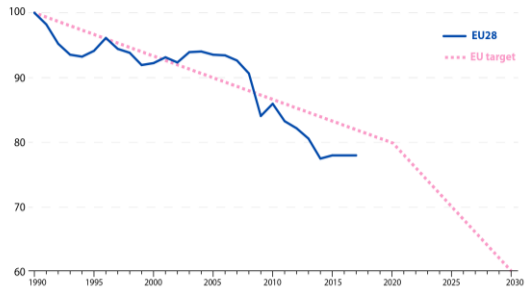

Figure 1.1: Greenhouse gas emissions (%), 1990-2017 (Index 1990 = 100), European Environment Agency

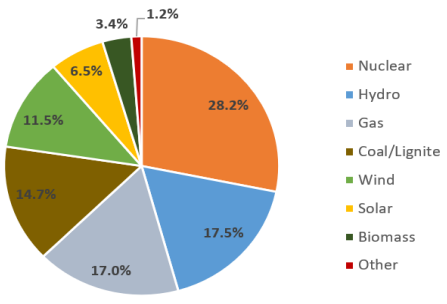

Figure 1.2: Distribution of energy sources in the European region *(Gordon, 2019)*

The explosion in renewables expected in the coming years is directly connected with the rise of HVDC system installations. The ENTSO-E Ten-Year Network Development Plan (TYNDP) 2014 report shows a prediction of the share that each technology will have by 2030 in the European region:

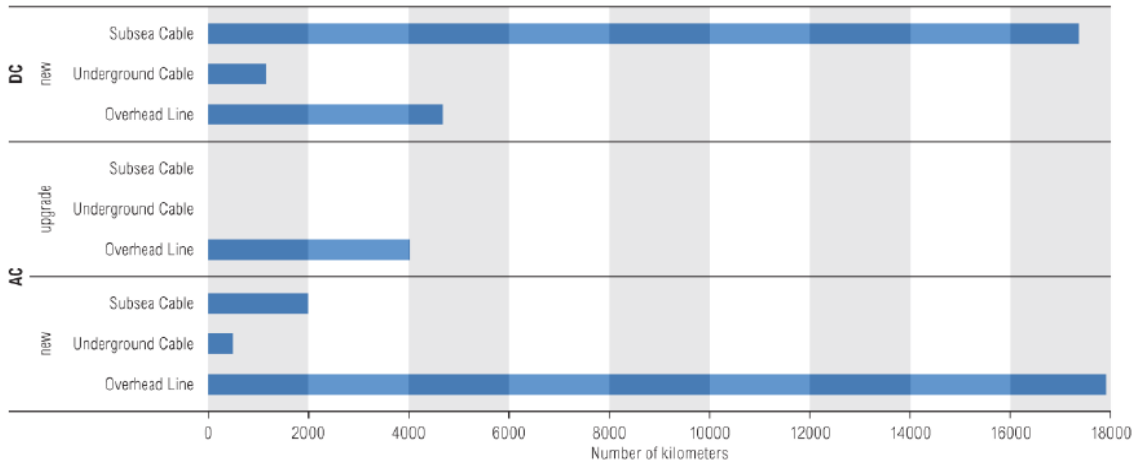

Figure 1.3: TYNDP 2014 investment portfolio – breakdown per technology *(TYNDP, 2014)*

This scenario anticipates the installation approximately 48000 km of new or upgraded lines that correspond to 120 projects. AC technology will still remain on the foreground with 21000 km of new lines and upgrades of 4000 km. The reason is that it is still reliable and easy to implement in most inland applications. However, HVDC is only slightly behind with approximately 23000 km of new DC lines scheduled for the next decade.

All the above lead us to the conclusion that HVDC is a technology that is increasingly gaining momentum and can be an asset of great importance in the road to a sustainable future.

1.2. History

At the dawn of the electricity supply industry, a race was taking place between the supporters of alternating current (AC) and direct current (DC) for the technology that would prevail as the main method of electricity distribution. Eventually AC was the one which emerged as the winner and therefore gradually took over almost all domestic, industrial and commercial supplies of electricity to consumers, while maintaining its dominance to this day (Peake, 2010).

DC was already been used for electricity distribution from early on, as Edison developed the first urban system for electric lighting in London's Holborn Viaduct in 1882. The innovation made more cities to heavily invest in DC power systems. However, the first full AC power system in the world was a reality in 1886 (Massachusetts). The impressive results AC delivered compared to low-voltage DC in long-distance transmission applications, led it to impressive milestones such as first hydro-electric power plant which was built by Nikola Tesla and George Westinghouse in 1895. These circumstances brought the gradual abandonment of DC until the early 20th century (Guarnieri, 2013).

The challenges that AC systems faced in the process didn't take long to appear, as the size of electricity production systems increased overtime. The industry had to overcome major obstacles that came to surface from the growing power demand that made necessary the

power capacity increase of undersea cables, due to the difficulties in increasing their voltage, as well as their range. In addition, the development of very large hydroelectric power plant projects in remote areas, relatively far from load centers discouraged the usage of AC systems to transmit large amounts of electricity over long distances.

For this type of scenarios, high voltage direct current (HVDC) seemed like an ideal solution by offering better efficiency and greater capacity than AC systems. The advantages of the usage of DC transmission systems were recognized already from 1920, and proved them suitable for those types of challenging applications. However, despite the optimistic promises, the concept of HVDC was held back by the lack of technology for the mercury-arc valves that were needed to convert AC to DC and vice versa. It was in 1929 when the mercury arc rectifier was presented as a potential converter technology, after Uno Lamm achieved to increase the withstood voltage of the valves. But it was only in 1954 that the technology had matured enough in order to be used in a commercial project for the development of the Gotland HVDC link, in order to provide the island with cheap hydropower (Guarnieri, 2013). This innovation opened the way for other successful projects, eleven in total.

Meanwhile the silicon semiconductor thyristor made its appearance as a viable alternative for the mercury arc valves of HVDC systems. The new technology, the thyristor valve, made its debut in HVDC applications in 1970, breaking the boundaries set by its predecessor and reducing the existing limitations of HVDC as it was utilized in Current Source Converter (CSC) systems. Later, in an attempt to improve thyristors, Insulated-Gate Bipolar Transistor (IGBT) was developed in 1984, which opened the way for Voltage Source Converter (VSC) HVDC systems with the first experimental project in 1997.

Since then, significant progress has been made in increasing the voltage, power capacity and length of the transmission lines, thus giving breath to the wider development of renewables and larger interconnection projects in general. This takes place at a time when the efficiency and stability of electricity supply systems plays a critical role in the collective attempt for decreased reliance on fossil fuel power generation on a global scale, along with the demand for cheap, clean electric energy. (Peake, 2010)

1.2.1. The Gotland HVDC link

The world's first fully commercial HVDC transmission system was commissioned on a Swedish island named Gotland, located 90km from the Swedish east coast in 1954.

The high cost of the electric energy produced on the island of Gotland had negative effect on the local economy resulting in depopulation and unemployment. The solution to this growing problem came from the decision of the Swedish government to commission and finance a transmission link that would connect Gotland to the mainland, to boost the island's industrial sector. (Hoel, 2004)

Figure 1.4: Gotland HVDC Link

That was the decision that led to the creation of the Gotland HVDC link, the world's pioneering high voltage direct current transmission system. It was capable of transferring 20 megawatts of power over a 96-kilometer long submarine cable that connected Västervik on the mainland and Ygne on the island of Gotland (ABB , 2018). For the project, two 12-pulse converters were used with a total nominal voltage capacity of 100kV, each one with two anodes connected in parallel, rated at 100A (Guarnieri, 2013).

Since then new upgrades have taken place to the existing project along with the development of the thyristor technology, which enabled converter stations to be simplified. The addition of two more cables in 1983 (Gotland 2) and 1985 (Gotland 3) allowed for total transmission capacity of 250 MW, with the maximum of 320 MW, at a nominal voltage of 150 kV. The new links were designed to operate independently or together by forming a bipolar link. The original cable and terminal equipment (Gotland 1) ware taken out of service and dismantled in 1986 when the latest link (Gotland 3) started to operate (ABB , 2018).

Today the fossil fuel generation on the island has completely shut down while the increasing power demand has been covered and the supply safety is secured. A new upgrade was scheduled in 2017 for enabling more renewable energy integration and boosting the grid's reliability.

In the table below, information about the projects that incorporated mercury arc valves are presented:

*Hybrid operation: mercury-arc valves and thyristor valves (1991)

Name	Year of Commission	Voltage (kV)	Capacity (MW)	Length (km)	Current State
Gotland, Sweden	1954	100	20	96	Upgraded
Cross Channel Link, France – England	1961	100	160	64	Shut Down 1984
Konti-Scan 1, Denmark – Sweden	1964	250	250	87	Upgraded
Volgograd-Donbass	1964	400	750	475	Upgraded
Corsica – Italy	1965	200	200	304	Upgraded
Sakuma, Japan	1965	125	300	-	Upgraded
Benmore – Haywards, New Zealand	1965	250	600	40 undersea 535 overhead	Upgraded*
Vancouver Island, Delta – North Cowichan	1968	260	312	42 undersea 33 overhead	Upgraded to AC
Pacific DC Intertie, US	1970	400	1440	1362	Upgraded
Manitoba Hydro, Nelson River - Winnipeg	1971	450	1620	895	Upgraded
London, HVDC Kingsnorth	1972	266	-	60	Shut Down 1987

Table 1.1. Mercury-Arc Era HVDC schemes (Haglöf, 2004)

1.3. HVDC vs HVAC

HVDC is a technology that substitutes the traditional high voltage alternating current (HVAC) for electric power transmission in areas where the latter cannot compete with. The major advantages of HVDC technology are presented in the following lines.

1.3.1. Asynchronous System Connection

The main advantage of HVDC systems is that it allows the interconnection of separate AC networks. In fact, a DC line is the only practical method for connecting asynchronous AC systems, i.e. systems of different frequency or same frequency but different phase angle. DC transmission lines enhance the networks stability in power swings and can also protect them from tipping in overload situations (Wang & Redfern, 2010). Furthermore, asynchronous interconnection offers better protection by preventing cascading blackouts to transmit from a sector of a larger power network to another, which can possibly cause blackouts (Breuer, Hartmann, Povh, Retzmann, & Teltsch, 2004).

Whereas load changes that take place throughout an AC network can cause sectors to become asynchronous and thus, isolated, DC systems aren't affected and the power flowing through the HVDC interconnection tends to stabilize the AC network (Breuer, Hartmann, Povh, Retzmann, & Teltsch, 2004). In DC networks, the rating and direction of power flow can be controlled directly and manipulated accordingly in order to support other AC networks located at the other end of a DC interconnection, resulting in increased system capacity and flexibility (Wang & Redfern, 2010). These properties of increased stability and utility make HVDC technology a widespread solution for energy distribution networks around the world.

1.3.2. Long Distance Power Transmission

HVDC systems provide substantially greater efficiency in applications where bulk power delivery over long distances is needed, especially in cases that require the use of underground or submarine transmission lines. Regarding the conductors, underwater cables have increased effective capacitance compared to overhead cables. This means that additional heavy currents are needed to continuously charge and discharge the line's capacitance, resulting in energy losses, thus limiting its ability to transmit current to long distances (Rajpoot S., Rajpoot P., & Gupta K., 2017). Furthermore, the high requirements for reactive power compensation in long distance AC transmission applications, combined with the increased losses, raise the total cost dramatically (Wang & Redfern, 2010). This problem does not persist in DC lines, where the line capacitance is only charged once when the interconnection is energized for the first time (Grant, 2017). HVDC systems high voltage utilization means that lower current passing through the DC interconnections, which combined with the absence of the skin effect, gives us significantly less line loses compared to an AC system of similar size, thus eliminating distance constraints. Lower line losses along with remarkable economic benefits give HVDC systems a profound advantage for long distance power distribution.

Skin effect is a phenomenon existing in AC systems. It refers to the tendency of the current to distribute unevenly inside the conductor, by having larger density near its surface which decreases as we get closer to the center. This effect becomes more intense in higher frequencies and is responsible for greater loses due to the Corona discharge phenomenon,

which causes the ionization of the air around the conductor and makes it to become conductive. Therefore, the skin effect reduces drastically amount of useful current traveling through the conductor. DC systems operate in zero frequency and therefore they don't suffer from the consequences of the skin effect.

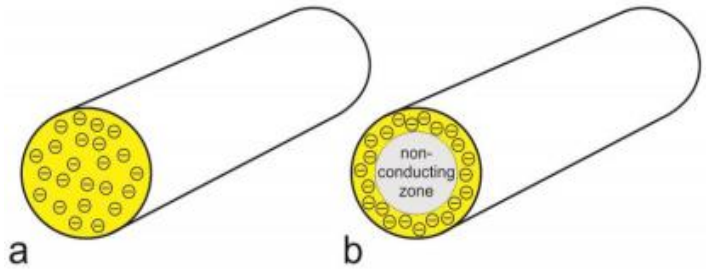

Figure 1.4: The Skin effect in DC (a) and AC (b) conductors *(Ardelean & Minnebo)*

1.3.3. Economic Efficiency

Compared to HVAC, HVDC systems require less conductors to transmit the same amount of electric power, because it substitutes the need for three-phase transmission. For establishing a bipolar HVDC configuration we can use only two lines instead of three. Moreover, conductors operated with DC can carry nearly 40% more power than AC. This is due to the fact that HVDC systems can operate at voltage levels which are as high as the peak voltage of an AC system. The effective voltage of an AC system is equivalent to its RMS value, that is, 71% of its peak voltage. (Khazaei, Idowu, Asrari, Shafaye, & Piyasinghe, 2018) On the other hand, the effective voltage of an HVDC system is equal to its operating voltage. Therefore, HVDC has the capacity of more power transmitted per conductor, while also requiring less conductors to transmit the same amount of power. As a result, projects based on HVDC technology need less infrastructure and take over less space, which directly translates to cost savings. As an example, the Three Gorges Project in Chine would require 5 x 500kV AC lines compared to the 2 x ±500kV, 3000MW bipolar DC lines it currently utilizes (Wang & Redfern, 2010).

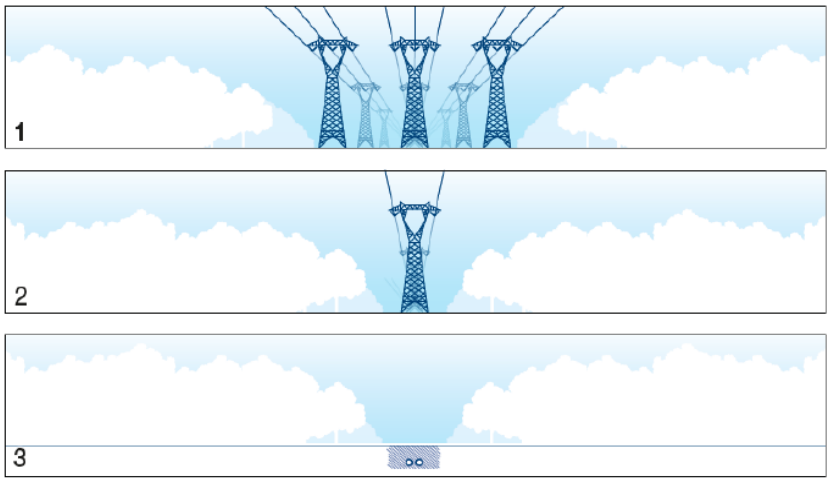

Figure 1.5: Conductor Layout, (1) AC overhead line, (2) DC overhead line, (3) DC land cables *(Khazaei, Idowu, Asrari, Shafaye, & Piyasinghe, 2018)*

However, HVDC systems are also expensive to build and operate, with their biggest expenses being the converter stations. The economic advantages of HVDC really stand out when utilized for long distance transmission. As the distance between the converter stations increases, DC lines gain a significant edge compared to AC, which justifies the large investment cost. The next figures compare AC and DC by showing the relation between the distance of the terminals and the corresponding investment cost, as well as the power losses of DC lines:

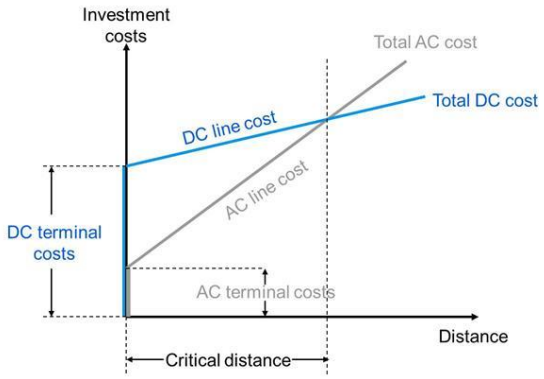

Figure 1.6: AC vs DC cost comparison *(ABB, n.d.)*

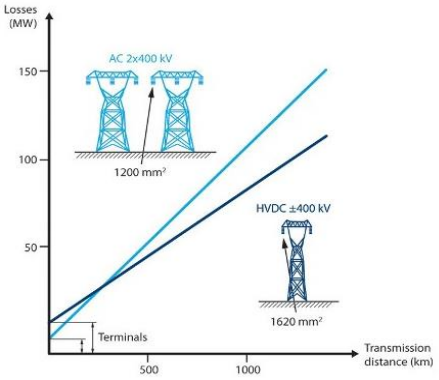

Figure 1.7: AC vs DC losses comparison *(ABB, n.d.)*

The point on which DC exceeds the performance of AC, called break-even distance, is found at line distances approximately 600 – 800 km long. For submarine cables, this point starts from just 60 km. From this point on, DC outperforms AC by having a lower rate of total cost increase, despite the fact that DC's investment cost is significantly greater. All the above immediately prove the economic benefits of HVDC in long distance power transmission (Ardelean & Minnebo).

Below two examples are shown that compare the losses of HVDC and HVAC respectively:

	Voltage (kV)	**Power (MW)**	**Length (km)**	**Losses (%)**
AC	800	3000	1000 / 2000	6.7/ 10
DC	800	6400	1000 / 2000	3.5 / 5

Table 1.2: Examples comparing AC and DC losses *(Ardelean & Minnebo)*

1.3.4. Environmental Benefits

Another advantage in the connection of different AC systems by using HVDC lines is that building new power stations near the load centers becomes unnecessary once it is possible to bring electric energy from distant locations. The efficiency they offer subsequently leads to a significant boost in the use of renewables. HVDC has made offshore wind farms feasible which, as the technology progresses, are becoming a more widespread alternative (Khazaei, Idowu, Asrari, Shafaye, & Piyasinghe, 2018). Moreover, the fewer lines that are needed for HVDC transmission allow us to build DC lines in environmentally sensitive areas. Less infrastructure means less space occupied, thus limiting environmental impact (ABB, n.d.). Additionally, the absence of alternating electro-magnetic fields, skin effects, more efficient energy transmission and lower losses lead to relatively reduced environmental issues in general (Wang & Redfern, 2010).

The next table presents a summary of the comparison between HVAC, CSC and VSC HVDC systems classifications:

	HVAC	CSC – HVDC	VSC – HVDC
Capacity distance dependent	✓	×	×
Power Losses	Distance dependent	2-4%	5-10%
Back-Start capability	✓	×	✓
Voltage level Transform	✓	×	✓
AC System Support	Limited	Limited	Large Range
Fault Limitation	×	✓	✓
Short-circuit level limitation	×	✓	✓
Evolution in components	Not expected to decrease	Semiconductor costs decrease over time	Semiconductor costs decrease over time
Visual Impact	Higher	Lower	Lower
Protection Systems	Advanced	Limited	Limited
Control Strategies	Acceptable in normal conditions	Fast	Fast
Corona Phenomena	Yes	No	No
Radio Interference	High	Limited	Limited
Audible Noise	High	Low	Low
Emissions (O_3, N_2)	High	Low	Low

Table 1.3: Comparison between HVAC, CSC and VSC HVDC systems *(Oulis Rousis & Anaya-Lara, 2015)*

1.4. Disadvantages of HVDC

1.4.1. Cost

The cost for building an HVDC transmission system varies and depends on a number of factors. DC converter stations have the largest share of the total construction costs and are more expensive than common ac substations of similar capacity. The reason for that is the great number of additional components and power electronics necessary to get technical performance of certain quality.

Furthermore, the power capacity of the system, the type of transmission medium (overhead, underwater, underground), the power electronics used, converters, transformers, safety requirements and many more can affect the total cost in many different ways (Rudervall, Charpentier, & Sharma, 2000). In the next figure, the typical cost structure for the converter stations is presented:

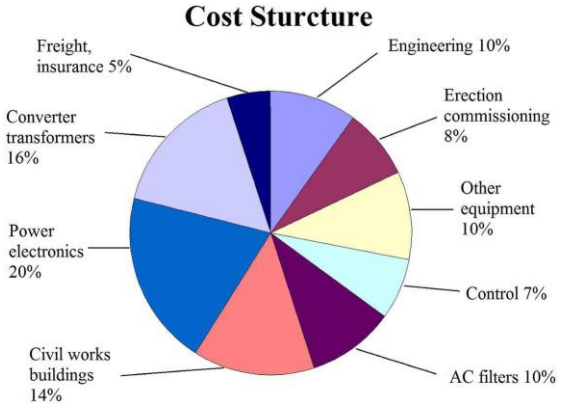

Figure 1.8: HVDC Converter cost structure *(Wang & Redfern, 2010)*

It is rather obvious that when it comes to building an HVDC system, the majority of the total cost comes from electronic components related to the operation of the converter stations. The following tables contain an estimation of CSC and VSC projects (Pierri, Binder, Hemdan, & Kurrat, 2017), respectively:

Specifications	Unit Cost [Mio €]
1000 MW, 400 kV	81 – 104
2000 MW, 500 kV	150 – 184
3000 MW, 600 kV	196 - 230

Table 1.4: CSC-HVDC project cost estimation.

Specifications	Unit Cost [Mio €]
500 MW, 300 kV	75 – 92
850 MW, 320 kV	98 – 105
1250 MW, 500 kV	121 - 150
2000 MW, 500kV	144 - 196

Table 1.5: VSC-HVDC project cost estimation.

Another element that adds to the total investment cost is cable installation. Cable installation costs may vary significantly depending on the type of HVDC system and also the nature of the application. A rough estimate of the price range is between 230 to 977 € per meter, although it can be affected by number of different factors. The cost skyrockets for subsea cable installations, as it appears in the table below:

Installation Type	Total Cost [1000 €/km]
Single cable, single trench	345 – 805
Twin cable, single trench	575 – 1035
2 single cables, 2 trenches, 10m apart	690 - 1380

Table 1.6: Subsea cable installation cost estimation.

1.4.2. Harmonics

Electronic converters and power electronics in general produce harmonics during the conversion process from AC to DC and vice versa. Today's HVDC systems utilize multiple connected converters, which combined lead to a significant increase of the harmonics injected into the transmission lines. Harmonics are considered one of the most serious problems in modern HVDC systems. The power quality is greatly affected along with the operation of other electronic components, and can even lead to system oscillation. In worst case scenarios, harmonics can become a possible cause of system failure.

1.4.3. System Stability Issues

Huge amounts of power are usually transmitted through HVDC interconnections between individual AC systems. In case a disturbance occurs, it is possible that it may have serious consequences to the system's transient stability.

Commutation failures during the conversion can be also an issue if the system faces a disturbance. These types of failures can even stop the flow between the converter stations. Circuit breakers and power relays are often used to prevent the system from destabilization. During a commutation error, the HVDC system draws significantly more

reactive power than it does in normal circumstances. This can often lead to voltage instability if the AC grid (Khazaei, Idowu, Asrari, Shafaye, & Piyasinghe, 2018). For most commutation failures in the DC connections, the AC system is responsible. Moreover, the large AC harmonic filters in HVDC systems can cause serious over-voltage issues during fault recovery. Thankfully, this is partially offset by the satisfactory fault protection of HVDC systems (Wang & Redfern, 2010).

In conclusion, despite their great advantages, HVDC systems are still experiencing some challenges that need to be resolved, especially as we move towards a future where increasingly more projects are going be commissioned.

1.5. Applications

HVDC can be found in numerous applications. As the technology continues to progress, the world increasingly adopts the benefits it has to offer. More and more projects appear that take advantage of DC power transmission and its capabilities, that without them, it would be hardly feasible to implement.

1.5.1. Offshore Wind Farms

The progress of HVDC technology is of major importance for the reinforcement and further development of renewable energy for it to be used on a wider scale, not only for Europe, but also on a global level.

We have already mentioned the importance of HVDC technology for electric energy distribution between remote regions, which makes it an ideal solution for bringing renewable energy from removed production points to the growing load centers. Their economic and practical benefits make HVDC networks the most suitable method to support the growing trend for offshore wind energy. Offshore wind farms are a clear demonstration of exemplary use of HVDC technology for long-distance transmission of renewable energy.

By the end of 2020, European Union's Member States aim to meet 35% of their total energy demand by renewables, with around 16% of the production coming from wind farms alone. This is an equivalent of 200 - 220 GW in installed wind power, able to produce approximately 495TWh of electricity (Wind Europe, 2017). It is estimated that by the 2030, the total capacity of offshore wind farms alone in European region will reach 15 GW with an electricity production of 563TWh. This is an equivalent of 12.8 – 16.7% the its total power demand and will lead to an annual decrease of CO2 emissions by 292 Mt. Consequently, the market of wind turbines will experience annual investments of approximately 16.5 billion euros (E.W.E.A., van Hulle, & others, 2010).

The increase of wind farms installed in Europe in the current decade is presented in the next chart:

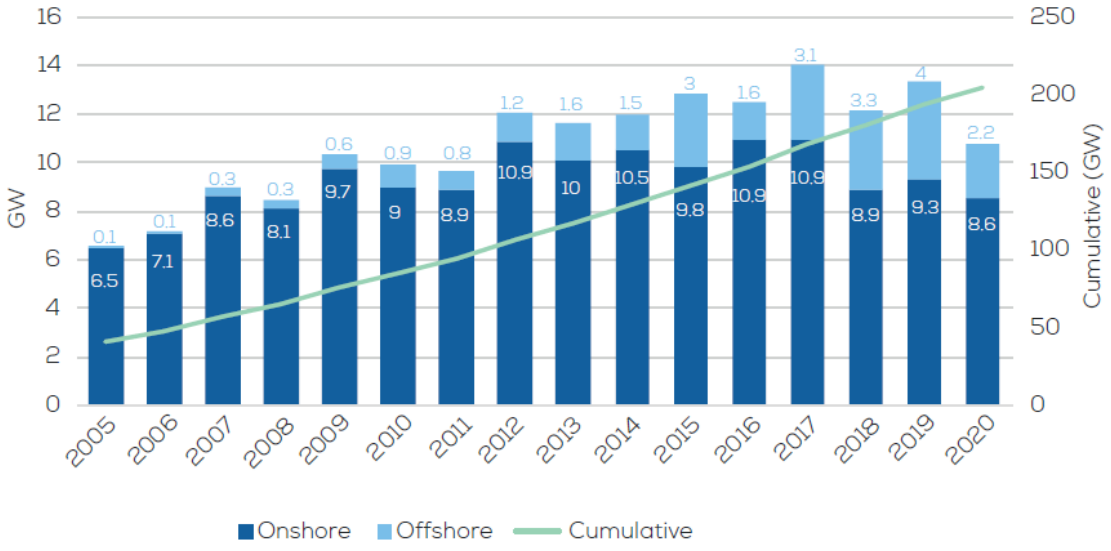

Figure 1.9: Wind energy market outlook in EU, Wind Energy Central Scenario *(Wind Europe, 2017)*

This explosion of offshore wind farms is a result of the significant advantages it has to offer, compared to onshore installations. Offshore wind farms offer considerably more energy output than onshore due to the higher wind speeds available, which however comes with increased cost (Pierri, Binder, Hemdan, & Kurrat, 2017). HVDC makes the extra investment worth it by efficiently transmitting power with rather low losses in the process. For the reasons explained earlier, AC is a poor choice when it comes to transmitting power through submarine cables due to their high electric capacitance. Thus, HVDC stands as the only viable solution for this purpose.

The fact that offshore wind turbines are installed far away from the public eye means loosened noise restrictions, thus allowing bigger dimensions for the rotors as well as faster rotation speeds. Furthermore, for the same reason, offshore wind farms cause minimal aesthetic issues, thus limiting visual pollution in their local region (Grant, 2017).

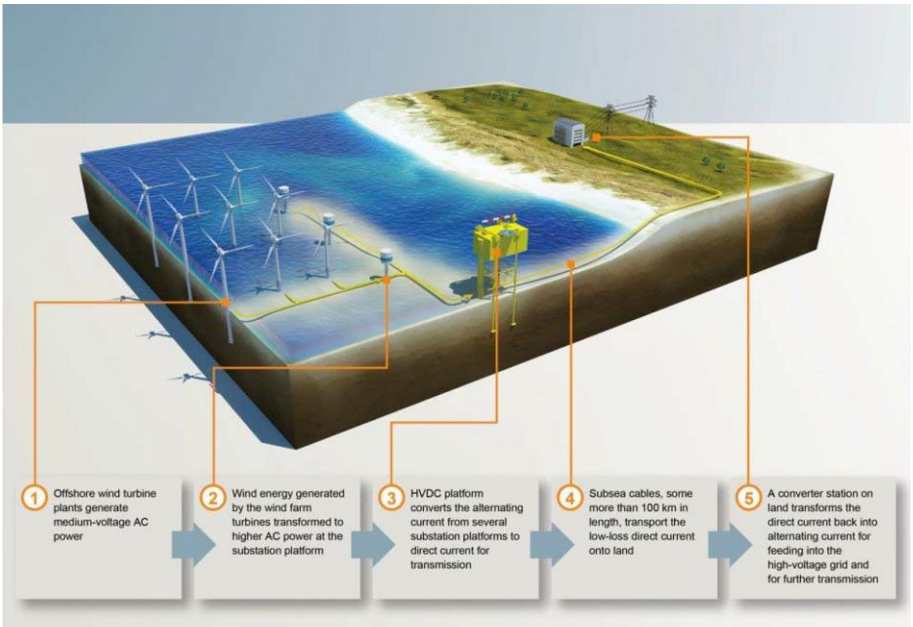

Figure 1.10: HVDC transmission with offshore wind *(Khazaei, Idowu, Asrari, Shafaye, & Piyasinghe, 2018)*

1.5.2. Shore to Offshore

Characteristics like back-start capability, dynamic voltage control and self-commutation, make VSC-HVDC systems excel in transmitting power to isolated areas. Islands and offshore oil, or gas production platforms can benefit from these properties by using power coming from shore through subsea cables (Pierri, Binder, Hemdan, & Kurrat, 2017).

Moreover, HVDC interconnections can be deployed to transport clean power from renewables, generated on shore, to supply offshore installations or remote areas, thus making them cheaper to operate due to the reduction of diesel fuel consumption, while also reducing their emissions (Khazaei, Idowu, Asrari, Shafaye, & Piyasinghe, 2018).

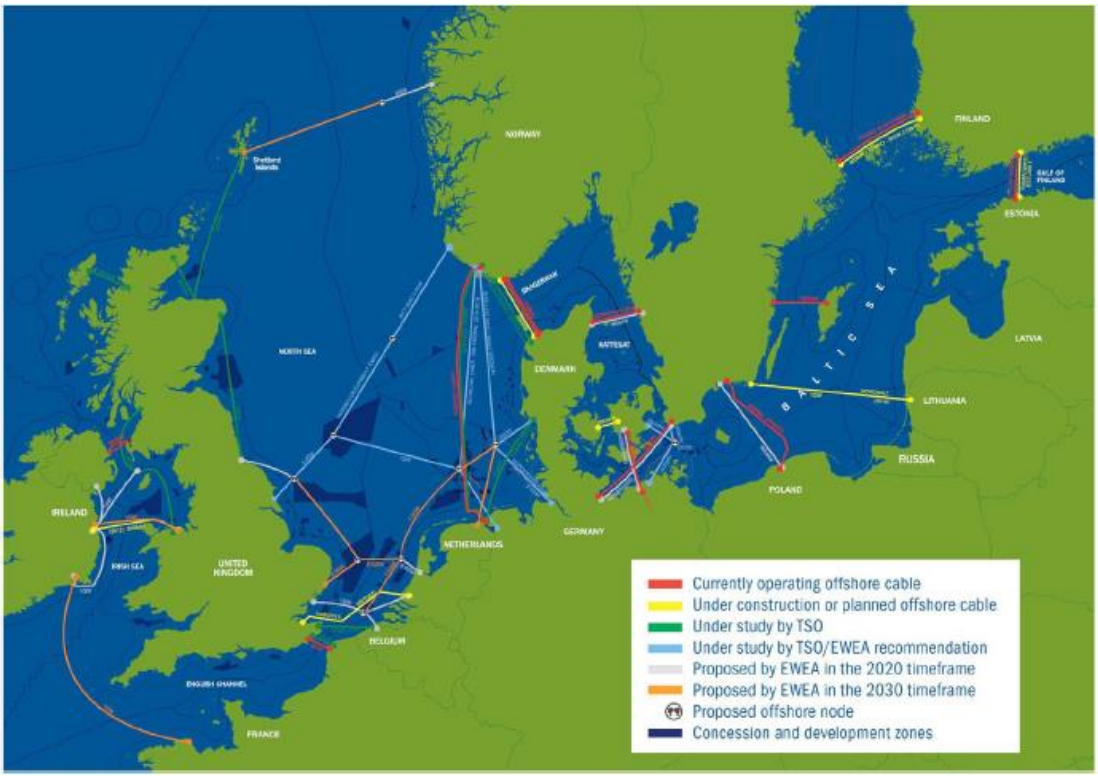

Figure 1.11: Offshore DC grid as proposed by EWEA *(Khazaei, Idowu, Asrari, Shafaye, & Piyasinghe, 2018)*

1.5.3. Large Power System Interconnection

As HVDC continues to find its way to more applications, the world moves progressively towards to the interconnection of larger electric systems. The undeniable technical and economic benefits of the technology have opened the way for power distribution across large regions and countries, but have also enabled the trade of electric energy between them.

The efficiency HVDC systems present in long-distance power transmission makes them ideal for interconnecting large systems together and forming larger grids that can exchange power dynamically, based on their current demand status. Systems are given the ability to buy or sell electric power to others, based on their current demand and operation cost of their production units. A system during peak hours can buy power from neighboring systems of greater capacity to cover the extra demand, possibly at a lower cost than if it produced the same power itself. Therefore, DC interconnections enable the systems to cooperate and also profit in the process.

Moreover, expanding interconnected networks of electric systems in Europe are gradually leading to the formation of a more economic, stable and stronger, large electrical supergrid. Trade of clean power is made a lot easier and efficient, thus helping Europe to further participate in power trading and furtherly utilize renewables for clean energy. HVDC makes it feasible to trade solar energy from southern to northern areas where solar energy is abundant during summer, while wind energy during winter can be transmitted from northern to southern Europe. The concept of the European supergrid is predicted to become a reality before 2050 (Pierri, Binder, Hemdan, & Kurrat, 2017).

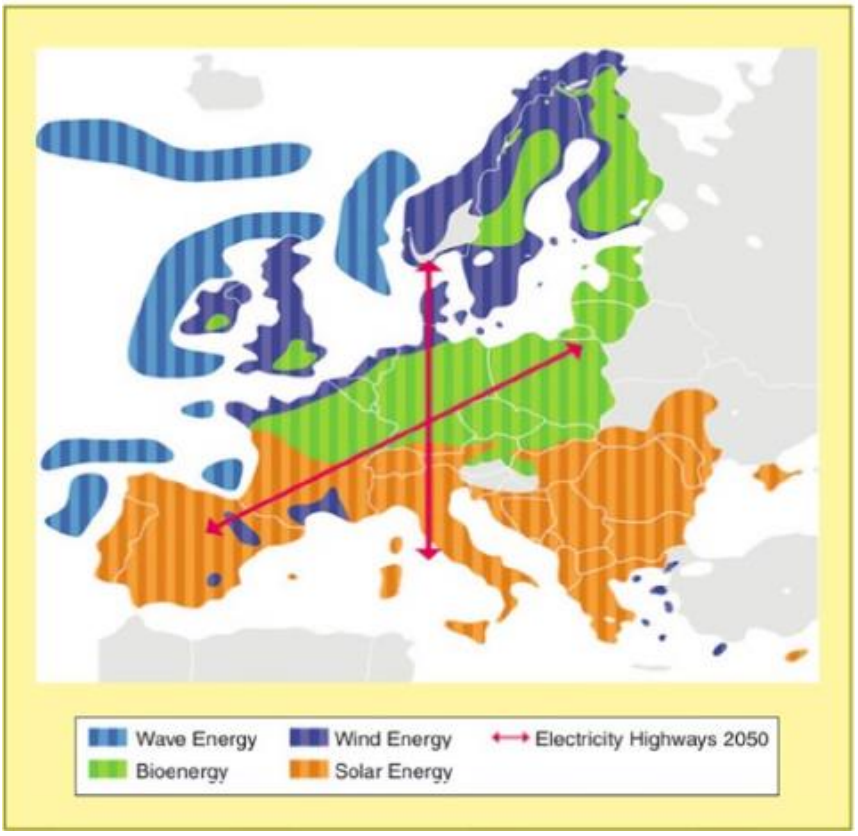

Figure 1.12: Location of renewable energy sources *(Sanchis, et al., 2014)*

1.5.4. Real World Projects

i. NORDLINK

A pioneering HVDC project that has nearly reached its completion is the NordLink. It will connect the grids of Norway and Germany with a subsea HVDC power cable more than 600 km long, which makes it Europe's longer interconnection. It will utilize the first full bipole VSH-HVDC converter with a rating of 525 kV and 1400 MW.

Figure 1.12: NORDLINK HVDC (right), *(Callavik, Lundberg, & Hansson, 2015)*

This project will enable the exchange of clean power between the two countries grids, with Norway being a leading producer of hydropower and Germany, an active investor of wind and solar power production (Callavik, Lundberg, & Hansson, 2015).

The trial operation of the NordLink will start in December 2020. It is expected to be fully functional by March 2021. The interconnection of the two regions will extend their power markets, encourage renewables and potentially bring down the electricity prices (Statnett , 2018).

More European HVDC projects are presented in the following table, along with their main characteristics:

ID	Project	Location	Year commissioned	Supplier	Power rating [MW]	DC Voltage [kV]	Converter type
1	Gotland	Sweden	1954	ABB	20	± 100	LCC
2	Cross Channel BP	France-UK	1985	CGEE Alsthom/GEC	2000	± 270	LCC
3	Fenno-Skan	Finland-Sweden	1989	ABB/Alcatel	500	400	LCC
4	Skagerrak 3	Norway-Denmark	1993	ABB	500	± 350	LCC
5	Sacoi	Italy-Corsica-Sardinia	1993	ANSADO	300	± 200	LCC
6	Baltic Cable	Sweden-Germany	1994	ABB	600	450	LCC
7	Kontek	Denmark-Germany	1995	ABB/NKT	600	400	LCC
8	Hellsjön	Sweden	1997	ABB	3	± 10	VSC
9	Gotland HVDC Light	Sweden	1999	ABB	50	± 60	VSC
10	Swepol Link	Sweden-Poland	2000	ABB	600	± 450	LCC
11	Tjaereborg	Denmark	2000	ABB	7	9	VSC
12	Grita	Greece-Italy	2001	Pirelli/ABB	500	400	LCC
13	Moyle Interconnector	Ireland-Scotland	2001	Siemens	2x250	2x250	LCC
14	Troll A	Norway	2004	ABB	2x40	± 60	VSC
15	Konti-Skan 1	Denmark-Sweden	2005	AREVA	250	± 250	LCC
16	Estlink	Estonia-Finland	2006	ABB	350	± 150	VSC
17	NorNed	Norway-Netherlands	2008	ABB	700	± 450	LCC
18	Storebaelt	Denmark	2010	Siemens	600	400	LCC
19	Valhall	Norway	2011	ABB	78	150	VSC
20	Sapei	Italy-Sardinia	2011	ABB	1000	± 500	LCC
21	BritNed	UK-Netherlands	2011	Siemens	1000	± 450	LCC
22	Romulo	Spain-Mallorca	2011	Siemens	2x200	± 250	LCC
23	East-West-Interconnector	Ireland-UK	2012	ABB	500	± 200	VSC
24	INELFE	France-Spain	2015	Siemens	2000	± 320	VSC
25	Skagerrak 4	Norway-Denmark	2014	ABB	700	500	VSC
26	Estlink 2	Estonia-Finland	2014	Siemens	670	± 450	LCC
27	NordBalt	Sweden-Lithuania	2015	ABB	700	± 300	VSC
28	NorGer	Norway-Germany	2015	t.b.d.	1400	± 450–500	LCC
29	Nemo	UK-Belgium	2017[a]	t.b.b.	1000	320–500	VSC
30	Alegro	Belgium-Germany	2019[a]	t.b.d.	500–1000	t.b.d.	VSC
31	NORD.LINK	Norway-Germany	2020[a]	ABB	1400	± 525 kV	VSC

[a] Scheduled.

Table 1.6: European HVDC projects *(Pierri, Binder, Hemdan, & Kurrat, 2017)*

ii. Jinping – Sunan Link

The Ultrahigh Voltage Direct Current (UHVDC) project of Jinping – Sunan, commissioned in 2013, bears the title most powerful transmission line in the world. It connects the two regions with a cable almost 2000 km long. It is rated at 800 kV with a capacity of 7200 MW, which can reach up to 7600 MW in continuous overload. The thyristor-based converters have the ability to withstand more than 5000 Amperes of DC current, in two-hour overload conditions, at 7920 MW. (ABB , n.d.)The project was designed to eliminate the power shortage in Eastern China, by delivering power from the hydropower station in Jinping. (C-EPRI Electric Power Engineering Co., Ltd , n.d.)

Figure 1.13: Jinping – Sunan HVDC Link *(ABB , n.d.)*

The map below gives an overview the impact of HVDC technology around the world. Numerous projects of various ratings have been installed, interconnecting regional and national networks, while more have already been commissioned:

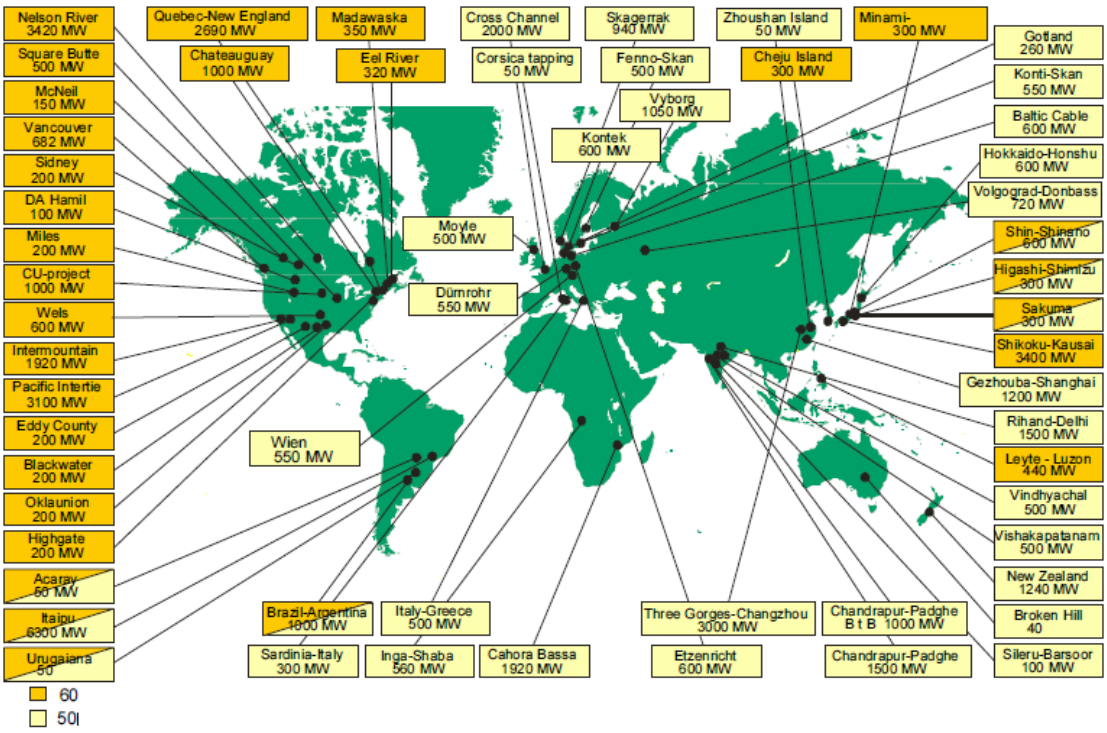

Figure 1.14: HVDC projects around the world *(Rudervall, Charpentier, & Sharma, 2000)*

Chapter 2: Theoretical Background

This chapter demonstrates the technical aspects of HVDC technology, from its first steps until today. Here we present the fundamental components of HVDC over the course of time, starting from the mercury-arc valve up to the advanced silicon-based semiconductors used nowadays in projects of great scale around the world. Also, the basic topology of an HVDC interconnection is described and different types of converters and configurations are presented. The chapter continues by making a short analysis on the nature of harmonics and their side effects in the operation of electrical grids. Finally, the principals of power flow and optimal power flow analysis are examined.

2.1. HVDC Converter Technologies

2.1.1. Mercury Arc Rectifier

The mercury arc valve was invented by Peter Hewitt in 1901 and was the technology that was firstly used for converting AC to DC and vice versa. It was a bulb that required a large glass envelope to operate and had already reached its maximum operating potential by the end of WWI due to size limitations. During 1930s and after continuous improvements, the mercury-arc rectifier had spread widely and started to make its way to the first HVDC projects (Tiku, 2014).

A mercury arc rectifier consists of an evacuated chamber (glass tube) and three or more electrodes. At the bottom of the tube there is a pool of mercury at very low pressure which forms the cathode, while a carbon electrode at the top forms the anode. When a given amount of current heats the mercury pool, it vaporizes and an arc can be struck within the chamber causing the ionization of mercury vapor that conducts electrons from the cathode to the anode (Peake, 2010). While mercury emits electrons freely, the same doesn't happen for the carbon anode that emits very few when heated. As a result, the current of electrons can only pass through the tube in one direction, similarly to a diode, which allows the tube to rectify alternating current. Therefore, the valve can maintain high currents at low arc voltages, making an effective rectifier. (Normandin, n.d.).

Despite the progress made on developing more robust mercury – arc valves, their demanding cooling techniques, high maintenance cost and significant environmental risk due to the toxicity of mercury compounds, made them easily replaceable by the more reliable and cost-effective semiconductor rectifiers. The age of mercury – arc rectifiers officially ended in the 1960s when solid state devices begun to emerge (Normandin, n.d.).

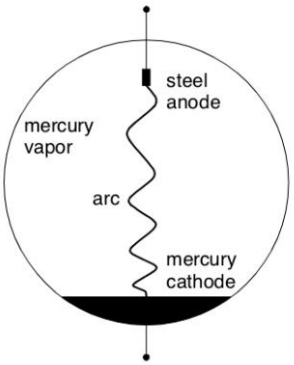

Figure 2.1: Mercury-Arc Valve *(Electrical Power Engineering, n.d.)*

2.1.2. Thyristor

The silicon-controlled rectifier (SCR) or thyristor, was proposed by William Shockley in 1950 and industrialized in 1956 by power engineers at General Electric (G.E.) (Guarnieri, 2013). The name thyristor became universally accepted later. At first the usage of thyristor was misjudged, and was considered as a tiny device that can only cope with small power ratings, comparable to the transistor. Their vital difference was the switching abilities of the former (Pyakuryal, 2013). Later on, it served as an alternative of the mercury arc rectifier for controlling alternating currents, where high voltages are involved.

The thyristor is a solid – state semiconductor device with four layers of alternating P and N-type materials. It consists of three terminals, the anode, the cathode and the gate. The outer highly doped zones are the emitting zones, whereas the inner, lower doped layers are the base zones. Thyristor layers act as bi-state switches that conduct as long as a current pulse is applied to the gate, and the voltage across the devise is not reversed. Thyristors have three states of operation: reverse blocking mode (off state), forward blocking mode (off state) and forward conduction mode (on state) (Huang, Uder, Barthelmess, & Dorn, 2008).

Figure 2.2: Thyristor symbol (left) and schematic diagram (right) *(Khatri, 2018)*

Thyristors cannot be considered as ideal switches because of several imperfections compared to an ideal switch. Non-ideal behavior is present in both off and on-state of the thyristor. Due to voltage applied during the off-state, an off-state current flows both in the forward and in the reverse direction. Furthermore, while at the on-state the thyristor shows significant voltage drop during conduction. As a result, considerable power losses must be expected for typical currents of several kA. (Huang, Uder, Barthelmess, & Dorn, 2008).

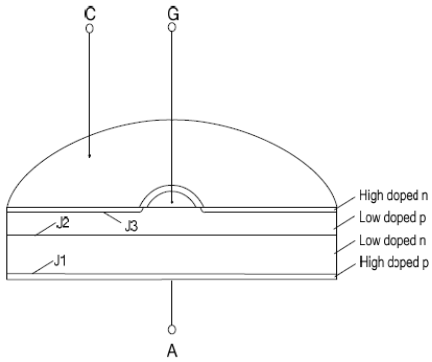

Figure 2.3: Schematic cross section illustration of a high- power thyristor

Figure 2.4: High power thyristors made of 4", 5" and 6" silicon wafer

Thyristor's sizes may vary and directly depend on its voltage rating. The typical diameter length of a modern high-power thyristor is around 4 to 6 inches. Six- inch thyristors with 8kV blocking voltage was developed for applications that require higher current capabilities, such as HVDC systems (Huang, Uder, Barthelmess, & Dorn, 2008). For high-blocking voltages, the thyristor requires a thick N-base region and therefore a high ON-state voltage drop, which implies increased losses. The reach-through effect gives us the only option of reducing the P-base and P-anode thickness to reduce the on-state losses (Baliga, 2010).

Thyristors have come a long way, and today are available with blocking capability that exceeds 8000 V and are able to conduct 5000A in the on-state. A modern thyristor device has the ability to control over 40 MW of power, which makes it appealing for HVDC systems. The high effectiveness of just a single thyristor unit means that fewer devices are needed for the operation of the converter stations. Due to their advantages, thyristors are chosen for numerous HVDC and Ultra-HVDC projects around the world. (Baliga, 2010)

2.1.3. Thyristor Valve

Modern thyristors stand out for their high blocking capability, but when high voltage withstand capability is required, a series or parallel connection of multiple thyristors is necessary, which all together compose a thyristor valve.

The thyristor, or solid-state valve, is basically a layout of thyristors located inside the converter stations at either end of a transmission link, converting AC to DC current or vice versa. It has been the backbone of the high-power electronics industry used in HVDC transmission systems until today in Current source (CSC) converters (Klaka, 2015). The term 'valve' is carried over from the mercury arc valve days and is applied until today. Through the years the thyristor technology has been refined and significant progress has been made to the quality of their design. Since the early seventies, when high voltage thyristor valves made their commercial debut in HVDC transmission systems, there has been a constant improvement in their blocking performance along with their current carrying capability.

The increase of thyristor's power rating goes hand in hand with increased demand for larger HVDC power transmission projects. While the semiconductors are optimized for each HVDC project with respect to voltages and especially the on – state losses, the blocking voltage of about 8kV per thyristor has been established as an optimum of overall operation losses. However, new designs of 9kV per thyristor have been introduced recently, aimed for plants with current ratings at the lower range (Stomberg, Abrahamsson, & Saksvik, 1996). At the same time, the enhancement of their characteristics over the years had a great impact on decreasing the components of the thyristor valve. "To transmit the same amount of power as the beginning of the thyristor – era in HVDC – technique, only about 5% of the thyristors (and snubber circuits) are necessary today" (Huang, Uder, Barthelmess, & Dorn, 2008). Consequently, there has been a significant improvement in their reliability and an overall simplification on their design. Today's valve setups follow a rather elegant approach by been clean structured, compact, and also easy to assembly and maintain.

Thyristor valves can be built with different configurations of thyristors in series, including their auxiliary electronics. They are usually found in twelve-pulse group using three

quadruple valves. The valve is built up with one or more layers of thyristors connected in series, depending on its required voltage capacity of the application. Today, HVDC valves can reach voltages up to 800 kV, and may consist from up to 120 thyristors (Huang, Uder, Barthelmess, & Dorn, 2008).

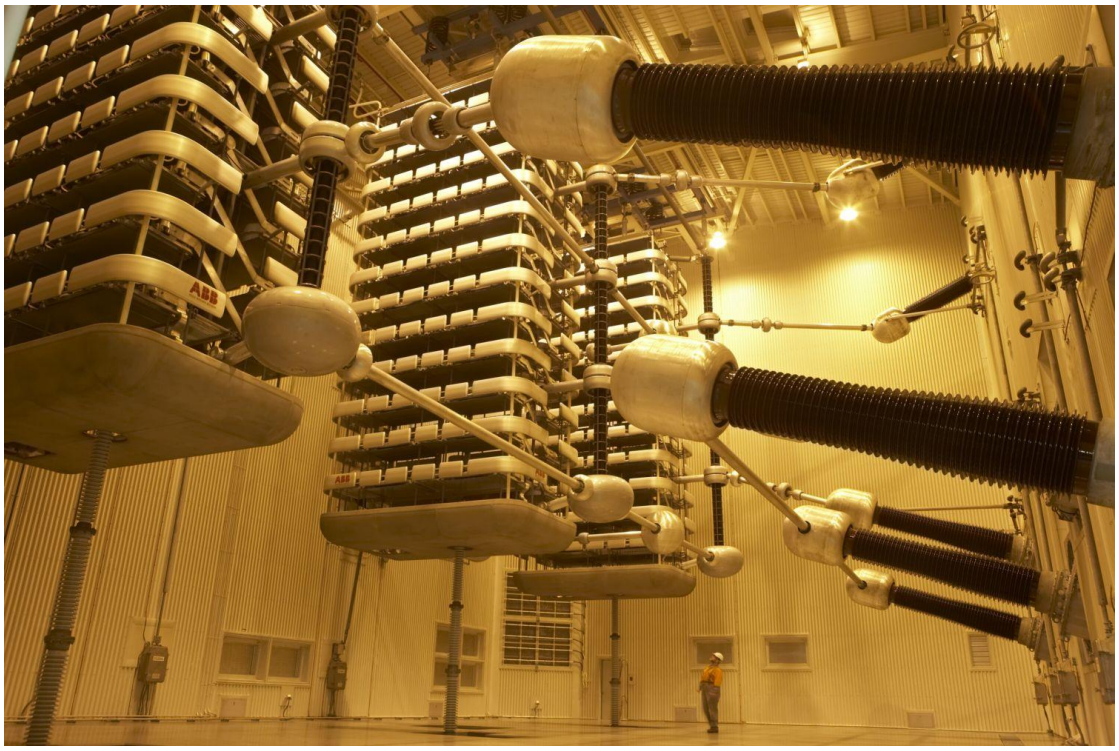

Figure 2.5: HVDC Pole 2 thyristor valve hall at Haywards in the New Zealand HVDC Inter-Island scheme *(Marshelec)*

The above image is from a real-world example of the utilization of thyristor valves. This is from the valve hall of pole 2 of the HVDC Inter-Island project (1991), which connects the North and South Island of New Zealand. Thyristor valves can be seen with 12 layers (trays) with 4 modules of series connected thyristors each. The converter's nominal rating is 560 MW with a voltage of 350 kV (ABB, n.d.).

2.1.4. IGBT

The newly introduced IGBT, or Insulated Gate Bipolar Transistor, was introduced in the family of power electronic devices in the early 1980s that comes from the combination of Power MOSFETS and Power BJTs, while keeping the best from both worlds.

IGBTs are characterized by the excellent conduction properties of the former, and the high input impedance, the exceptional switching capabilities with the voltage control offered by the latter. Furthermore, they don't preserve the poor characteristics, like the low input impedance, inferior switching performance and current control of PBJTs, and the bad conduction properties of the PMOSFET. Therefore, the result of the two is a device that mixes an insulated gate of the MOSFET with the output performance of a BJT. This combination is evident from the symbol used for the IGBT:

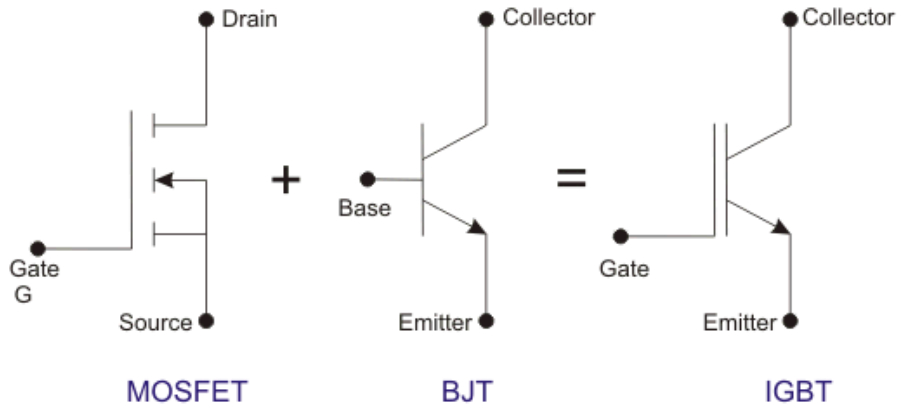

Figure 2.6: IGBT symbol as an amalgamation of MOSFET and BJT symbols *(Electrical 4U, 2019)*

IGBT is a three terminal device that includes a Gate, an Emitter and a Collector. It has a structure closely related to the MOSFET, with the difference of having a collector with an injected layer of p^+, instead of just a n^+ substrate like the MOSFET's drain. In order to bring an IGBT to the ON state, both the gate (V_{GE}) and the collector (V_{CE}) should be at a positive potential with respect to the emitter. Additionally, the gate should have a sufficient voltage ($V_{GET} > V_{GE}$). This leads to the creation of an inversion layer below the gate, which allows current to flow with direction from the collector to the emitter. We turn it off by simply changing the gate signal to zero, or making it slightly negative. Below is presented a comparison between the three devices we mentioned:

	Power Bipolar	**Power MOSFET**	**IGBT**
Voltage Rating	High < 1kV	High < 1kV	Very High >1kV
Current Rating	High < 500 A	Low < 200A	High > 500A
Input Drive	Current, h_{FE}	Voltage, V_{GS}	Voltage, V_{GE}
Input Impedance	Low	High	High
Output Impedance	Slow	Fast	Medium
Cost	Low	Medium	High

Table 2.1: Comparison of Transistor technologies *(Electronics Tutorials, n.d.)*

IGBTs are widely used in power electronics, for the construction of inverters, converters and also power supplies, where there is high demand for decent switching speeds and good conduction properties. They offer significantly more power gain than bipolar transistors while having less input losses than the MOSFET. Therefore, IGBTs make an ideal solution for HVDC system applications, and specifically VSC converters (Electronics Tutorials, n.d.).

2.1.5. VSC Valve

VSC converter valves consist of several modules of IGBTs, depending on the desired rated voltage we want to achieve. A typical IGBT valve module has an IGBT, a voltage divider and a gate unit. The module also includes a water-cooled heat sink for highly efficient heat dissipation. More IGBT modules are used in order to reach currents of higher rate (Devi, Ch, & Nagaraju, 2012).

The valves are installed inside the valve hall where they can be arranged as three or four layer valve towers. They form structures that in some cases suspend from the roof, while in other cases they stand on a higher level relative to the floor. A dedicated cooling system is responsible for keeping the valves in lower temperatures.

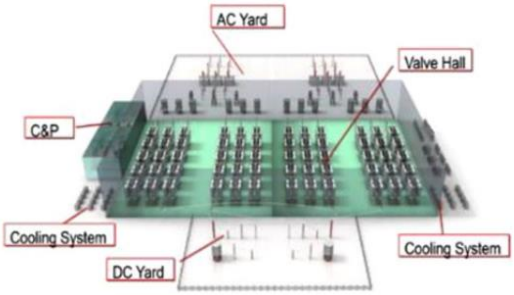

Figure 2.7: Typical VSC-HVDC converter station layout *(An, Tang, & Wang, 2017)*

The next figure shows the valve hall of Skagerrak 4 VSC-HVDC scheme in Scandinavia (Jovcic & Ahmed, High Voltage Direct Current Transmission: Converters, Systems and DC Grids, 2015):

Figure 2.7: Valve hall of 500 kV, 700 MW Skagerrak 4 Modular Multilevel Converter (MMC) *(ABB, 2016)*

2.2. HVDC Transmission System

HVDC systems convert the AC current to DC to transmit power from an AC network to another. The conversion takes place inside the valve hall where the HVDC converter is located. The current flows through the transmission medium, chosen according to the needs of the particular application. It then arrives at the other end of the interconnection, where there is another converter substation that performs the conversion from DC to AC. The power is then injected to the respective AC network.

The converter station located at each end of the interconnection can either be used as a rectifier or an inverter, depending on the direction of the power transmission as power transfer can be done from both sides. In the case which the voltage at the rectifier is greater than the voltage at the inverter, the power is transmitted with direction from the rectifier's end to the inverter. Otherwise, the power flows from the inverter to the station the rectifier is located. During the conversion, reactive power is consumed by the converters that needs to be compensated.

DC Current through interconnection (Wang & Redfern, 2010):

$$I_{dc} = \frac{U_f - U_i}{R}$$

- $U_f > U_i$: power flow from the rectifier to the inverter
- $U_f < U_i$: power flow from the inverter to the rectifier

I_{dc}: the current passing through the DC transmission line
U_f : the voltage at the rectifier
U_i : the voltage at the inverter
R : the resistance along the transmission line

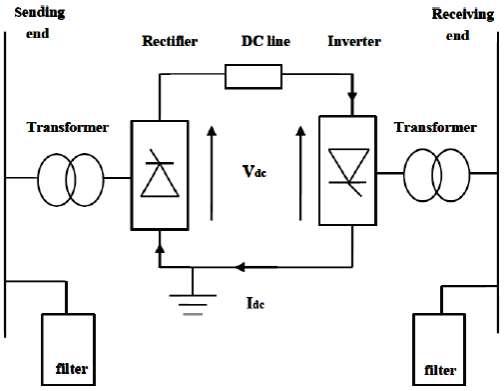

Figure 2.7: HVDC System basic layout.

The layout of an HVDC system is presented in the following example of a typical subsea interconnection:

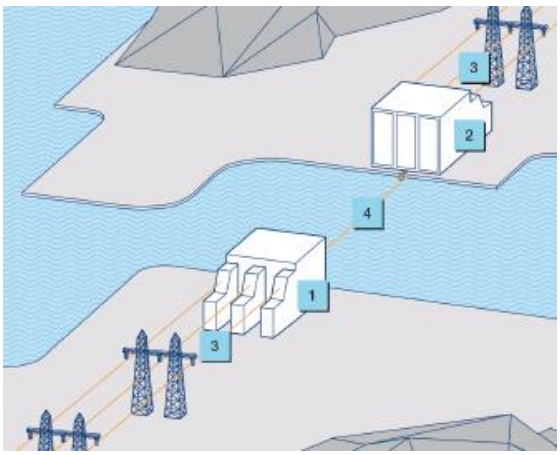

1: HVDC Converter Station Rectifier
2: HVDC Converter Station Inverter
3: Alternating Current (AC)
4: Direct Current (DC)

Figure 2.8: Basic components of an HVDC link (left) *(Grant, 2017)*

2.2.1. HVDC Components

Converter stations are crucial for the operation of the system and are responsible for the quality of the power injected to the DC lines. They require a number of different electronic components for their operation:

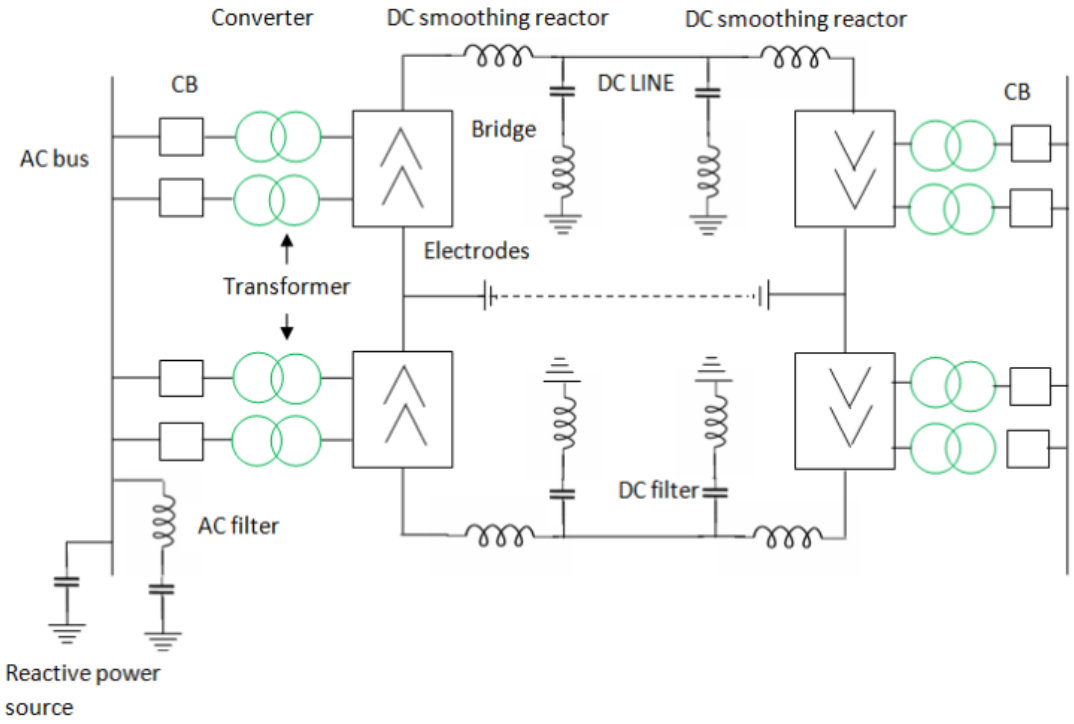

Figure 2.9: HVDC key components overview *(Electrical4U, 2019)*

Depending on the type of application, thyristor or VSC valves can be used in several different configurations. The transformers used on both ends are for adjusting AC voltage levels to that of DC, while also contribute to the commutation reactance. In HVDC systems, single phase transformers with three windings are often used, but the configurations may vary based on the project's requirements. AC filters are necessary for limiting the number of harmonics of AC current produced during the conversion, and the impact of reactive power. Capacitor banks are necessarily installed for the compensation of reactive power consumed by the converters. This is achieved by installing capacitors in series between the converter valves and the respective transformer. In VSC systems, less filters are needed due to the fact that harmonics in these cases are directly related to the frequency of the PWM. Finally, DC filters are placed in order to reduce harmonics that are injected into the transmission line, which can interfere with other electronics and especially telecommunication systems. DC filters are mandatory when the system uses overhead transmission lines. (Khazaei, Idowu, Asrari, Shafaye, & Piyasinghe, 2018)

Another important aspect of HVDC systems is the transmission medium. Depending on the type of application, overhead cables are used for power transmission on land, which are mostly bipolar, and submarine cables for transmission through sea. Solid and oil-filled are the types of cables used more often, with the former being the less costly alternative and doesn't have any length limitations. The second has a maximum length of 60 km but can withstand more pressure, which makes it ideal for submarine transmission, in comparison with the solid type that can be used no more than 1000 m deep. Power cables

technologies are progressing with rather quick pace, and are still introducing new types of cables with better performance. (Rudervall, Charpentier, & Sharma, 2000)

These components can also be seen in the following graphic representation:

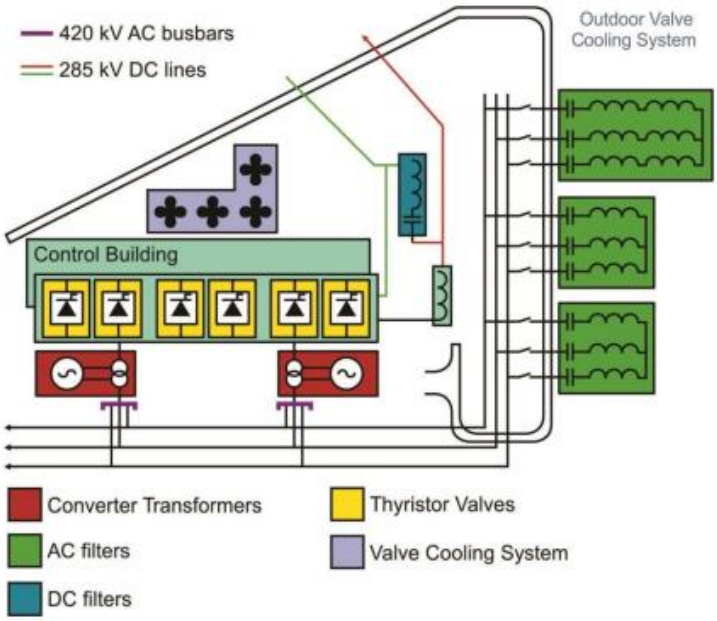

Figure 2.10: Simplified layout of a conversion station *(Ardelean & Minnebo)*

2.3. HVDC Types

HVDC technology has undergone long way since it was firstly introduced for commercial purposes of long - distance energy distribution. Nowadays we distinguish two types of HVDC, depending on the switching devices used inside the converter: CSC – HVDC and VSC – HVDC.

2.3.1. CSC – HVDC

Conventional HVDC technology is a well-tested method that has already been used in numerus projects around the globe, offering high power transmission capacity. CSC uses thyristor valves as switching devices, making it work like a Line Commutated Converter (LCC). That is because the thyristor can be switched off only when the current passing through it is zero, thus needing line voltage for commutation. CSC – HVDC is a suitable method for long distance, high voltage bulk power transmission, given that it ignores the effect of capacitance along the transmission lines. Other examples of CSC applications are the connection of two unsynchronized AC grids or grids with different frequencies. With the utilization of source-current inverters we achieve voltage rectification through a six or twelve - pulse controlled thyristor bridge (Wang, Bertling, Le, Mannikoff, & Bergman, 2011):

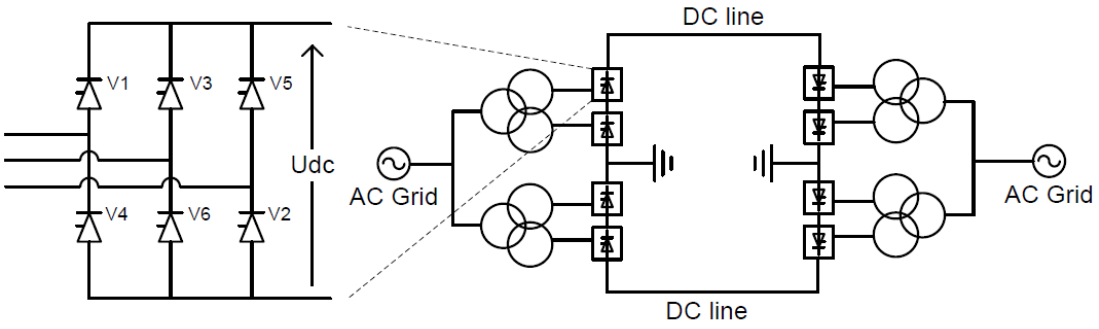

Figure 2.11: 6-pulse valve (left) and bipolar configuration (right)

Rectifiers are circuits that convert alternating current and voltage to direct using either diodes or appropriately controlled thyristors as switching elements. A pair of switching elements (valves) corresponds to each phase of power, one of them allowing current to pass through when voltage is negative, and one for when voltage is positive. Two valves in the bridge that belong to different phases are conducting at any time, thus giving a DC output synthesized by two of the three AC phase voltage in series. For controlled bridges, thyristors determine the switching elements of the circuit. Thyristors conduct when they receive a trigger pulse and only if they are positively polarized. Consequently, real power output control can be achieved by sending the trigger pulses accordingly.

2.3.1.1. Back-to-Back CSC-HVDC Systems

This configuration includes two converters installed at the same station. The two terminals are connected with very short DC cables, with the purpose of supporting asynchronous interconnection between AC systems that operate at different frequencies. The power transmission is controlled by the HVDC system with reduced losses in the process due to the limited size of the DC lines, and are designed to operate at low voltages for lower cost (Jovcic & Ahmed, High Voltage Direct Current Transmission: Converters, Systems and DC Grids, 2015).

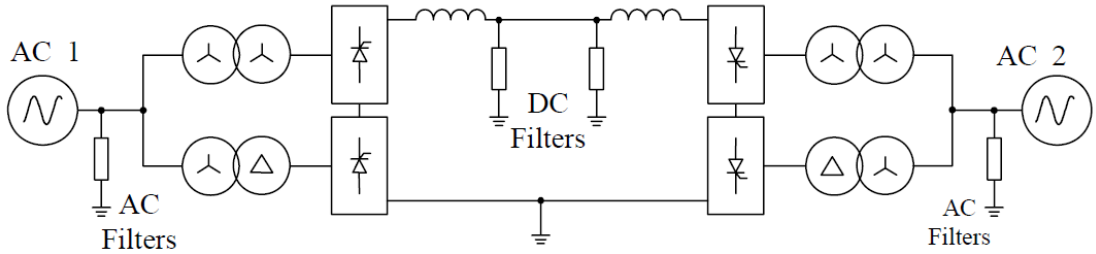

Figure 2.12: Back-to-back CSC-HVDC system with 12-pulse converters *(Agelidis, Demetriades, & Flourentzou, 2006)*

2.3.1.2. Monopolar CSC-HVDC Systems

There are two types of monopolar HVDC systems: monopolar systems with ground return and monopolar systems with metallic return (Eremia, Liu, & Edris, 2016) .

i. Monopolar System with Ground Return

A system like that consists of multiple 12-pulse converter units connected in series or parallel at each terminal. The terminals are interconnected with a single conductor and they both have a ground or sea electrode built that ensures continuous operation. While being a cost – effective method for HVDC transmission, this method may cause interference to nearby structures or systems and can also involve magnetic field effects.

ii. Monopolar System with Metallic Return

In this case the system consists two conductors of high and low voltage respectively. The neutral is attached to one converter station and connects to the station's grounding grid or to a ground electrode, while the other terminal remains ungrounded.

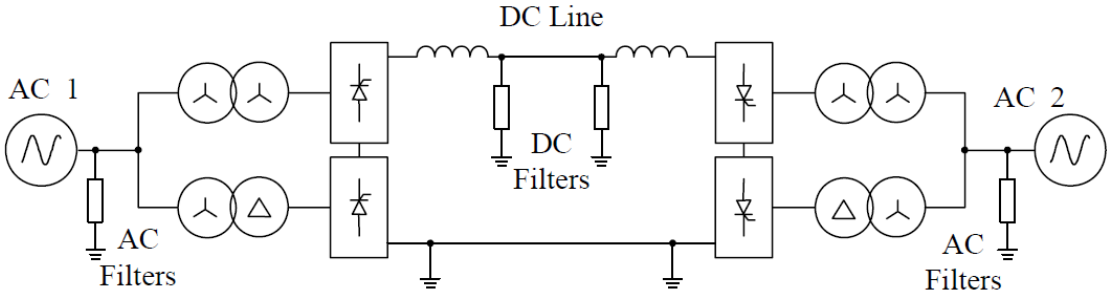

Figure 2.13: Monopolar CSC-HVDC system with 12 pulse converters.

2.3.1.3. Bipolar CSC-HVDC Systems

The most prevalent configuration of CSC-HVDC systems in applications where the transmission of power happens by using overhead lines. The bipolar systems basically consist of two monopolar systems that uses two converters at each terminal, one that connected amidst earth and the positive pole while the other remains connected amidst earth and the negative pole. Each of these systems can operate independently, using earth as the return path thus greatly enhancing the reliability of the simple monopole system. Therefore, in case one converter or high voltage conductor is out of service, the healthy pole can continue to transmit power, using earth as the return path. In an extreme scenario where a converter outage occurs at any of the two poles, the healthy pole conductor can be used as the return path. In normal operation, the two poles try to maintain equal DC voltage and current so that the neutral current is theoretically zero with deviation around 1% (Agelidis, Demetriades, & Flourentzou, 2006).

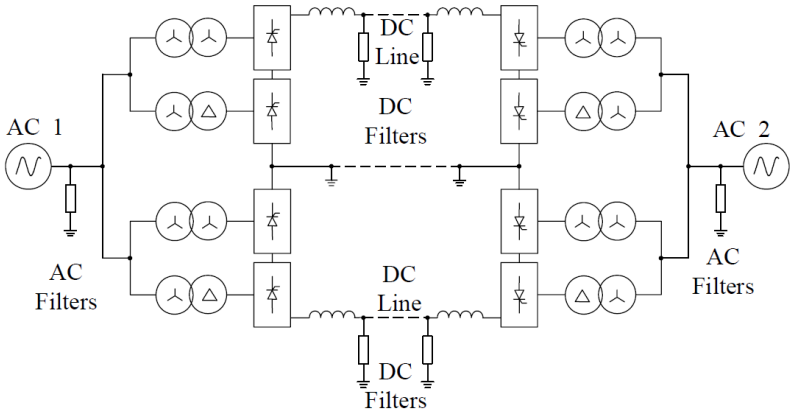

Figure 2.14: Bipolar CSC-HVDC system with one 12-pulse converter per pole *(Agelidis, Demetriades, & Flourentzou, 2006)*

2.3.1.4. Multiterminal CSC-HVDC Systems

The term refers to an HVDC system that consists of more than two sets of converters. This configuration involves more complexity than a two terminal point-to-point system in order to maintain sophisticated control and communication between the transforming stations. Below is a block diagram of a multiterminal CSC-HVDC that employs 12-pulse converters on each pole:

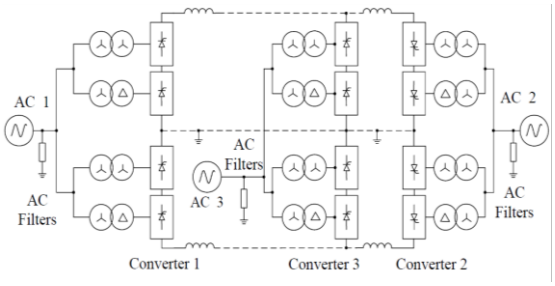

Figure 2.15: Multi-terminal CSC-HVDC system-parallel connected

Here converters 1 and 3 can operate as rectifiers while converter 2 operates as an inverter, and vice versa. We can achieve a number of different combinations by switching the connections of a converter using mechanical switches (Agelidis, Demetriades, & Flourentzou, 2006).

Currently only two multi-terminal CSC-HVDC (MTDC) systems are in operation in the world. The difficulties in using this type of technology arise from its inefficient power control capabilities, but mostly due to the inability to change the power flow direction without changing the polarity of the converter. This limits us to the development of multi-terminal CSC systems with one-way power flow capability (Buigues, Valverde, Etxegarai, Eguia, & Torres, 2017).

2.3.2. VSC - HVDC

The term stands for Voltage Sourced Converters. This technology offers a rather simpler and more economical approach, by using two-level converters consisting of Insulated Gate Bipolar Transistors (IGBT) combined with Pulse-Width Modulation (PWM) control method.

A typical voltage source valve operates based on IGBTs connected in series that work as switching devices to distribute the high blocking voltage. Anti-parallel freewheeling diodes are responsible for the converter's four – quadrant operation because of their property of eliminating flyback, a small voltage spike caused by sudden reduction of the current supplying an inductive load (ELPROCUS, n.d.). Furthermore, capacitors are used on the dc side to offer power flow control and also to smooth voltage ripples and filter out dc side harmonics. In those type of converters, the AC output of each phase is switched between two discrete voltage levels that translate to the positive and negative DC voltage terminals, generating a square waveform. Thus, the use of PWM is recommended in order to reduce the high harmonic distortion generated (Wang, Bertling, Le, Mannikoff, & Bergman, 2011).

A rather significant drawback of this technology is the high-power losses due to the demand for high switching frequencies of the IGBTs. However, the two-level topology can be used as a basis for the creating of converters with three, four, or more levels. It is certain that multilevel topologies offer some important improvements that are greatly appreciated in HVDC applications (Agelidis, Demetriades, & Flourentzou, 2006).

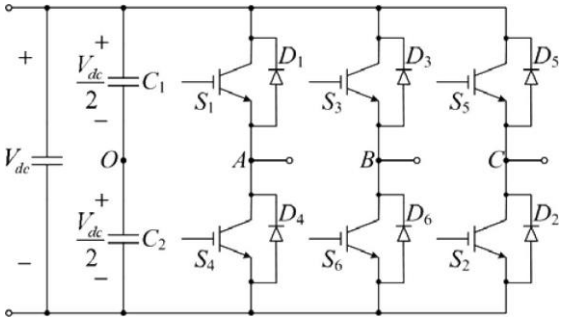

Figure 2.16: Conventional three-phase two-level VSC topology (Agelidis, Demetriades, & Flourentzou, 2006)

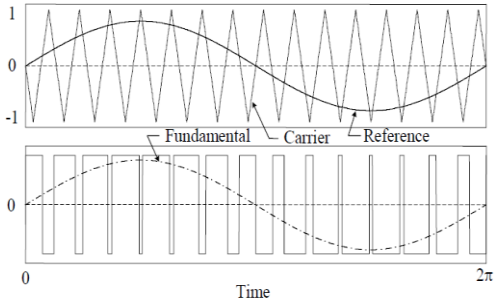

Figure 2.17: Two-level sinusoidal PWM method: reference (sinusoidal) and carrier (triangular) signals and line-to-neutral voltage waveform.

2.3.2.1. Monopolar and Bipolar VSC - HVDC

All the configurations we discussed earlier about CSC are also available for VSC-HVDC systems. VSC systems can be installed in monopolar and bipolar topologies for power transmission, although they are most commonly used as symmetrical monopoles. In this type of configuration, the system is controlled as a single unit (monopole) while it operates as a bipole, using two cables of negative polarity.

Symmetrical monopole configurations were used in early VSC-HVDC systems, where cable voltage ratings were limited and have only recently reached 320 kV, and therefore this was the only solution for achieving the proper DC voltage level between the two poles. Moreover, full bipolar topologies were not necessary, due to the low voltage levels and power ratings of the installed VSC transmission systems (Jovcic & Ahmed, High Voltage Direct Current Transmission: Converters, Systems and DC Grids, 2015).

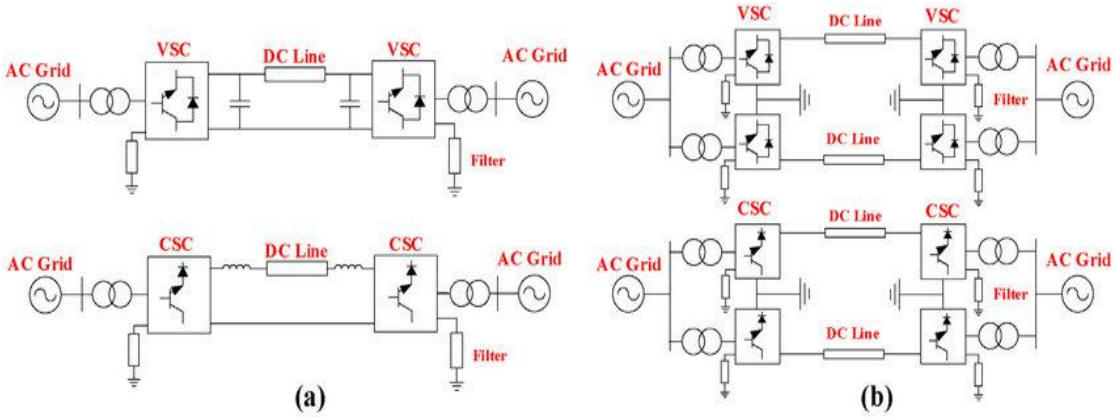

Figure 2.18: Comparison of (a)Monopolar VSC/CSC-HVDC and (b)Bipolar VSC/CSC-HVDC *(Khazaei, Idowu, Asrari, Shafaye, & Piyasinghe, 2018)*

2.3.2.2. Multi-level VSC-HVDC

This technology is also available with names such as HVDC Plus or HVDC Light. It utilizes multiple modular multilevel converters to gain significant benefits, providing HVDC applications an enticing alternative to traditional two-level topologies.

To produce quality sinusoidal output voltage waveform closer to the fundamental frequency, while maintaining lower switching losses in comparison with two-level VSC. Better power quality means smaller and cheaper output (AC) filters because of the reduced harmonic components in voltage and current.

Each switch module in reality consists of two IGBTs (valves) with anti-parallel diodes, connected in series. Using the typical two-level topology, we can construct a converter of three or more levels. The basic principal behind the operation of MMC is that each module has three switch modes:

- S1 is turned on and S2 is turned off. The capacitor is inserted into the circuit, the module contributes with voltage to the phase voltage
- S1 is turned off and S2 is turned on, the capacitor is bypassed.
- S1 and S2 are both turned off, the module is blocked when the capacitor voltage is higher than outside voltage.

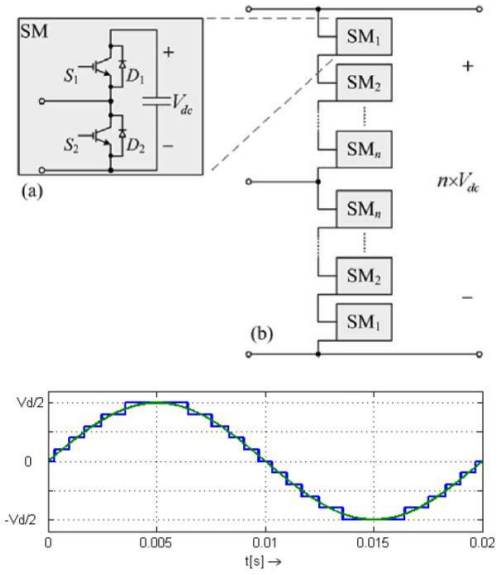

Figure 2.19: Upper Right: Modular multilevel converter topology, (a) Structure of one submodule (SM) and (b) Phase leg. Lower Right: ac line voltage waveform (Wang, Bertling, Le, Mannikoff, & Bergman, 2011)

This method greatly reduces the switching losses seeing that a module needs to switch on and off significantly less times. By adding more modules for each phase leg, we can attain an output closer to a sinusoidal waveform.

2.3.2.3. Multi-Terminal VSC-HVDC

VSC systems are most suitable for Multi-Terminal (MT) applications than CSC due to the fact that it's easier to establish parallel connections with common DC voltage, and additionally, to control the direction of the power without interruption (Pan, et al., 2008). The application of CSC is troublesome in these cases and may result in an unreliable MT system.

MT systems are considered have significant back-start, AC/DC voltage control capabilities. Their operation requires power management within the limits of the operating voltage limits that will ensure their reliable operation. The lower voltage limit is defined by the maximum of the operating AC voltage of all converter stations of the system, whereas the upper limit is specified by the rating of the DC cables and the forward blocking capacity of the IGBTs (Mohammadi, 2018).

VSC MT systems are a newly introduced concept and are especially preferred for renewable energy production integration and for strengthening large interconnected AC grids. Only a few projects exist today but more are planned and are expected to be implemented in the coming years.

2.3.3. Advantages and Disadvantages

New generation topologies of VSC have been developed that offer loss reduction up to almost half of the original level. Such a topology is the Modular Multilevel Converter (MMC) which uses cascaded connection logic. The diode-clamped NPC topology is presented below along with that of the actively clamped topology. The last was introduced as an improvement to the original NPC, capable of solving the loss distribution problem of its predecessor (Wang, Bertling, Le, Mannikoff, & Bergman, 2011):

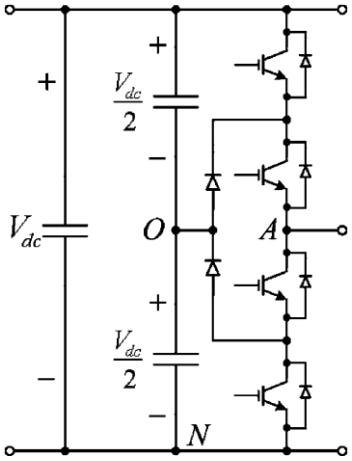

Figure 2.20: NPC phase leg

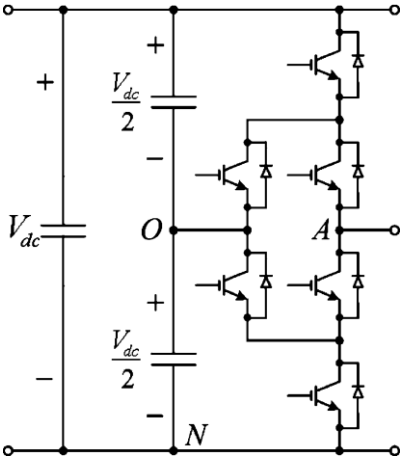

Figure 2.21: ANPC phase leg

Compared to CSC, VSC provides us with the ability to have independent and fast control over the real and reactive power, giving us the ability of regulating voltage and frequency in order to keep them stable. The real power can be kept within the limits of the converter, thus making the DC network injecting or absorbing from the AC grid. Therefore, VSC systems show great utility in the control of the power flow on demand (Pan, et al., 2008).

VSC converters can be controlled as an idea voltage source, which makes it viable to connect a VSC system to a weaker AC grid, or one that doesn't possess a generation source and therefore, has a relatively low short-circuit level (Agelidis, Demetriades, & Flourentzou, 2006).

The need for large harmonic filters is reduced because of the fast dynamic response offered by PWM, which is higher than that of the phase-controlled operation (Agelidis, Demetriades, & Flourentzou, 2006). High switching frequencies (1-2 kHz) make it possible to separate the fundamental voltage frequency from the sidebands. Therefore, the harmonic components around the switching frequency are cut off, allowing us to use less costly harmonic filters with lower losses (Jovcic & Ahmed, High Voltage Direct Current Transmission: Converters, Systems and DC Grids, 2015).

VSC systems also perform well during AC faults, due to their ability to actively control the AC voltage and current. In case of an AC disturbance, the converter remains in operation and provides voltage support to the AC networks during and after the fault's occurrence (Jovcic & Ahmed, High Voltage Direct Current Transmission: Converters, Systems and DC Grids, 2015). Moreover, VSC systems provide back-start capability. This means that they are able to start and restore power to an AC network that doesn't heave operating generation units, thus eliminating the necessity for a start-up generator (Agelidis, Demetriades, & Flourentzou, 2006).

The capabilities of VSC-HVDC make it valuable for various fields of applications (Pan, et al., 2008):

- Supply of small, isolated remote loads
- Power supply to islands and city centers
- Makes remote small-scale generation feasible
- Transmission of power generated offshore through undersea lines
- Multi-terminal configurations

It is understandable that VSC is an asset of great importance for the feasibiity in a great number of applications that HVDC technology is involved. However, the technology shows some weaknesses compared to CSC that are summed up in the following lines:

PWM method incorporates the high switching frequency of the IGBTs which leads to significant power losses, as a tradeoff to the improved control it offers. That stands as a drawback in high-power applications based on VSC, where the high-frequency switching of the IGBTs is followed by increased conduction loss (Wang, Bertling, Le, Mannikoff, & Bergman, 2011). However, multi-level topologies achieve to partially resolve the issue.

VSC applications come with a higher cost than CSC, mostly because of the very large number of semiconductors (IGBTs) needed, contributing to the more economical design of thyristor valves that requires less thyristors. IGBT modules also have greater footprint than that of thyristor modules (Jovcic & Ahmed, High Voltage Direct Current Transmission: Converters, Systems and DC Grids, 2015).

Most importantly, VSC systems face serious issues with DC faults. The clearance of the fault is usually done by AC circuit breakers, however, the converter's reconnection after circuit breaker tripping can be really time consuming (Jovcic & Ahmed, High Voltage Direct Current Transmission: Converters, Systems and DC Grids, 2015).

Bellow follows a list of real-world projects that utilize VSC technology:

Project Name	Year of Commission	Power rating	Number of circuits	AC voltage	DC voltage	Length of DC cables	Comments and reasons for choosing VSC-HVDC	Topology	Semi-contactors
Hellsjön, Sweden	1997	3 MW ±3 MVAr	1	10 kV (both ends)	± 10 kV	10 km Overhead lines	Test transmission. Synchronous AC grid.	2-level	IGBTs (series connected)
Gotland HVDC Light, Sweden	1999	50 MW -55 to +50 MVAr	1	80 kV (both ends)	± 80 kV	2 × 70 km Submarine cables	Wind power (voltage support). Easy to get permission for underground cables.	2-level	IGBTs (series connected)
Eagle Pass, USA	2000	36MW ±36 MVAr	1	138 kV (both sides)	± 15.9 kV	Back-to-back HVDC Light station	Controlled asynchronous connection for trading. Voltage control. Power exchange.	3-level NPC	IGBTs (series connected)
Tjæreborg, Denmark	2000	8 MVA 7.2 MW -3 to +4 MVAr	1	10.5 kV (both sides)	± 9 kV	2 × 4.3 km Submarine	Wind power. Demonstration project. Normally synchronous AC grid with variable frequency control.	2-level	IGBTs (series connected)
Terrenora Interconnection (Directlink), Australia	2000	180 MW -165 to +90 MVAr	3	110 kV – Bungalora 132 kV – Mullumbimby	± 80 kV	6 × 59 km Underground cable	Energy trade. Asynchronous AC grid. Easy to get permission for underground cables.	2-level	IGBTs (series connected)
MurrayLink, Australia	2002	220 MW -150 to +140 MVAr	1	132 kV – Berri 220 kV – Red Cliffs	± 150 kV	2 × 180 km Underground cable	Controlled asynchronous connection for trading. Easy to get permission for underground cables.	3-level ANPC	IGBTs (series connected)
CrossSound, USA	2002	330 MW ±150 MVAr	1	345 kV – New-Heaven 138 kV – Shoreham	± 150 kV	2 × 40 km Submarine cables	Controlled synchronous connection for power exchange. Submarine cables.	3-level ANPC	IGBTs (series connected)
Troll A offshore, Norway	2005	84 MW -20 to +24 MVAr	2	132 kV – Kollsnes 56 kV - Troll	± 60 kV	4 × 70 km Submarine cables	Environment, CO_2 tax. Long submarine cable distance. Compactness of converter on platform electrification.	2-level	IGBTs (series connected)
Estlink, Estonia-Finland	2006	350 MW ±125 MVAr	1	330 kV – Estonia 400 kV – Finland	± 150 kV	2 × 31 km Underground 2 × 74 km Submarine	Length of land cable, sea crossing and non-synchronous AC systems.	2-level	IGBTs (series connected)
NORD E.ON 1, Germany	2009	400 MW	1	380 kV – Diele 170 kV – Borkum 2	± 150 kV	2 × 75 km Underground 2 × 128 km Submarine	Offshore wind farm to shore. Length of land and sea cables. Asynchronous system.	------	IGBTs (series connected)
Caprivi Link, Namibia	2009	300 MW	1	330 kV – Zambezi 400 kV – Gerus	350 kV	970 km Overhead lines	Synchronous AC grids. Long distance, weak networks	--------	IGBTs (series connected)
Valhall offshore, Norway	2009	78 MW	1	300 kV – Lista 11 kV – Valhall	150 kV	292 km Submarine coaxial cable	Reduce cost and improve operation efficiency of the field. Minimize emission of green house gases.	2-level	IGBTs (series connected)

Table 2.2.: VSC-HVDC projects around the world along with their characteristics *(Agelidis, Demetriades, & Flourentzou, 2006)*

The next table showcases the properties of both CSC and VSC-HVDC technologies and puts them in comparison to provide us with a better understanding of their utilities:

OHTL: Overhead Transmission Line

	CSC – HVDC		VSC - HVDC	
Power Transmission	OHTL	Cable	OHTL	Cable
Maximum Volt. level	800 kV	500kV	≤ 640 kV	≤ 640 kV
Maximum Power rating	<7500 MW		< 1600 MW	
Maximum Distance	Unlimited		Unlimited, expected voltage drop over line	
Convert Station Footprint	200 x 120 x 20m (600MW)		120 x 50 x 11 (550 MW)	
Real Power Control	Continuous, 10% min. load		Continuous, fast, no limit	
Reactive Power	50 – 60% of converter power rating		Fully Controllable	
Reactive Power Compensation	Reactive power banks, harmonic filters		Reactive Power provided or consumed by demand	
AC Voltage Control	Slow		Continuous, fast response	
Power Reversal	DC voltage reversal		DC voltage reversal	
Filter Equipment	High Demand		PWM-Low, Multilevel-None	
Grid Connection Requirements	Strong Network		Weak or even passive supply network	
Back start/island supply	Not available		Available	
Typical Power Loss in the two converters at full power	1.7%		1.2 – 1.4%	
Cost	Lower		Higher	

Table 2.3: Detailed comparison CSC & VSC technologies *(CIGRE, 2012)*

2.4. Harmonic Content

During the conversion of sinusoidal voltage into dc voltage in medium-voltage and high-power applications, harmonic components are injected to the grid due to the operation of the switching elements of the circuit. A harmonic is a voltage or current at a multiple of the fundamental frequency of the system, which is the harmonic with the lowest frequency. The production of harmonics is caused by nonlinear loads and their presence in a power system degrades the power quality and can lead to many different complications. Such harmonic problems can be transformer overheating and decreased power factor due to distorted voltage waveforms (Grady, 2006). They can also cause the defective operation of protective relays. In the most severe cases harmonics may induce apparatus dielectric failure due to circuit resonance, causing significant damage (Pyakuryal, 2013).

For the reasons mentioned above today's standards (IEEE standard 519-1992, Utility Limits) strongly dictate that the amount of harmonic distortion produced should not exceed a specified value. Specifically, any individual harmonics should be under 3% while at the same time total harmonic distortion (THD_v) must not go beyond 5%.

Total harmonic distortion is defined as the root mean square (RMS) voltage value of all the harmonic frequencies, except the first one, divided by the RMS voltage of the fundamental frequency, as shown in the following equation:

$$THD_V = 100\frac{\sqrt{\sum_{h\neq 1} V_{Sh,rms}^2}}{V_{S1,rms}}$$

$V_{Sh,rms}$: RMS voltage of the h-th harmonic
$V_{S1,rms}$: RMS voltage of the fundamental frequency

An appropriate method to meet the desirable harmonic content standards in high – power applications is the usage of multi – pulse rectifiers. These rectifiers consist of more than one 6-pulse rectifier in parallel connection, and are usually met in 12, 18 and 24-pulse configurations. Power is supplied to the rectifiers through transformers consisting of a number of secondary windings, with each secondary winding supplying one of the individual 6-pulse rectifiers. This type of rectifiers is capable of reducing the line harmonic distorting through phase-shifting transformers that block lower order harmonics generated by the 6-pulse rectifiers. Therefore, this ability makes the use of LC filters or power factor compensators unnecessary (Pyakuryal, 2013).

A twelve – Pulse Bridge has basically the same operation principals with a six – pulse bridge, for the reason that it consists by two six – pulse bridge circuits connected in parallel. A supply transformer is connected to both bridges creating a 30^o phase shift between them. This phase shift is a result of the two sets of secondary windings inside the transformer, the one in delta (Δ) and the other in star (Y) connection. Thanks to that, many of the characteristic harmonics of lower frequencies (5^{th} and 7^{th}), which are present in six – pulse bridge applications, are removed, thus making the twelve – pulse bridge suitable for high-power rectifiers (Grady, 2006).

Chapter 3: Power Flow Analysis

The next chapter is an introduction to the methods of power flow and optimal power flow analysis and their applications in the modern electric power grids. It focuses on the application of optimal power flow for AC-DC networks and ends with a brief presentation of Matpower Simulation tool.

3.1. Power Flow

Power flow analysis is used for the study of the behavior of an Electric Power System under specific load conditions in the steady-state sinusoidal operation. The quantities calculated using the load flow analysis are the voltages of each one of the network's buses and the power flows through a given number of power lines and transformers in order to cover the total system demand (Vovos & Γιαννακόπουλος, 2008).

Power flow analysis is a tool of great importance for determining the optimal state of operation of an electric power system. Although a system can cover its power demand through multiple ways of power distribution, it is critical to do it by choosing the most efficient and cost effective from all the possible alternatives and orchestrate the system's operation accordingly in order to achieve economic load dispatch.

Furthermore, the application of power flow analysis is necessary when future changes or extensions are planned for an existing electric power system. This is due to the importance of studying the effects of such changes on the system's operation, but also evaluating the performance and effectiveness of different solutions in order to choose the finest amongst them. Interventions of that kind can be the development of new production units, the supply of imminent load increase, the routing of new transmission lines across the network and also the interconnection of individual electric systems.

Another field in which the value of power flow analysis is important is the determination of a system's operation in cases where one or more power production units or transmission lines go out of service for a variety of reasons. It is essential for system operators to be able to calculate the effects in different load conditions within the systems and also obtain data for situations of transient stability, short-circuits and other disturbances.

For the successful development of a power flow computational program, two basic issues must be addressed: the mathematical description of the problem and the application of a numerical method for the solution of the resulting equations.

The first one can be dealt using Nodal analysis for the formulation of the mathematical model. The direct application of this method is not feasible as the system load is represented by complex powers while generators cannot be depicted as voltage sources, because their behavior is closer to that of power sources. The second matter can be resolved by using recursive techniques since an analytical solution can't be formulated due to the nonlinearity of the equations.

The resulting solutions must satisfy the two laws of Kirchhoff and the constraints:

- The limits of active/reactive power sources should not be exceeded
- The tap changer thresholds of the control transformers should also not be exceeded
- Transmission lines and transformers must not be overloaded
- The bus voltages should stay within the prescribed levels

Furthermore, the system should be able to satisfy all of the above constraints at maximum load conditions, as well as during events that cause sudden state changes. (Vovos & Γιαννακόπουλος, 2008)

3.1.1. AC Power Flow

The process of solving the standard Power Flow problem for both AC and DC requires solving a set of equations of the following structure:

$$g(x) = 0 \tag{3.1}$$

The above formula represents the functions that express a subset of the nodal power balance equations of the system, with unknown voltage quantities (Zimmerman & Murillo-Sánchez, 2019).

Specifically, for the solution of the AC Power Flow problem, a reference bus is needed to with the purposes of being a real power slack and provide a voltage angle reference. By convention, we chose one generator bus to serve as a reference bus. Whereas the voltage angle's value is known, the real power generation at this particular bus remains unknown to avoid overspecification of the problem. For the rest of the system's buses, their generator real power injection (Pg) and also the voltage magnitude (Vg) are predefined, and usually operate as PV buses. Buses that don't generate power, and instead operate as consumers (loads) represent the power demand inside the system and are given the classification PQ. Their injections of real (Pd) and reactive power (Qd) are also specified.

For the solution of the problem, real and reactive power parameters are taken into consideration. Therefore, the power balance equation that expresses the bus voltages and generator injections in complex matrix form, is split into two new functions, one regarding its real, and the other the respective reactive components:

$$g_S(V_m, S_g) = S_{bus}(V) + S_d - C_g S_g = 0 \Rightarrow \tag{3.2}$$

$$g_P(\Theta, V_m, P_g) = P_{bus}(\Theta, V_m) + P_d - C_g P_g = 0 \tag{3.3}$$

$$g_Q(\Theta, V_m, Q_g) = Q_{bus}(\Theta, V_m) + Q_d - C_g Q_g = 0 \tag{3.4}$$

The above functions include the values of the voltage angles Θ, the corresponding voltage magnitudes V_m and generator injections Pg, Qg. C_g is a $n_b \times n_g$ matrix of the generator connections. If an element (i, j) is 1, this indicates that generator j is located at the $i-th$ bus. In a different case it is set to 0.

For the formation of the g(x) function, we take the left side of the previous power balance equations 2, 3 for the PV and PQ buses respectively, along with the loads, generator injections, voltage magnitudes, and the reference angle:

$$g(x) = \begin{bmatrix} g_P^{\{i\}}(\Theta, V_m, P_g) \\ g_Q^{\{j\}}(\Theta, V_m, Q_g) \end{bmatrix} \begin{matrix} \forall i \in I_{PV} \cup I_{PQ} \\ \forall j \in I_{PQ} \end{matrix} \quad (3.5)$$

The unknown voltage values, voltage angles of non-reference buses, as well as the voltage magnitudes at PQ buses are included in the following vector:

$$x = \begin{bmatrix} \theta_{\{i\}} \\ u_m^{\{j\}} \end{bmatrix} \begin{matrix} \forall i \notin I_{ref} \\ \forall j \in I_{PQ} \end{matrix} \quad (3.6)$$

A system of nonlinear equations is formed, with $n_{pu} + 2n_{pq}$ equations and unknowns in total. The term n_{pu} expresses the number of PV buses, and n_{pq} the number of buses classified as PQ. The real power balance equation that remains after solving x can be then used for the computation of the slack bus's real power injection. The reactive power balance equations left $(n_{pu} + 1)$ give us the corresponding reactive power injections.

3.2. Optimal Power Flow

One of the most important optimization problems for the operation of power systems is the optimal power flow (OPF) problem. It's an extension of the power flow analysis and its aim is the optimal scheduling and distribution of an electric system's power production and demand, in a way that satisfies certain constraints based on the system's capabilities. The main goal is to solve the problem of economic dispatch of the system's generation units in a way that minimizes their operating cost, and consequently that of the whole system (Zimmerman & Murillo-Sánchez, 2019).

The optimal power flow can be seen as a minimization problem that takes the following form:

$$\min_x f(X) \quad (3.7)$$

$$s.t.\, g(X) = 0 \quad (3.8)$$

$$h(X) \leq 0 \quad (3.9)$$

$$x_{min} \leq x \leq x_{max} \quad (3.10)$$

In the above formula, $f(x)$ is the objective minimization function that consists of the polynomial cost of generator injections. It attempts to estimate vector X, which contains several control variables. The equality constraints are the power balance equations and are given inside $g(x)$. The inequality constraints $h(x)$ include the branch flow limits, whereas the bounds x_{min} and x_{max} indicate the generator injections, reference bus angles and voltage magnitudes (AC), that the solution should satisfy.

3.2.1. AC Optimal Power Flow

For the standard AC OPF, the optimization vector x includes the n_b x 1 vectors of voltage angles Θ and the respective magnitudes V_m, the n_g x 1 vectors containing the real and reactive power injection P_g and Q_g of the generators, thus:

$$x = \begin{bmatrix} \Theta \\ V_m \\ P_g \\ Q_g \end{bmatrix} \tag{3.11}$$

The objective minimization function f(x) derives from the sum of all the polynomial cost functions of the respective real and reactive power injections (Zimmerman & Murillo-Sánchez, 2019), f_P^i and f_Q^i, for all generators (n_g), and is formulated below:

$$f(P_g, Q_g) = \sum_{i=1}^{n_g} f_P^i(p_g^i) + f_Q^i(q_g^i) \tag{3.12}$$

As equality constraints we take the $2n_b$ nonlinear real and reactive power balance equations (3.3) and (3.4). For the inequality constraints, we use the branch flow limits of the total n_l branches. Each branch has a set of two branch flow limits, one regarding the $from$ end, while the other is about the to end. These limits are expressed as nonlinear functions of the bus magnitudes and voltage angles:

$$h_f(\Theta, V_m) = \left|F_f(\Theta, V_m)\right| - F_{max} \leq 0 \tag{3.13}$$

$$h_t(\Theta, V_m) = \left|F_t(\Theta, V_m)\right| - F_{max} \leq 0 \tag{3.14}$$

The vector F_{max} contains the flow limits and has the proper units, depending on the type of constraint.

Although power flows are usually expressed as apparent power flows in MVA, there are two more forms that the flow constraints can be expressed:

$$F_f = \begin{cases} S_f(\Theta, V_m), & apparent\ power \\ P_f(\Theta, V_m), & real\ power \\ I_f(\Theta, V_m), & current \end{cases} \tag{3.15}$$

The magnitudes of S_f, P_f and I_f are defined by the equations:

$$I_f = Y_f V \tag{3.16}$$

I_f: $n_l \times 1$ vector of the branch currents at the $from$ ends of the branches
Y_f: $n_l \times n_b$ system branch admittance matrix of the $from$ end buses
V: corresponding n_l bus voltages

The current injection can be used to formulate the equations of the complex power injections at the $from$ end, as functions of the complex bus voltages:

$$S_f(V) = \left[C_f V\right] I_f^* = \left[C_f V\right] Y_f^* V^* \tag{3.17}$$

The real power injection at the $from$ end of each branch is equal to the real part of the apparent power injection, therefore:

$$P_f = R\{S_f\} \tag{3.18}$$

It can also be calculated by the following equation:

$$P_f(\Theta) = B_f\Theta + P_{f,shift} \tag{3.19}$$

P_f: $n_l \times 1$ vector of the branch flow at the $from$ end of each branch
Θ: bus voltage angles
$P_{f,shift}$: n_l vector whose $i-th$ element is equal to $-\theta_{shift}^i b_i$

$$P_{shift}^i = \theta_{shift}^i b_i \begin{bmatrix} -1 \\ 1 \end{bmatrix} \tag{3.20}$$

Where b_i is defined as series reactance x_s^i and tap ratio τ^i for each $i-th$ branch as:

$$b_i = \frac{1}{x_s^i \tau^i} \tag{3.21}$$

B_f: branch shunt susceptance at the $from$ end bus

$$B_f = [B_{ff}\ (C_f - C_t)] \tag{3.22}$$

3.3. Matpower Description

Matpower's main feature is the solution of power flow and optimal power flow problems. Its highly extensible OPF architecture that offers simple and yet sophisticated control over system parameters and constraints makes it ideal for the purposes of this thesis. Its functionality includes the solution of steady – state power system simulation and optimization problems, some of them are mentioned below (MATPOWER, n.d.):

- Power Flow (PF)
- Continuation power flow (CPF)
- Extensible optimal power flow (OPF)
- Unit commitment (UC)
- Stochastic, secure multi-interval OPF/UC

In order to proceed to the desired implementation, it is necessary that each time the appropriate input data needed for sufficiently defining all the relevant power system parameters have been prepared. Additionally, an objective function should be defined to run the specific simulation. After a successful run of the simulation, the output data are displayed on the screen and can also be saved in data structure files where the user can access them.

Matpower also provides a considerable number of test electric system models and also already implemented files for the execution of several functions on the existing models. These examples contain the typical system case structured layouts where the data needed

for the description and simulation of a system are stored. The user can access those data in m - files, modify or delete elements and then observe and draw conclusion about the behaviour of a system as it changes to adapt to the given circumstances. Modifications can be made to a given system by adding or removing buses, relax or constrict magnitude constrains or even change the fundamental characteristics of the system, such as bus/generator voltages, real or reactive power etc. (Zimmerman, Murillo-Sánchez, & Thomas, MATPOWER: Steady-State Operations, Planning, and Analysis Tools for Power Systems Research and Education, 2011).

3.3.1. Data Formats

Matpower uses MATLAB M-files or MAT-files that each one defines and returns a MATLAB struct in plain text format, which can be edited by any standard text editor. Every struct contains the description of a system model in struct fields, while each field holds data for a specific aspect of the system's operation in columns. The basic fields of the struct are **baseMVA**, **bus**, **branch**, **gen** and **gencost**, with the last one being optional. All together form a typical MATPOWER case which can be loaded into variables that give us access to the contents of any struct field. Below follows the presentation of the basic struct fields along with lists of their attributes. (Zimmerman & Murillo-Sánchez, 2019)

The **baseMVA** field is a scalar that holds the used power base through which the system's quantities are expressed as per-unit.

The **bus** field is type of matrix (as the rest of the fields) and contains the unique system's bus ids in ascending order along with other necessary information about each bus's properties.

Bus Data		
Name	**Column**	**Description**
Bus_ID	1	bus number (positive integer)
Type	2	bus type (1 = PQ, 2 = PV, 3 = ref, 4 = isolated)
Pd	3	real power demand (MW)
Qd	4	reactive power demand (MVAr)
Gs	5	shunt conductance (MW demanded at V = 1.0 p.u.)
Bs	6	shunt susceptance (MVAr injected at V = 1.0 p.u.)
Area	7	area number (positive integer)
Vm	8	voltage magnitude (p.u.)
Va	9	voltage angle (degrees)
Base_KV	10	base voltage (kV)
Zone	11	loss zone (positive integer)
Vmax	12	maximum voltage magnitude (p.u.)
Vmin	13	minimum voltage magnitude (p.u.)

Table 3.1: Bus Data structure field.

The next field contains the data needed for branch description and also the power exchanges between system's buses.

Branch Data		
Name	**Column**	**Description**
Fbus	1	"from" bus number
Tbus	2	"to" bus number
R	3	resistance (p.u.)
x	4	reactance (p.u.)
b	5	total line charging susceptance (p.u.)
rateA	6	MVA rating A (long term rating), set to 0 for unlimited
rateB	7	MVA rating B (short term rating), set to 0 for unlimited
rateC	8	MVA rating C (emergency rating), set to 0 for unlimited
Ratio	9	transformer off nominal turns ratio
Angle	10	transformer phase shift angle
status	11	initial branch status, 1 = in-service, 0 = out-of-service
argmin	12	minimum angle difference, (degrees)
argmax	13	maximum angle difference, (degrees)

Table 3.2: Branch Data structure field.

The data regarding the definition of a system's generators are kept in the **gen** field. Its columns include information about the operation and output of each generator inside the system:

Generator Data		
Name	**Column**	**Description**
Gen_bus	1	bus number
Pg	2	real power output (MW)
Qg	3	reactive power output (MVAr)
Qmax	4	maximum reactive power output (MVAr)
Qmin	5	minimum reactive power output (MVAr)
Vg	6	voltage magnitude setpoint (p.u.)
mBase	7	total MVA base of machine, defaults to baseMVA
Status	8	machine status (> 0 = in-service, <= 0 out-of-service)
Pmax	9	maximum real power output (MW)
Pmin	10	minimum real power output (MW)
Pc1	11	lower real power output of PQ capability curve (MW)
Pc2	12	upper real power output of PQ capability curve (MW)
Qc1min	13	minimum reactive power output at PC1 (MVAr)
Qc1max	14	maximum reactive power output at PC1 (MVAr)
Qc2min	15	minimum reactive power output at PC2 (MVAr)
Qc2max	16	maximum reactive power output at PC2 (MVAr)
Ramp_agc	17	ramp rate for load following/AGC (MW/min)
Ramp_10	18	ramp rate for 10-minute reserves (MW)
Ramp_30	19	ramp rate for 30-minute reserves (MW)
Ramp_q	20	ramp rate for reactive power (2 sec timescale) (MVAr/min)

Table 3.3: Generator Data structure field.

The field **gencost** is an optional struct field where the data related to the operation cost of each generator are being stored:

Generator Cost Data		
Name	**Column**	**Description**
Model	1	cost model, 1 = piecewise linear, 2 = polynomial
Startup	2	startup cost in US dollars
Shutdown	3	shutdown cost in US dollars
Ncost	4	number N = n + 1 of data points defining an n-segment piecewise linear cost function, or of coefficients defining an n-th order polynomial cost function
Cost	5	parameters dening total cost function f(p) begin in this column, units of f and p are $/hr and MW (or MVAr),

Table 3.4: Generator Cost Data structure field.

3.3.2. Solving a Matpower Case

Before executing a simulation for a given system, we must first use the "loadcase" command in order to load the system's data into a Matlab structure that will include the elements from all the fields mentioned above. This command lets us store a system's characteristics into a typical struct variable and thus gain access to them the way we would with a normal structure's fields. This gives us the option to manipulate these data as we see fit and run the desired simulations.

>> mpc = loadcase(casefilename)

The mpc variable is the structure where all system data will be loaded inside proper fields and from there used to run simulations. Necessarily, the loadcase command's single attribute is the name of the .m case file that contains those data in text format.

Now that our case is properly set up for further processing, we are ready to solve it using one of Matpower's available simulation commands. For the purposes of this thesis, it was required the solution of optimal power flow problems for several individual systems was required, thus the command "runopf" was used extensively.

>>[RESULTS, SUCCESS] = runopf(CASEDATA, MPOPT, FNAME, SOLVEDCASE)

After the execution of an optimal power flow (AC OPF by default), the command optionally returns a RESULTS struct and a SUCCESS flag. The RESULTS struct contains all the fields that also exist inside the MATPOWER case given as input, that is bus, branch, gen, etc. but with solved voltages, power flows etc. The SUCCESS flag is returned as a second output argument and indicates whether the solution was successful (success = 1) or not (success = 0). The command also includes four input arguments. The first argument corresponds to a MATPOWER case struct or a string containing the name of the file with the case data (in this example, the variable "mpc"). MPOPT is a MATPOWER options struct to override default options. It can be used to specify the solution algorithm, output options, termination tolerances, and more. The FNAME argument lets us specify the name of the file to which the pretty-printed (solved) output will be stored. Finally, SOLVEDCASE corresponds to the name of the file to which the solved case will be saved as a MATPOWER case format (Zimmerman & Murillo-Sánchez, 2019).

Chapter 4: Proposed Optimal Power Flow Method for Electric Power Systems with HVDC Interconnections

The next chapter discusses the approach followed in the development of the main subject of this work, which is the optimization of large electric power systems with interconnections of HVDC technology. Here we address the topic of linear interpolation and its utilization for the implementation of the optimization algorithm. Then we present the fundamental components used for the modeling of our implementation. The chapter ends with the presentation of the algorithm and the thorough description of its functionality.

4.1 Problem Statement

In the following lines we present the main target of this thesis that deals with the determination of the optimal point of operation of a large electric system composed by multiple individual AC electric systems interconnected with HVDC technology. This can be reached by redistributing the power production between the cooperating systems in a way that minimizes the total system cost while sufficiently covering each one's power demands.

In a large electrical grid, each subsystem can be considered as an autonomous electrical grid that maintains its own power production units to cover its local power demand. In our case, the sub-systems are interconnected via dedicated long-distance DC transmission lines which allow them exchange power. Multiple subsystems interconnected by multiple transmission lines establish a complex network with enhanced stability, capacity, and the ability to achieve a more economical global state of operation. This is because cheaper electric systems are capable of providing power to others by increasing their power production. A relatively cheap electric system will increase its power output by a permissible amount and supply others with energy, while consequently increasing its operating cost. On the other hand, it is advantageous for an expensive system to accept the amount of power coming from a relatively cheaper by lowering its power production by the same amount, and consequently reducing its cost. Therefore, in an ideal scenario, a zero-sum game takes place between the power exchanging nodes which will eventually lead to the alteration of the existing power flows and the power distribution throughout the large power system in general. The power production required for the operation of the whole system will be dispatched to the subsystems with the less costly production units, thus minimizing the total cost.

For the purposes of this thesis, we assume that the subsystems do not possess any information about the operating status and cost of the ones they are interconnected with. For this reason, the optimal point of operation of the total large system can be reached by iteratively generating power offers for exchange between the subsystems. Each system can make offers to increase or decrease its production, and thus to inject or absorb power respectively. Each set of valid offers are equivalent to power transactions through the DC

interconnections that, when committed, will bring the total system one step closer to the global system optimal operation point.

This whole process is orchestrated by the integrated power system manager, the role of whom will be carried out by our algorithm. The system manager has access to each subsystem's data and also the authority to evaluate and approve the power offers taking place. As we previously mentioned the amount of the exchanged power gradually increases by each iteration. For an offer to be valid, the system's manager makes sure that as the offers increase in magnitude, the systems involved satisfy all the constraints of power flow analysis. The changes must also contribute to the minimization of the total system cost before the transaction can be executed. After a number of iterations, we reach a marginal point where no more transactions can be approved due to optimal power flow constraint violation, or because the optimization has reached a minimum. This state can be considered as the optimal point of operation of the whole system.

4.2. Linear Interpolation

The method of linear interpolation is the least complex of all existing interpolation techniques in terms of computing requirements and performs reasonably well in a variety of problems, even in cases where the latter are rather challenging.

Interpolation is mainly used in practical situations where a quantity y is uniquely determined by the value of another quantity x, but we are unable to figure out the specific form of dependence between them, that is the function that correlates the two quantities $y = f(x)$. This dependence can be calculating by measuring the values of x and y in different situations. Therefore, by measuring a number of y values that correspond to different values of x we can calculate a number of the y_i = f(xi) values of the unknown $f(x)$ function, and by generalizing these results, we are able determine the value of $f(x)$ for all other values of x. Interpolation is the prediction we make in the case in which x is located between the smallest and the largest of the x_i values.

Being the most widespread interpolation technique, linear interpolation is used as an effective approach for non-linear problems, by basically making the assumption that $f(x)$ is linear on the interval $[x_1, x_2]$. From the previous assumption derives the following formula of linear interpolation:

$$f(x) = \frac{x-x_1}{x-x_2} \cdot f(x_2) + \frac{x_2-x}{x_2-x_1} \cdot f(x_1) \qquad (4.1)$$

The advantage of such a method comes from the fact that the computation of linear functions requires the least intensive calculations. The simplicity and elegance of this approach made it appealing for our optimization problem (Pownuk & Kreinovich, 2017).

4.3. DC Transmission Lines

The solution of the optimization problem to minimize the total cost of a large electric power system relies on the presence of DC interconnections and their bulk power-transmitting properties. To successfully simulate the DC transmission lines interconnecting different subsystems in Matpower, it is necessary to use a reliable model that sufficiently embeds their properties.

4.3.1. Active Power Modeling

In a schematic representation of an electric power grid, a DC transmission line is attached to the buses belonging to the subsystems it interconnects. Depending on the current operation state of both systems, one of them will increase its power production by a specific number of megawatts to supply the other, whereas the last one will accept the incoming power and be able to drop its power production by the same amount. Power flows between the two AC systems through the respective system buses via the mediated DC interconnection, and is injected to the corresponding electric grid, thus contributing to meet its power demand.

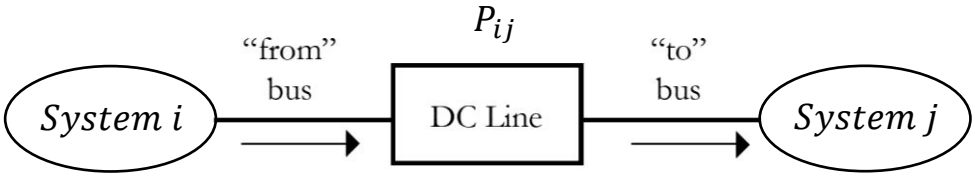

Figure 4.1: DC Interconnection basic layout

The DC line through which the power exchange between two systems happens can by modeled in Matpower as a set of two 'dummy' loads attached to the proper system buses, as shown in figures 1 and 2. One load has positive capacity, drawing active power from the system it is attached to, at the 'from' end of the line. This represents the power production surplus that will travel through the interconnection. The other load is attached at the 'to' end of the DC line and has a negative capacity, thus simulating the behavior of a generator, injecting the respective amount of power to the system at the other end of the interconnection.

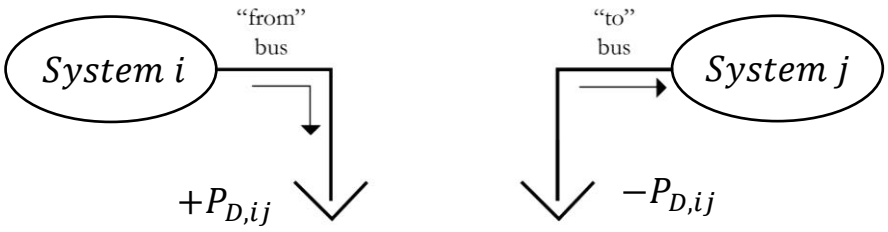

Figure 4.2: Equivalent modeling of the DC interconnection with dummy loads

After successfully establishing a DC interconnection, we can simulate the power exchanges that will take place between the interconnected systems during the execution of the optimization algorithm. An offer of power production increase is equivalent to a temporary active power increase of the relevant 'from' bus production by a fixed number

of megawatts, and can be simulated by attaching a positive 'dummy' load. The opposite applies in the case of the 'to' bus, where the power production decrease is represented by the subtraction of an equal amount of power. Basically, we treat the DC interconnection as a set of 'dummy' loads that drain active power from one system and provide it to another by decreasing the last's power production. These sets of loads of opposite capacity constitute a trustworthy tool for integrating and simulating the DC transmission lines and the power exchanges between the participating systems.

4.3.2. Reactive Power Modeling

An issue that arises is the modeling of the reactive power of the converters placed at the ends of the DC lines that goes along with the active power traveling through the them. Whereas the 'dummy' loads we use do a decent job in simulating the active power transactions between interconnected systems, they are not able to model the reactive power consumed by the converters on each end of the DC transmission line.

To model these properties in Matpower, we considered to additionally attach 'dummy' generators on the buses that will operate as converter stations, located on both ends of each interconnection. The role of these generators will be to supply/absorb the proper amount of reactive power, depending on the 'dummy' loads applied on the respective buses that simulate the interconnection's power transactions. To avoid any intervention with the current power production of the systems, we need to set the 'dummy' generators active power production to zero. At the same time, we set the maximum amount of reactive power equal to 60% of the maximum permissible real power rating of the respective DC line's transformer:

$$P_{Q,max} = P_{G,max} \cdot 0.6$$

$$P_{Q,min} = -P_{G,max} \cdot 0.6$$

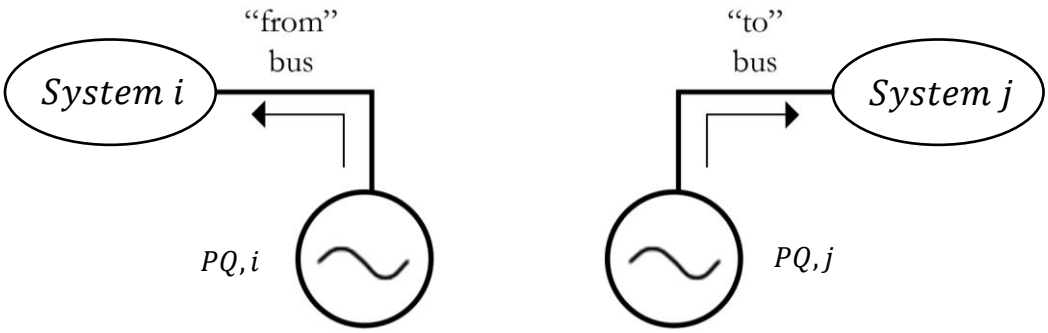

Figure 4.3: Dummy generators for reactive power compensations of the DC interconnected buses

Due to the reason that the properties and characteristics of the components described above fully comply with the principles governing the operation of HVDC networks, it is safe to assume that their use makes it feasible to properly model the DC transmission lines using Matpower. Therefore, we can proceed with confidence to the implementation of the optimization algorithm.

4.4. Optimization Algorithm

The main task of our algorithm is the simulation and handling of multiple power transactions with the purpose of reaching the optimal state of operation, by taking advantage of HVDC technology's properties. However, the minimization of a large system's total operating cost in a network consisting by individual sub-systems is a process that requires external action. This process is performed by the general system manager, whose role is modelled by our objective function and the constraints of the global interconnected power system. For the purposes of this thesis, the design of the optimization function is based on the principals of linear interpolation.

4.4.1 Algorithm Description

We already know that the operating cost of an electric system is shaped to a large extent by its power production cost. However, the relation between power production and operation cost is nonlinear. This limits our ability to formulate a function that describes the generator's production curve, and generally to predict the operating cost of an electric system in different states. For this reason, linear interpolation can be used in order to calculate the system's cost in a small operating range. Linear interpolation helps us approach the nonlinear function that describes the cost of a system under different load conditions by treating it as a simple linear function.

Our goal here is to reach the optimal point of operation of a large electric power system, that is, the operation state where it meets its total power demand with the minimum possible cost. To achieve this, each individual sub-system will make offers, to increase or decrease its power production accordingly. Every power production exchange is a new state of operation where a subsystem has a different operating cost. The linear interpolation technique suggests that in order to determine the value of the function f(x), we have to assume that the function is linear within a specific interval [x1, x2]. In our case, the value of the function f(x) corresponds to the operating cost of a specified subsystem, calculated for a given amount of power production (x) in megawatts. This interval is determined by the set of offers made by that particular subsystem, to increase its production by ΔP_+ megawattsor to reduce it by the opposite amount.

4.4.2. Power Offer Distribution

The implementation of the algorithm requires first to calculate each subsystem's cost for its current production. Given that a system i produces Pi megawatts of power, its operating cost is determined by the value of the function F(Pi) and can be calculated through optimal power flow. After that, it is necessary to simulate the power offers that each system is going to make. As mentioned earlier, all subsystems will make a set of offers at each round of the negotiations. First, an offer ΔP_+ to increase their power power production, and a respective offer ΔP_- to decrease it. In our implementation, we demonstrate two possible ways that these offers can be fairly distributed for every subsystem:

Method 1:

In order to express a system's offer to alternate its local power production by ΔP megawatts, we can attempt to attach this amount as 'dummy' loads by splitting it equally between all the system's buses. More specifically, for each n-th bus of a system i, with N buses in total, during the k-th iteration, the new dummy loads are:

$$dummy\ load\ n(k+1) = dummy\ load\ n(k) + \frac{\Delta P}{N} \qquad (4.2)$$

For example, if a system offers 10MW and consists of ten buses in total, each bus should increase its current production by 1MW. This ensures that the increase in power will be uniformly distributed and reduces the likelihood of overloading particular buses.

Method 2:

Another way to distribute the power offers in a system is to apply the offers only to the buses that are participating in a DC interconnection. This is a more realistic approach, considering that the power exchange in real world HVDC systems happens between the systems(buses) of the interconnected converter stations. The offer is divided between the DC buses of each subsystem proportionally, according to their current respective 'dummy' loads, that have already been applied to them. Therefore, for a system i with j DC buses, and current 'dummy' loads L_j, the new 'dummy' loads that will be applied to each bus at k-th iteration, in addition to the previous ones, are:

$$dummy\ load\ j(k+1) = dummy\ load\ j(k) + \Delta P \cdot \frac{L_j}{sum(L_1 + \cdots + L_j)} \qquad (4.3)$$

This technique ensures that additional power is assigned to the DC buses contributing more megawatts to the interconnections they are involved in.

After the proper distribution of the offers for every subsystem, we are able to determine the operating cost of the particular system $F(Pi + \Delta P_+)$ through optimal power flow analysis. The same procedure is followed to simulate offers of power production decrease, although this time we do it by attaching negative 'dummy' loads, allowing us to determine the operating cost $F(Pi + \Delta P\_)$

4.5. Objective Function

In order to apply linear interpolation to our problem, we should subtract the two costs and then divide the result by the absolute value/measure of the difference of the opposite offers, i.e. the interval in which we assume the linearity of the cost function. The resulting value is then multiplied by the sum of the power flowing though all interconnections belonging to the particular system we examine. Finally, the result of the multiplication will be added to the current system cost.

$$\min \quad \sum_i \left\{ F_i(P_i) + \frac{F_i(P_i + \Delta P_{i+}) - F_i(P_i + \Delta P_{i-})}{\Delta P_{i+} - \Delta P_{i-}} \cdot \sum_j P_{ij} \right\} \qquad (5.4)$$

The power of each of the interconnections (P_{ij}) will be decided by our objective function in a way that the total operating cost of the system will be minimized. This process is executed for each $i-th$ subsystem that consists our large electrical network. If a subsystem i has j interconnections attached to it, the objective function calculates the power P_{ij} that will travel through each one of them, with the purpose of minimizing the rest of the formula. When summed together, these costs should provide us with the overall minimum cost we can possibly achieve based on the offers ΔP made by the systems. The resulting values of the vector P_{ij} indicate the power that will travel through each DC interconnection and will be applied as 'dummy' loads on the proper buses of the respective systems.

This process is executed iteratively, and for every iteration, additional offers are made. After the last transaction was committed successfully and the calculated values of P_{ij} were attached to the proper interconnected buses, the newly modified systems will be given as input for the execution of the next iteration. At this time, their current operating costs $F(P_i)$ have changed due to the new power flows on the interconnections, and should be calculated again through optimal power flow analysis. The same set of power offers is applied for the calculation of the respective costs, $F(P + \Delta P_+)$ and $F(P + \Delta P_-)$. The data are again fed into our objective function, giving us a vector containing new 'dummy' loads. These will again slightly improve the total system operating cost after applying them in addition to the preceding ones. By performing this process iteratively, the results are gradually leading the overall system to more economical operating states. Consequently, the iterative sum of the values of the P_{ij} vector, which correspond to each $j-th$ interconnection, gives us the optimal power of the respective interconnection. Therefore, by applying the final results of the algorithm as 'dummy' loads on the proper buses, we get the individual system cases that together form a large system which operates optimally because of the calculated DC interconnections.

		Objective Min. Function Results (P_{ij})			
	F(Pi,iter)	**Conn. 1**	**Conn. 2**	**…**	**Conn. j**
Iter. 1	F(Pi,1)	$P_{D1,1}$	$P_{D2,1}$		$P_{Dj,1}$
Iter. 2	F(Pi,2)	$P_{D2,1}$	$P_{D2,2}$		$P_{Dj,2}$
…	…	…			
Iter. n	F(Pi,n)	$P_{D1,n}$	$P_{D2,n}$		$P_{Dj,n}$
Optimal Connections		sum($P_{D1,1}$: $P_{D1,n}$)	sum($P_{D2,1}$: $P_{D2,n}$)		sum($P_{Dj,1}$: $P_{Dj,n}$)

Table 4.1: Final DC interconnections forming by iteratively stacking up 'dummy' loads

The above table shows the gradual formation process of the 'dummy' loads for each $i-th$ system. A set of new interconnection values is produced at every $n-th$ iteration step, which stack up during the execution. After attaching the 'dummy' loads, the systems are introduced to a new production state F(Pi,n), where the next optimization step will be based on. The sum of the 'dummy' loads for a particular interconnection gives us its final value.

4.5.1 Constraints

The implementation of the objective function must be accompanied by proper constraints which will ensure the applicability of its results. It is important to point out that in order for the output values to be valid every time the objective minimization function is evaluated, their sum inside the vector P_{ij} must be within the interval $[\Delta P_+, \Delta P_-]$, specified by the offers made at the current optimization step. The purpose of this approach define that the solution should come from the interval where we assume the linearity of the function we attempt to minimize. On a more practical level, it is sensible that the power of the interconnections should not exceed the maximum offers the $i-th$ system is willing to make. The constraints we described are formulated below:

$$\Delta P_{i-} \leq \sum_j P_{ij} \leq \Delta P_{i+} \tag{5.5}$$

It is also vital that we should keep an eye on the final results, which must not exceed the maximum power rating of the DC interconnections. Therefore, the algorithm should perform checking for the accepted 'dummy' loads, attached on the respective DC buses during the progression of the algorithm, and make sure that their sum until this point meets the following criterion:

$$\left| \sum_j P_{ij,accepted} \right| \leq P_{ij,max} \tag{5.6}$$

In the last case, the algorithm ignores the solution that violated the particular constraint and keeps the last successfully optimized cases. That is, before the error occurred.

For an offer to be valid, the system manager should make sure that the systems involved satisfy all the constraints of power flow analysis too. After a number of iterations, we may reach a point where no more transactions can be approved due to optimal power flow constraint violation or potential cost increase. Specifically, it is possible that changing a systems production output by attaching 'dummy' loads, may result to exceeding the system's generation capabilities or bus voltage limits. This will lead to an error during the execution of the 'runopf()' function. The 'dummy' loads must also contribute to the minimization of the total system cost before a transaction can be committed. Thus, the algorithm should ignore results that lead to increased total cost. Moreover, it should terminate if it detects a considerable increase in the resulting total operating cost, in case it exceeds a certain boundary.

In any of these situations, the algorithm stores the results that gave us the minimum cost during a certain point of the execution and that at the same time satisfy all the constraints we described above. When the proper conditions are met, the system manager approves and commits the transactions by making the final 'dummy' loads permanent, which are practically the optimal DC interconnections of our large electric power system.

4.5.2. Objective Function Implementation

The implementation of the optimization algorithm which will iteratively minimize the system's total operating cost was accomplished by the utilization of the fmincon, a nonlinear programming solver function of Matlab.

The general purpose of this function is to determine the values of a nonlinear multivariable function by trying to satisfy multiple constraints at the same time, in a way that will minimize its output. Below follows the mathematical description of fmincon:

$$\min_{x} f(x) \; such \; that \begin{cases} c(x) \leq 0 \\ ceq(x) = 0 \\ A \cdot x \leq b \\ Aeq \cdot x = beq \\ lb \leq x \leq ub \end{cases} \tag{5.7}$$

Practically, the job of the function is to evaluate the variable(s) x that will give us the minimum value of the total objective function $f(x)$. To achieve that, fmincon takes into consideration a number of different equality and inequality constraints. A and b are matrices or vectors used in inequality constraints, whereas Aeq and beq in equality constraints, regarding the variable x. Additionally, $c(x)$ is a nonlinear constraint and $ceq(x)$ serves as a linear constraint. The variables lb and ub consist the lower and upper bounds of x. (and determine the interval of its possible values). They too can be passed as vectors or matrices. Variable x itself can also be handled as a vector or matrix, though the respective constraints should be customized accordingly.

There are many ways in which fmincon can be implemented in Matlab. For the needs of our problem, we will take advantage of fmincon's ability to determine a solution by solely relying on the nonlinear inequalities $c(x)$. These constraints are about the calculation of the desired solutions. The output values in every iteration must be determined in a way that their sum does not exceed or fall beyond the amount of power offered by a subsystem at that particular iteration.

The general implementation of fmincon in Matlab is described below:

x = fmincon(fun,x0,A,b,Aeq,beq,lb,ub,nonlcon)

The first argument (fun) is used for passing the function we want fmincon to minimize, whereas the second (x0) is a matrix/vector used for initializing the values from which fmincon will start the minimization attempt. The argument nonlcon is a function that accepts a vector x and returns two arrays, $c(x)$ and $ceq(x)$, which are the nonlinear constraints the function should always satisfy. The size of all the mentioned arrays should be equal to the total number of subsystems participating in the power exchange game. Fmincon allows us to ignore the other types of constraints that are not necessary for the algorithm's implementation.

Therefore, our algorithm passes the objective function into fmincon, each time using the proper operating costs, which are calculated based on the offers made at the particular iteration. At the same time, it keeps the respective offer constraints updated during the execution, ensuring that the results come from the permissible range of values.

4.6. Simulation Model Characteristics

As previously mentioned, an interconnection is modeled by a set of equal and opposite 'dummy' loads. Thus, to simulate the resulting j interconnections, a set of $2j$ 'dummy' loads need to be applied in a way that will indicate the true direction of the power flowing between the systems. The default direction of the power flow is determined by the order in which the user defines the data involved in an interconnection. The input data are declared inside a .txt file where the user provides necessary information for the definition of the DC interconnections in Matpower ("from'/ 'to' system/bus, r, x, b, rateA etc.). Therefore, if a value of the resulting vector Pij is positive, it means that the power flow is identical to the one originally declared by the user for the corresponding $j-th$ interconnection. In a different case, a negative value means that power flows in the opposite direction from the one declared. The respective 'from' bus becomes a 'to' bus and therefore a negative 'dummy' load should be applied.

The systems are uninformed about the operating status of their nearby subsystems and thus power offers should increase iteratively in order to gradually reach the optimal state of operation. The initial offers ΔP are predetermined and are common for all the systems participating in the optimization process. It makes sense to initialize the starting offers by assigning them a relatively considerable number of megawatts, considering that we have to do with large systems. Hence, values between 10 and 100 MW, depending on the capacity of the systems, seem reasonable. At every iteration, this amount is applied to the Matpower cases carrying the results (Pij) of the previous optimization step. It is possible that at some point the increasing 'dummy' loads attached on the DC buses will lead to optimal power flow failure due to constraint violations at least one of the system cases. For this reason, the offers should be able to adapt dynamically, and therefore decrease by an amount of dp megawatts. In the event of failure, the changes made to the systems by the latest offers should be reverted and the optimization step will have to be repeated, this time with slightly lower offers than the previous. Given that the initial set of offers have values ΔP_+ and $\Delta P\_$ megawatts, the new, decreased offers are:

$$\Delta P_+^{new} = \Delta P_+ - dp$$
$$\Delta P\_^{new} = \Delta P\_ + dp$$

The algorithm will try again to perform the optimal power flow function for the new offers. This process is repeated until we find again a valid set of offers that may allow the runopf() function to run successfully for all subsystems. Then we can safely proceed to the next optimization step and the evaluation of the objective function.

As the iterations succeed, sooner or later every set of offers will eventually lead the runopf() function into failure for any of the system cases, thus forcing the offers to further decrease. It is evident that as the algorithm progresses, the two offers will gradually converge around zero. Consequently, the decision variables will also decrease and converge in the same way, due to their direct correlation with the power offers made. The iteration at which the algorithm reaches this point of convergence is practically the one our system reaches the optimal state of operation. Before terminating the process, the results of the optimization

process are applied on the original system cases, establishing the permanent DC interconnections.

4.7. Algorithm Overview:

Below an analytical presentation of the optimization algorithm appears:

For the *i*-th system:

P_i: the current total power production of the i-th system

$F_i(P_i)$: the current total production cost of the i-th system

ΔP_{i+}: the power production increase offered by the i-th system

ΔP_{i-}: the power production reduction offered by the i-th system

$F_i(P_i + \Delta P_{i+})$: the power production cost after the power increase by ΔP_{i+} of the i-th system

$F_i(P_i + \Delta P_{i-})$: the power production cost after the power decrease by ΔP_{i-} of the i-th system

P_{ij}: the power flow on the interconnection of systems i and j (decision variables that will be calculated by the optimization algorithm)

$P_{ij,max}$: the maximum power flow of the interconnection between the systems i and j

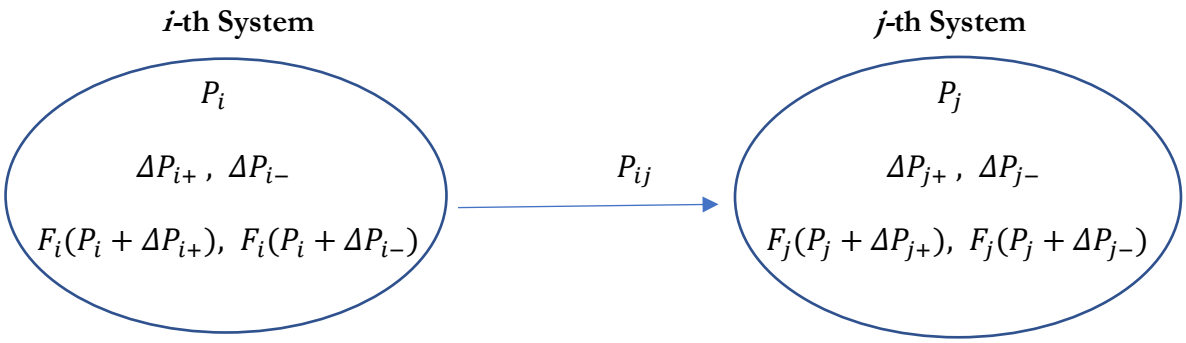

For each system *i* the following constraints apply:

$$\Delta P_{i-} \leq \sum_j P_{ij} \leq \Delta P_{i+}$$

$$|P_{ij}| \leq P_{ij,\max}$$

The objective function is:

$$\min \quad \sum_i \left\{ F_i(P_i) + \frac{F_i(P_i + \Delta P_{i+}) - F_i(P_i + \Delta P_{i-})}{\Delta P_{i+} - \Delta P_{i-}} \cdot \sum_j P_{ij} \right\}$$

A graphical representation of the algorithm is presented in the next figure, showing the abstract layout of a large electric power grid consisting of electric systems, interconnected with DC lines. The arrows indicate the direction of the power flow through the interconnections, which is modeled as power transactions between the DC buses. Multiple subsystems may be interconnected by one or more DC lines, with the potential of forming electrical networks of varied complexity.

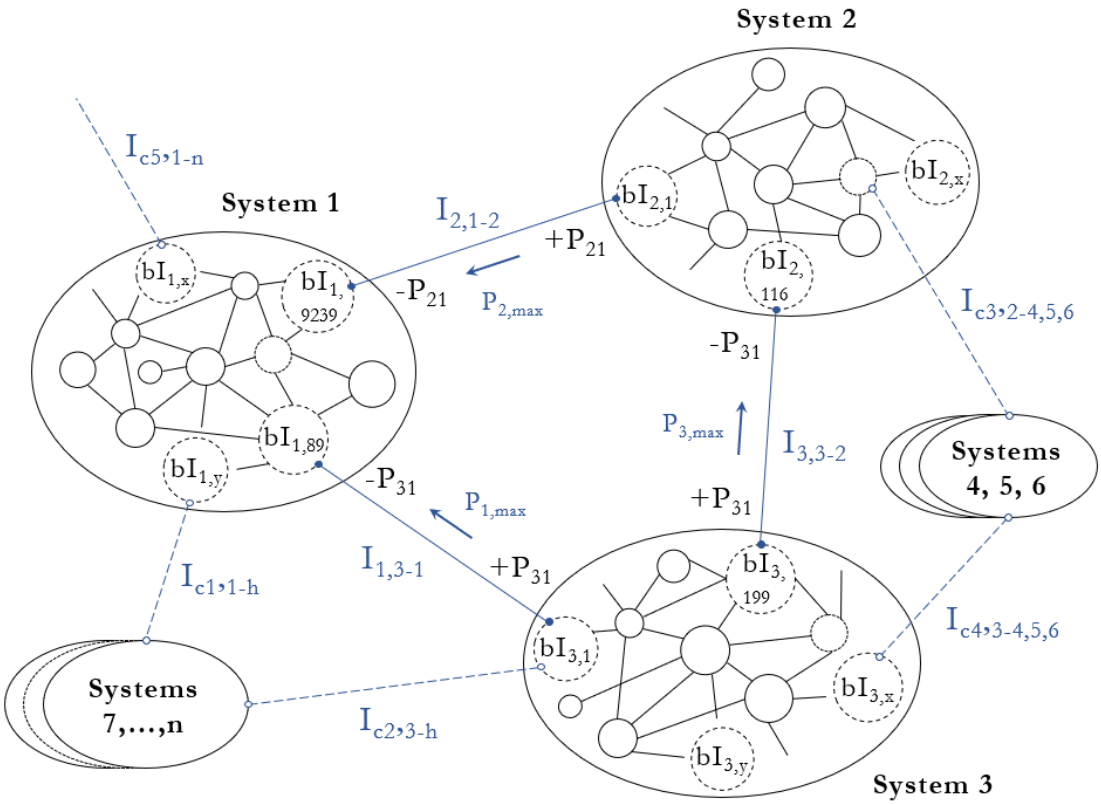

Figure 4.4: Graphical representation of a large electric power system with DC interconnections

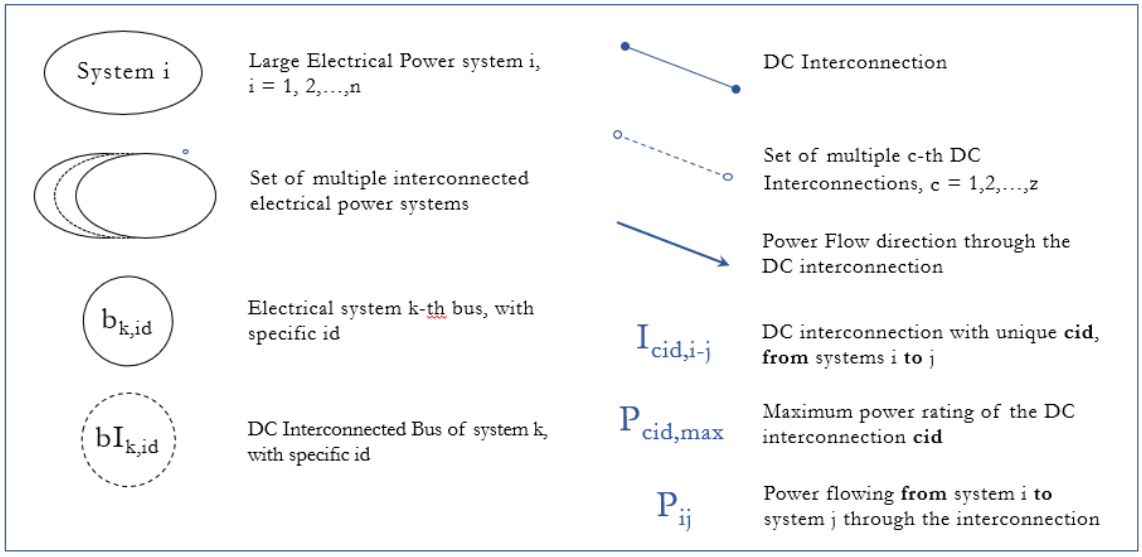

Figure 4.5: Legend with the symbol interpretations for figure 4.4

Algorithm: Calculate optimal DC interconnections

```
1: procedure FINDOPTIMALSTATE(i, j, systems, max_iterations, dp, fid)
2:         global F(i, 3)                                  //global matrix for storing system costs
3:         Initialize values of ΔP+, ΔP-
4:         for each system in systems{} do
5:                 cases = loadcase(systems{i})
6:         end for
7:
8:         iterations, error = 0
9:
10:        while error ≠ 1 and iterations ≤ max_iterations  do
11                 iterations++
12:                backup_cases = cases
13:                for each system i in temp_cases() do
14:
15:                        for j from 1 to 3 do
16:                                if j == 1
17:                                        tmp_cases(i) = backup_cases(i)        // F(Pi)
18:                                elseif j == 2
19:                                        tmp_cases(i) = ApplyOffers(ΔP+)    //F(Pi+ΔP+)
20:                                else
21:                                        tmp_cases(i) = ApplyOffers(ΔP-)     // F(Pi+ΔP-)
22:                                end if
23:
24:                                F(i, j) = getCost(runopf(tmp_cases(i)))   //get system cost for
27:                                                                          // respective offer
25:                                if runopf failed
26:                                        error = 1;
27:                                        cases = backup_cases;
28:                                        ΔP+ = ΔP+ – dp;
29:                                        ΔP-  = ΔP- + dp;
30:                                        break
31:                                end if
32:
33:                                if ΔP == 0
34:                                        Optimal_Cases = savecase(backup_cases);
```

```
35:                                     Terminate Process
36:                             end if
37:                     end for
38:
39:                     if error ≠ 1 do
40:                             [x, Fopt] = OBJ_MIN_FUNC(F)     // execute obj. min. function
41:
42:                             if Fopt,new < Fopt                      //store new optimal cases
43:                                     opt_cases = tmp_cases;
44:                                     opt_cost = Fopt_new;
45:                             elseif Fopt,new > Fopt + Fopt · 1%   //operation cost increase
46:                                     Terminate Process
47:                             end if
48:                             backup_cases = tmp_cases;       // store successfully optimized cases
49:
50:                             cases = ATTACH_DUMMY_LOADS (tmp_cases, i, x)
51:
52:                             printf("Optimization step successful")
53:                     else
54:     |       |               print ("Optimization step failed")
55:     |       |       end if
56:     |       end for
57:     end while
58:     Optimal_Cases = savecase(opt_cases);
59:     Extract(fid, exec_data);
60: end procedure
```

Execution Analysis:

Below are briefly described the steps that take place during the execution of the optimization process:

Optimization Algorithm Execution	
1	Initialize interconnection input, case files, starting offer set $\Delta P_+/\Delta P_-$ and maximum number of iterations
2	Load system cases that are about to be optimized, into proper Matlab structures for processing
3	Calculate the current operating cost F(Pi) of the i-th system through $runopf$
	• If runopf fails: decrease offers by dp MW each and repeat process
	• If offers converge to zero: **Terminate Process**
4	Distribute offers between the j DC buses system i proportionally, based on their current power demand
5	Calculate the new corresponding operating costs $F(Pi + \Delta P_+)$ and $F(Pi + \Delta P_-)$
	• If $runopf$ fails: decrease offers by dp MW each and repeat process
6	Store all three operating costs of the $i-th$ system into the properly indexed matrix F

7	**Repeat** process for all $n-th$ system cases: **go to** step 3
8	Feed contents of F matrix into the Objective Function
9	Get $fmincon$ results: Optimal Operating Cost ($Fopt$)
	• If new Fopt < Fopt: store new optimal cost
	• Else if new Fopt > Fopt * 1.01 (1%): **Terminate Process**
10	Get $fmincon$ results: Optimal Interconnections (x_j)
11	Attach resulting interconnections of $fmincon$ as opposite loads to the right DC buses, in a way that indicates the power flow's direction $(+x_{f,j}/-x_{t,j})$
12	Save new cases for further optimization
13	Proceed to next iteration
	• If maximum iterations limit reached: **Terminate Process**
14	**Repeat** process with the same offer set: **go to** step 3
15	Extract execution data and **Terminate Process**

Chapter 5: Method Evaluation

In this chapter we attempt to evaluate the functionality of the optimization algorithm we implemented. For this purpose, we performed tests for two different scenarios. The first is about a small electric system that serves as a model for validating the results' accuracy by putting them in comparison with those of Matlab's optimal power flow function. The second scenario aims to demonstrate the capabilities of the algorithm in optimizing a significantly larger system of similar topology, that meets the standards of today's HVDC systems.

5.1. Evaluation Model

In order to properly evaluate the reliability and robustness of our algorithm, we have to test its results in comparison to those of the already proven method of optimal power flow analysis, performed by Matpower's 'runopf' function. For this experiment, we will perform the optimization algorithm for a small electric system, consisting of three individual AC subsystems. These will be connected to each other by three DC interconnections. A topology like this is ideal to maintain a lower volume of data that can be consistently monitored during the execution, thus making the evaluation easier. Moreover, it ensures shorter running times and makes error detection easier. The schematic representation of the system we aim to optimize is the one shown in the following figure(5.1):

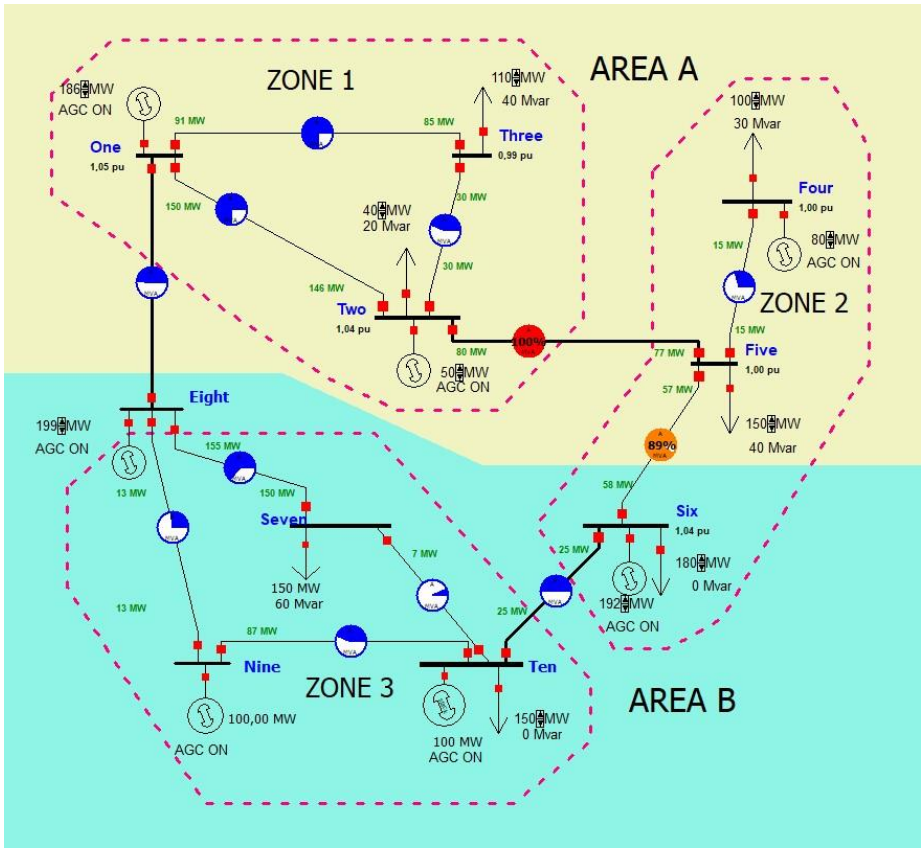

Figure 5.1: Integrated system topology, consisting of three interconnected subsystems

We can clearly see that the three individual subsystems are connected by the respective DC interconnections, forming a large electric power system. The systems are cooperating via the interconnections by performing optimal power flow in order to ensure optimal operation whole system. Below the characteristics of the full system are shown:

System	1	2	3	Total
Buses	3	3	4	10
Generators	2	2	3	7
Loads	2	3	2	7
Shunts	0	0	0	0
Branches	3	2	4	9
Transformers	0	0	0	0

Table 5.1: Integrated system characteristics

An overview of the data inside each system case is given in the following table:

System	Bus ID	Type	Pd	Qd	Pg	Qg
1	1	3	0	0	186.11	9.67
	2	2	40	20	50	133.78
	3	1	110	40	-	-
2	4	3	100	30	80	38.36
	5	1	150	40	-	-
	6	2	180	0	192.14	86.34

3	7 8 9 10	1 2 2 3	150 0 0 150	60 0 0 0	- 198.93 100 100	- 49.28 -27.88 -3.11

Table 5.2: Production data of the subsystems consisting the Integrated system

The characteristics of every DC transmission branch are next presented:

ID	From System	To System	From bus	To bus	R	X	b	rateA
1	3	1	8	1	0.006	0.05	0.01	400
2	1	2	2	5	0.008	0.024	0.09	400
3	3	2	10	6	0.016	0.048	0.15	500

Table 5.3: Characteristics of the initial DC interconnections

By running the optimal power flow function of Matpower, we will gain all the information we need about the power generation distribution throughout the system and more importantly, the power flow through each one of the interconnections. We will also determine the total operating cost of the system. This information is shown extensively in the results of the 'runopf' function in Matlab:

```
Objective Function Value = 58523.32 $/hr
================================================================================
|     System Summary                                                          |
================================================================================

How many?                How much?              P (MW)            Q (MVAr)
---------------------    -------------------  -------------  -----------------
Buses             10     Total Gen Capacity    2550.0       -11100.0 to 11100.0
Generators         7     On-line Capacity      2550.0       -11100.0 to 11100.0
Committed Gens     7     Generation (actual)    899.8             329.4
Loads              7     Load                   880.0             190.0
  Fixed            7       Fixed                880.0             190.0
  Dispatchable     0       Dispatchable          -0.0 of -0.0      -0.0
Shunts             0     Shunt (inj)            -0.0               0.0
Branches          12     Losses (I^2 * Z)       19.79            188.07
Transformers       0     Branch Charging (inj)    -                48.7
Inter-ties         2     Total Inter-tie Flow   253.8             133.8
Areas              2

                         Minimum                      Maximum
                  -------------------------  -------------------------------
Voltage Magnitude   0.900 p.u. @ bus 3          1.100 p.u. @ bus 10
Voltage Angle      -6.25 deg   @ bus 3         15.97 deg   @ bus 9
P Losses (I^2*R)             -                 2.73 MW    @ line 10-6
Q Losses (I^2*X)             -                40.00 MVAr  @ line 8-7
Lambda P           43.71 $/MWh @ bus 10        72.00 $/MWh @ bus 4
Lambda Q           -1.33 $/MWh @ bus 7          7.56 $/MWh @ bus 3
```

Bus Data								
Bus #	Voltage Mag(pu)	Voltage Ang(deg)	Generation P (MW)	Generation Q (MVAr)	Load P (MW)	Load Q (MVAr)	Lambda($/MVA-hr) P	Lambda($/MVA-hr) Q
1	0.947	6.629*	30.00	33.76	-	-	71.546	-
2	0.994	-4.095	30.00	89.23	40.00	20.00	62.971	-
3	0.900	-6.251	-	-	110.00	40.00	71.929	7.557
4	0.928	-5.591*	95.91	3.43	100.00	30.00	72.000	-
5	0.993	-5.588	-	-	150.00	40.00	61.371	0.202
6	1.057	-4.666	110.06	33.70	180.00	0.00	51.695	-
7	0.924	-4.360	-	-	150.00	60.00	53.571	-1.332
8	0.936	13.134	300.00	-8.85	-	-	64.437	-
9	0.939	15.967	116.90	-38.17	-	-	56.000	-
10	1.100	-1.996*	216.91	216.29	150.00	0.00	43.706	-
		Total:	899.79	329.39	880.00	190.00		

Branch Data								
Brnch #	From Bus	To Bus	From Bus Injection P (MW)	From Bus Injection Q (MVAr)	To Bus Injection P (MW)	To Bus Injection Q (MVAr)	Loss (I^2 * Z) P (MW)	Loss (I^2 * Z) Q (MVAr)
1	1	2	143.08	-37.83	-140.66	61.20	2.419	29.03
2	1	3	81.24	16.31	-79.18	-2.00	2.064	18.58
3	8	1	197.05	-32.53	-194.32	55.28	2.729	22.75
4	2	3	32.50	39.45	-30.82	-38.00	1.684	5.05
5	2	5	98.16	-31.42	-97.32	25.06	0.839	2.52
6	4	5	-4.09	-26.57	4.37	23.66	0.285	1.71
7	6	5	59.24	91.07	-57.06	-88.72	2.187	6.56
8	8	7	131.03	19.19	-129.03	20.82	2.000	40.00
9	7	10	-20.97	-80.82	20.97	97.14	0.000	16.32
10	10	6	131.91	48.12	-129.18	-57.37	2.734	8.20
11	8	9	-28.08	4.50	28.36	-3.11	0.277	1.38
12	9	10	88.54	-35.05	-85.97	71.03	2.569	35.97
						Total:	19.787	188.07

The data about each system's production are summed up in the next table:

System	Bus ID	Generation P (MW)	Generation Q (Mvar)	Load P (MW)	Load Q (Mvar)	Lambda $/MVA-hr
1	1	30	33.76	-	-	71.546
	2	30	89.23	40	20	62.971
	3	-	-	110	40	71.929
	Sum	**60**	**122.99**	**150**	**60**	**206.446**
2	4	95.91	3.43	100	30	72.000
	5	-	-	150	40	61.371
	6	110.06	33.7	180	0	51.695
	Sum	**205.97**	**37.13**	**430**	**70**	**185.066**
3	7	-	-	150	60	53.571
	8	300	-8.85	-	-	64.437
	9	116.9	-38.17	-	-	56.000
	10	216.91	216.29	150	0	43.706
	Sum	**633.81**	**169.27**	**300**	**60**	**217.714**
System Total		**899.78**	**329.39**	**880**	**190**	**609.226**

Table 5.4: Optimal power flow results of the Integrated system

It is obvious that the power production is concentrated at System 3 that generates almost 634 MW, followed by System 2 with 206 MW. Last one comes System 1 with only 60MW of power production. The reason for that is that the cost of power production at Zone 3 is cheaper than System 2, and especially System 1.

The last column of table 5.5 shows that even though System 3 is responsible for the bulk of production, it maintains a local cost similar to System 1, which generates ten times less the electric power. At the same time System 2 continues to be cheaper that System 1, despite generating three times more power. A comparison between the local operating costs for each MW produced by each system is presented in next table:

System	Generation (MW)	Lambda ($/MVA-hr)	Lambda/MW
1	60	206.446	**3.440**
2	205.97	185.066	**0.898**
3	633.81	217.714	**0.343**

Table 5.5: Subsystem costs per generated MW

We can see that Zone 3 is by far the cheapest and thus is expected to bear the most of the power generation taking place. Zone 2 is more expensive, but still a lot cheaper than Zone 1. The increased cost of Zone 1 makes it a less appealing for the optimal power flow solver. Therefore, the bulk power generation is assigned to the more economic systems. As we will see later, this is made possible by the exchange of power through the DC interconnections, which help the system solver achieve a more cost-effective state of operation.

The optimal power flow results show us additionally the amount of power flowing through each system branch, including the optimal DC interconnections:

Initial DC Interconnections								
Conn. ID	**Bus IDs**		**FROM**		**TO**		**LOSSES**	
	from	to	P(MW)	Q(Mvar)	P(MW)	Q(Mvar)	P(MW)	Q(Mvar)
1	8	1	197.05	-32.53	-194.32	55.28	2.729	22.75
2	2	5	98.16	-31.42	-97.32	25.06	0.839	2.52
3	10	6	131.91	48.12	-129.18	-57.37	2.734	8.2
Total			**427.12**	**-15.83**	**-420.82**	**22.97**	**6.302**	**33.47**

Table 5.6: OPF results of the DC interconnections

We can see that the total amount of real power transfer is almost equal to the that of the whole system. This proves the importance of the DC interconnections for achieving optimal power flow, and thus more efficient power distribution across the system that brings it to its optimal operation state. System 3 supplies System 1 with almost 195 MW, and System 2 with 130 MW through interconnections 1 and 3 respectively. Finally, System

1 injects approximately 98 MW to System 2. It is obvious that Zone 3 has a great power contribution to the rest of the system.

5.2. Separation of Small Power System Case Study to three autonomous subsystems

The algorithm we introduced will attempt to approach this particular optimal state by calculating the DC power flows using the objective function and constraints we formulated in the previous section. We are going to compare the results of our optimization algorithm to that of the 'runopf' of the previous paragraph function to validate its proper functionality and determine its accuracy.

In order to do so, it is necessary to break the initial power system into three autonomous subsystems by cutting off the existing interconnections. The new individual system cases will be given as input to the optimization algorithm. Below, the results of the optimal power flow are presented for the respective subsystems:

System 1:

```
Objective Function Value = 16268.92 $/hr
================================================================================
|     System Summary                                                           |
================================================================================

How many?                How much?              P (MW)            Q (MVAr)
---------------------    --------------------  -------------  -----------------
Buses                3   Total Gen Capacity     550.0         -400.0 to 400.0
Generators           2   On-line Capacity       550.0         -400.0 to 400.0
Committed Gens       2   Generation (actual)    152.0               48.6
Loads                2   Load                   150.0               60.0
  Fixed              2     Fixed                150.0               60.0
  Dispatchable       0     Dispatchable          -0.0 of -0.0        -0.0
Shunts               0   Shunt (inj)            -0.0                0.0
Branches             3   Losses (I^2 * Z)        1.99               6.44
Transformers         0   Branch Charging (inj)    -                 17.8
Inter-ties           0   Total Inter-tie Flow    0.0                0.0
Areas                1

                          Minimum                        Maximum
                  -------------------------  --------------------------------
Voltage Magnitude   1.068 p.u. @ bus 3          1.100 p.u. @ bus 2
Voltage Angle       4.78 deg   @ bus 3          7.90 deg   @ bus 2
P Losses (I^2*R)             -                 1.08 MW    @ line 1-3
Q Losses (I^2*X)             -                 3.23 MVAr  @ line 1-3
Lambda P           80.00 $/MWh @ bus 2         82.91 $/MWh @ bus 3
Lambda Q            0.00 $/MWh @ bus 2          0.86 $/MWh @ bus 3

================================================================================
|     Bus Data                                                                 |
================================================================================
 Bus      Voltage          Generation             Load          Lambda($/MVA-hr)
  #   Mag(pu) Ang(deg)   P (MW)   Q (MVAr)   P (MW)   Q (MVAr)     P        Q
-----  ------- --------  --------  --------  --------  --------  -------  -------
    1   1.098    6.629*    30.00     30.79       -         -      80.708      -
    2   1.100    7.898    121.99     17.83     40.00     20.00    80.000      -
    3   1.068    4.785       -         -      110.00     40.00    82.905    0.859
                         --------  --------  --------  --------
               Total:     151.99     48.62    150.00     60.00

================================================================================
|     Branch Data                                                              |
================================================================================
Brnch   From   To     From Bus Injection    To Bus Injection      Loss (I^2 * Z)
  #     Bus    Bus    P (MW)   Q (MVAr)   P (MW)   Q (MVAr)   P (MW)   Q (MVAr)
-----  -----  -----  --------  --------  --------  --------  --------  --------
   1      1      2    -43.75      1.37     43.91     -7.65     0.161      0.96
   2      1      3     73.75     29.43    -72.67    -32.07     1.076      3.23
   3      2      3     38.08      5.48    -37.33     -7.93     0.750      2.25
                                                             --------  --------
                                                    Total:     1.987      6.44
```

System 2:

```
Objective Function Value = 34110.51 $/hr
==========================================================================
|     System Summary                                                     |
==========================================================================

How many?                How much?              P (MW)            Q (MVAr)
---------------------    -------------------  -------------  -----------------
Buses               3    Total Gen Capacity     500.0         -400.0 to 400.0
Generators          2    On-line Capacity       500.0         -400.0 to 400.0
Committed Gens      2    Generation (actual)    436.8               80.4
Loads               3    Load                   430.0               70.0
  Fixed             3      Fixed                430.0               70.0
  Dispatchable      0      Dispatchable          -0.0 of -0.0        -0.0
Shunts              0    Shunt (inj)            -0.0                0.0
Branches            2    Losses (I^2 * Z)        6.85              20.55
Transformers        0    Branch Charging (inj)    -                10.1
Inter-ties          1    Total Inter-tie Flow    63.5               46.0
Areas               2

                          Minimum                      Maximum
                  -------------------------  --------------------------------
Voltage Magnitude   1.034 p.u. @ bus 2          1.100 p.u. @ bus 1
Voltage Angle     -16.56 deg   @ bus 2         -5.59 deg   @ bus 1
P Losses (I^2*R)             -                 5.74 MW    @ line 1-2
Q Losses (I^2*X)             -                17.22 MVAr  @ line 1-2
Lambda P          72.00 $/MWh @ bus 1         82.70 $/MWh @ bus 2
Lambda Q           0.00 $/MWh @ bus 1          1.34 $/MWh @ bus 2
```

```
==========================================================================
|     Bus Data                                                           |
==========================================================================
 Bus      Voltage          Generation             Load          Lambda($/MVA-hr)
  #   Mag(pu) Ang(deg)   P (MW)   Q (MVAr)   P (MW)   Q (MVAr)     P        Q
-----  ------- --------  --------  --------  --------  --------  -------  -------
    1  1.100   -5.591*   192.83      34.99   100.00      30.00   72.000      -
    2  1.034  -16.559       -          -     150.00      40.00   82.702    1.342
    3  1.072  -15.067    244.02      45.43   180.00       0.00   80.800      -
                        --------  --------  --------  --------
               Total:    436.85      80.41   430.00      70.00

==========================================================================
|     Branch Data                                                        |
==========================================================================
Brnch   From    To     From Bus Injection   To Bus Injection     Loss (I^2 * Z)
  #     Bus     Bus     P (MW)   Q (MVAr)   P (MW)   Q (MVAr)   P (MW)   Q (MVAr)
-----  -----   -----  --------  --------  --------  --------  --------  --------
   1      1       2     92.83      4.99    -87.09      6.54     5.740     17.22
   2      3       2     64.02     45.43    -62.91    -46.54     1.109      3.33
                                                              --------  --------
                                                    Total:     6.850     20.55
```

System 3:

```
Objective Function Value = 16979.32 $/hr
================================================================================
|     System Summary                                                           |
================================================================================

How many?                How much?              P (MW)            Q (MVAr)
---------------------    --------------------  -------------  -----------------
Buses               4    Total Gen Capacity    1500.0        -10300.0 to 10300.0
Generators          3    On-line Capacity      1500.0        -10300.0 to 10300.0
Committed Gens      3    Generation (actual)    303.3              96.2
Loads               2    Load                   300.0              60.0
  Fixed             2      Fixed                300.0              60.0
  Dispatchable      0      Dispatchable          -0.0 of -0.0       -0.0
Shunts              0    Shunt (inj)            -0.0               0.0
Branches            4    Losses (I^2 * Z)        3.32             36.19
Transformers        0    Branch Charging (inj)    -               0.0
Inter-ties          0    Total Inter-tie Flow    0.0              0.0
Areas               1

                         Minimum                      Maximum
                  -------------------------  ---------------------------------
Voltage Magnitude   1.017 p.u. @ bus 1          1.100 p.u. @ bus 2
Voltage Angle      -5.65 deg   @ bus 1          5.95 deg   @ bus 2
P Losses (I^2*R)             -                 2.60 MW    @ line 2-1
Q Losses (I^2*X)             -                25.99 MVAr  @ line 2-1
Lambda P           29.53 $/MWh @ bus 2        30.86 $/MWh @ bus 1
Lambda Q            0.00 $/MWh @ bus 4         0.27 $/MWh @ bus 1


================================================================================
|     Bus Data                                                                 |
================================================================================
 Bus      Voltage          Generation             Load          Lambda($/MVA-hr)
  #   Mag(pu) Ang(deg)   P (MW)   Q (MVAr)   P (MW)   Q (MVAr)     P        Q
----- ------- --------  --------  --------  --------  --------  -------  -------
    1  1.017   -5.645       -         -      150.00     60.00    30.861   0.271
    2  1.100    5.949    150.00     40.63       -         -      29.530     -
    3  1.098    3.535      0.00      2.20       -         -      30.026     -
    4  1.100   -1.996*   153.32     53.36    150.00      0.00    30.853     -
                         --------  --------  --------  --------
               Total:    303.32     96.19    300.00     60.00

================================================================================
|     Branch Data                                                              |
================================================================================
Brnch   From   To    From Bus Injection   To Bus Injection     Loss (I^2 * Z)
  #     Bus    Bus    P (MW)   Q (MVAr)   P (MW)   Q (MVAr)   P (MW)   Q (MVAr)
-----  -----  -----  --------  --------  --------  --------  --------  --------
   1      2      1    116.98     45.12   -114.38    -19.14     2.599     25.99
   2      1      4    -35.62    -40.86     35.62     46.54     0.000      5.68
   3      2      3     33.02     -4.49    -32.74      5.87     0.275      1.38
   4      3      4     32.74     -3.67    -32.29      6.82     0.450      3.15
                                                             --------  --------
                                                    Total:     3.324     36.19
```

A brief presentation of the optimal power flow results for each bus can be seen in the table 5.7:

System	Bus ID	Generation		Load	
		P (MW)	Q (Mvar)	P (MW)	Q (Mvar)
1	1	30	30.79	-	-
	2	121.99	17.83	40	20
	3	-	-	110	40
	Sum	**152**	**48.62**	**150**	**60**
2	4	192.83	34.99	100	30
	5	-	-	150	40
	6	244.02	45.43	180	0
	Sum	**436.85**	**80.42**	**430**	**70**
3	7	-	-	150	60
	8	150	40.63	-	-
	9	0	2.2	-	-
	10	153.32	53.36	150	0
	Sum	**303.32**	**96.19**	**300**	**0**
System Total		**892.12**	**225.23**	**880**	**130**

Table 5.7: OPF results for the Autonomous subsystems

The next table contains a summary of the production and the costs of each system case:

System	Generation		Load		Losses		Cost
	P(MW)	Q(Mvar)	P(MW)	Q(Mvar)	P(MW)	Q(Mvar)	$/hr
1	152	48.62	150	60	1.99	6.44	16268.92
2	436.85	80.42	430	70	6.85	20.55	34110.51
3	303.32	196.27	300	60	3.32	36.19	16979.32
Total	**892.12**	**298.31**	**880**	**190**	**12.16**	**63.18**	**67358.75**

Table 5.8: OPF results summary

Once again, the importance of the interconnections for the optimal operation of the system is highlighted. We can observe a radical difference in the production of each subsystem that directly leads to significantly larger operation costs. The changes are shown in the following table:

Systems	Load (MW)	Generation (MW)	
		AUTONOMOUS	INTEGRATED
1	150	152	60
2	430	436.85	205.97
3	300	303.32	633.81
Total	**880**	**892.12**	**899.78**
Cost ($/hr)		**67358.75**	**58523.75**

Table 5.9: Power generation comparison of the Autonomous subsystems and the Integrated system

We can see that System 3 doesn't hold the majority of the power production as it generates enough power just to supply its local power demand. Systems 1 and 2 generate more power and therefore increase the total system cost by at least 13%.

5.2.1. Optimization Results

The next step is to apply the three system cases our optimization algorithm to the three above described subsystems, along with the data of the DC interconnections. The cases

are given as a set of three separate .m files, whereas the interconnection's data are initialized inside a .txt file with the same fields as in the initial main system case. These data will be used to indicate the proper buses where the 'dummy' loads are going to be attached. The algorithm checks the validity of the input files and proceeds with the initialization of the respective data. An error message will be displayed if a file doesn't exist and the user will be prompted to enter again the corresponding file name. After the data entry is successful, the algorithm validates the system cases files by executing the 'runopf' function for each one and gets their initial operating costs for later reference. In case of failure, the algorithm is interrupted.

The execution of our algorithm also depends on other basic parameters, like the initial size of the power offers and the maximum number of iterations. Both parameters can have an impact on the execution speed of the whole process. For this experiment, we chose relatively small offers, knowing that the subsystems have limited power capacity due to their size. A set of starting offers equal to $\mathbf{\Delta P_+ = 20\ MW}$ and $\mathbf{\Delta P_- = -20\ MW}$ can be considered suitable. It is appropriate to set the power offer convergence/decrease step to 1 MW. We set the maximum number of iterations to 100 to allow the process to converge.

The algorithm was applied for the two different methods of power generation change offer distribution, introduced in the previous chapter. The first method is about dispatching the power offer evenly to a system's buses, whereas the second dictates the distribution of the offer only to the DC buses of a respective system, proportionally. Below the results of the algorithm for the two methods are presented:

The next table shows the final 'dummy' loads calculated by the objective function:

	Interconnection ID			**Total**
	1	**2**	**3**	
Method 1	158.35	67.35	195.65	421.35
Method 2	157.64	65.64	197.36	420.64
Integrated System	197.05	98.16	131.91	427.12

Table 5.10: Comparison between the DC interconnection results of Methods 1 and 2

The resulting 'dummy' loads are comparable with the power traveling through the interconnections of the initial integrated system, indicating that the algorithm pushes the system to the right direction regarding its operation state. This shows us that, while our algorithm approaches the optimal interconnections with accuracy, it reaches a new optimal state of operation by attempting different offer distributions.

The next table presents how the 'dummy' loads are distributed between the DC buses, forming the respective interconnections:

Optimal DC Interconnections								
Interconn. ID	**System IDs**		**Bus IDs**		**METHOD 1**		**METHOD 2**	
	from	to	from	to	**from**	**to**	**from**	**to**
1	3	1	8	1	158.35	-158.35	157.64	-157.64

2	1	2	2	5	67.35	-67.35	65.64	-65.64
3	3	2	10	6	195.65	-195.65	197.36	-197.36

Table 5.11: Layout of the resulting optimal DC interconnections

Method 1:

System	Bus ID	Generation		Load		Dummy Loads(MW)
		P (MW)	Q (Mvar)	P (MW)	Q (Mvar)	
1	1	30.1	22.92	-158.35	-	-158.35
	2	31.52	28.97	107.35	20	67.35
	3	-	-	110	40	
	Sum	61.62	51.89	59	60	
2	4	60.48	30.61	100	30	
	5	0.1	46.32	82.65	40	-67.35
	6	110.17	-8.49	-15.65	0	-195.65
	Sum	170.65	68.44	167	70	
3	7	-	-	150	60	
	8	157.85	34.08	158.35	-	158.35
	9	82.79	2.11	-	-	
	10	415.51	56.09	345.65	0	195.65
	Sum	656.15	92.28	654	60	
System Total		**888.42**	**212.61**	**880**	**190**	

Table 5.12: OPF results of Method 1 for the Autonomous subsystems

Method 2:

System	Bus ID	Generation		Load		Dummy Loads(MW)
		P (MW)	Q (Mvar)	P (MW)	Q (Mvar)	
1	1	30.1	22.91	-157.64	-	-157.64
	2	30.51	28.92	105.64	20	65.64
	3	-	-	110	40	-
	Sum	60.61	51.83	58	60	
2	4	60.55	30.6	100	30	-
	5	0.1	46.54	84.36	40	-65.64
	6	110.17	-6.13	-17.36	0	-195.65
	Sum	170.72	71.01	167	70	
3	7	-	-	150	60	-
	8	158.85	34.11	157.64	-	157.64
	9	82.79	1.97	-	-	-
	10	415.51	56.08	347.36	0	195.65
	Sum	657.15	92.16	655	60	
System Total		**888.42**	**215**	**880**	**190**	

Table 5.13: OPF results of Method 2 for the Autonomous subsystems

The 'dummy' loads that simulate the DC interconnections on the corresponding buses are presented above. It appears that the two methods give us practically the same results, with small deviations.

A summary of the previous tables along with the operating costs of the respective systems is next shown:

Method 1:

System	Generation		Load		Cost
	P(MW)	Q(Mvar)	P(MW)	Q(Mvar)	$/hr
1	61.62	51.89	59	60	9025.65
2	170.65	68.44	167	70	14105.9
3	656.15	92.28	654	60	32390.23
Total	**888.42**	**22.61**	**880**	**190**	**55521.78**

Table 5.14: OPF results summary of Method 1

Method 2:

System	Generation		Load		Cost
	P(MW)	Q(Mvar)	P(MW)	Q(Mvar)	$/hr
1	60.61	51.83	58	60	8944.72
2	170.72	86.93	167	70	14109.96
3	657.15	92.28	655	60	32444.56
Total	**888.48**	**231.04**	**880**	**190**	**55499.24**

Table 5.15: OPF results summary of Method 2

Method 2 slightly outperforms the first method in terms of total operating cost. While method 1 also gives us pretty accurate results, **method 2** is considered more appropriate due its more realistic approach towards the operation of HVDC systems. Therefore, we will use its results for evaluating our implementation.

The results of the algorithm are presented below, as calculated at each successful iteration of the optimization procedure:

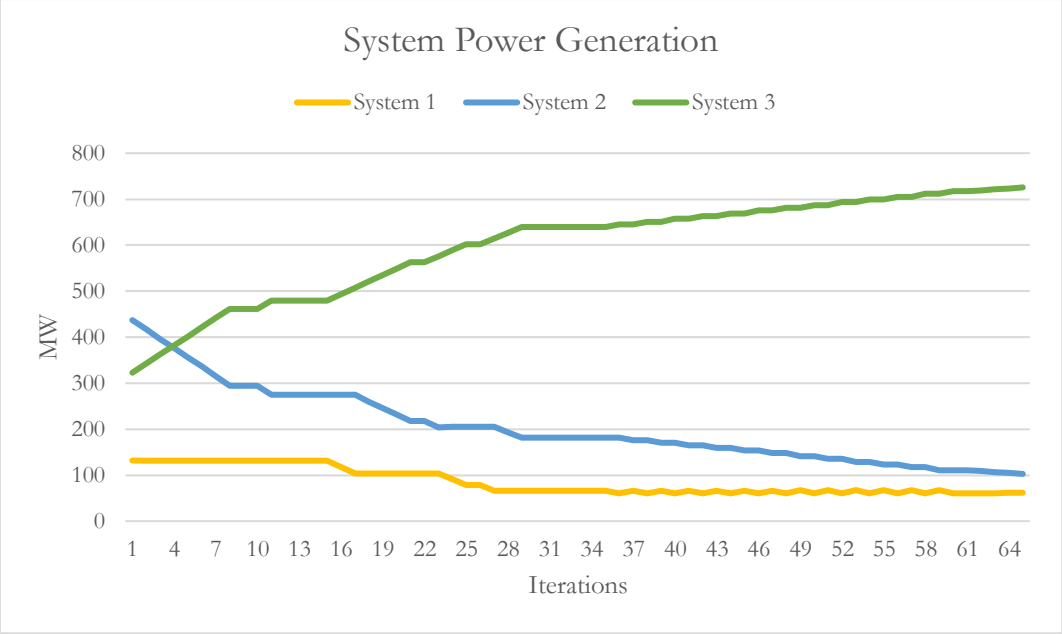

Figure 5.2: Real Power Production of the Autonomous subsystems during the execution process

We notice that by each iteration, the power generation of System 3 gradually increases, whereas that of Systems 1 and 2 decrease. System 1 reaches its optimal state of operation early, around the 25th iteration, and thus its production remains on the same level until the end of the process. The optimization for Systems 2 and 3 continues until the power offer limit is reached.

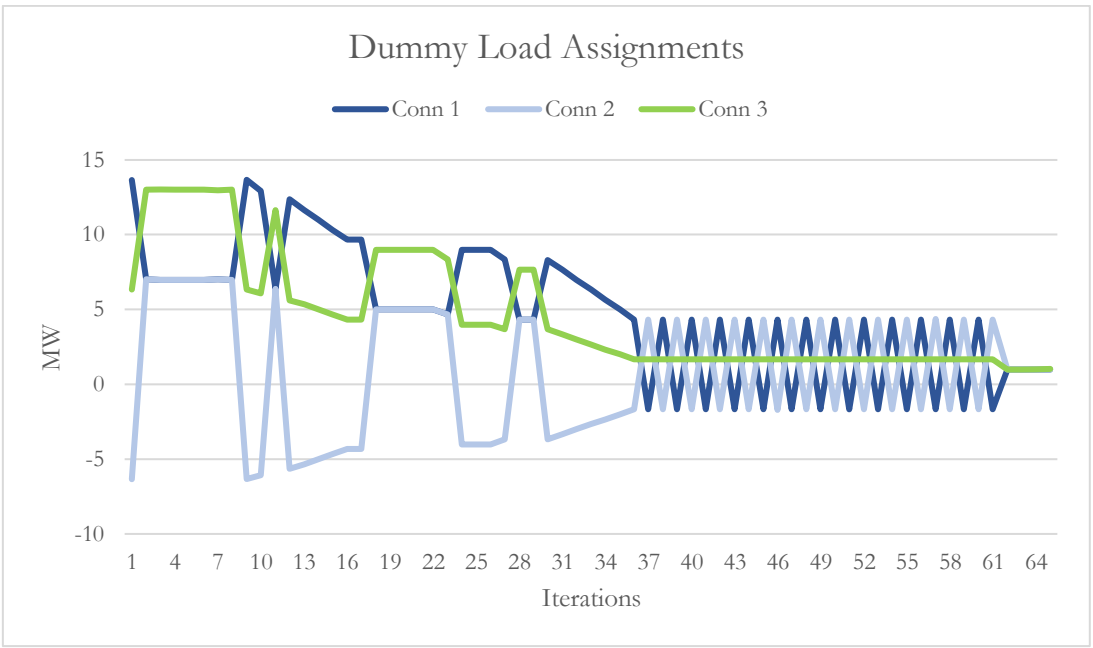

Figure 5.3: Fmincon resulting DC 'dummy' loads at each iteration of the execution process

Above are shown the results given by $fmincon$ at each iteration. These values represent the 'dummy' loads that iteratively add up to gradually form the optimal DC power flows on the interconnections. Each 'dummy' load is attached to the respective system dummy

buses, thus simulating each interconnection. We can see that the 'dummy' loads tend to converge in the course of the procedure, due to the fact that the set of the power offers is also converging. Around the 37-th iteration, interconnections 1 and 2 cannot be optimized further, and therefore they start to perform oscillations. The optimization continues for the 3rd interconnection until the last iteration. When it also reaches its optimal value, the resulting values of $fmincon$ fully converge and the execution is terminated.

We can see how the results of the objective function affect the total operating cost of the system cases we attempt to optimize, by taking a look at the next set of curves. One represents the total system cost calculated by the objective function and the other shows the actual operating cost. The latter is determined by using the 'runopf' function for each subsystem after attaching the 'dummy' loads, produced in that particular iteration, on the corresponding cases. By observing the graphs, we can see that the results are almost identical:

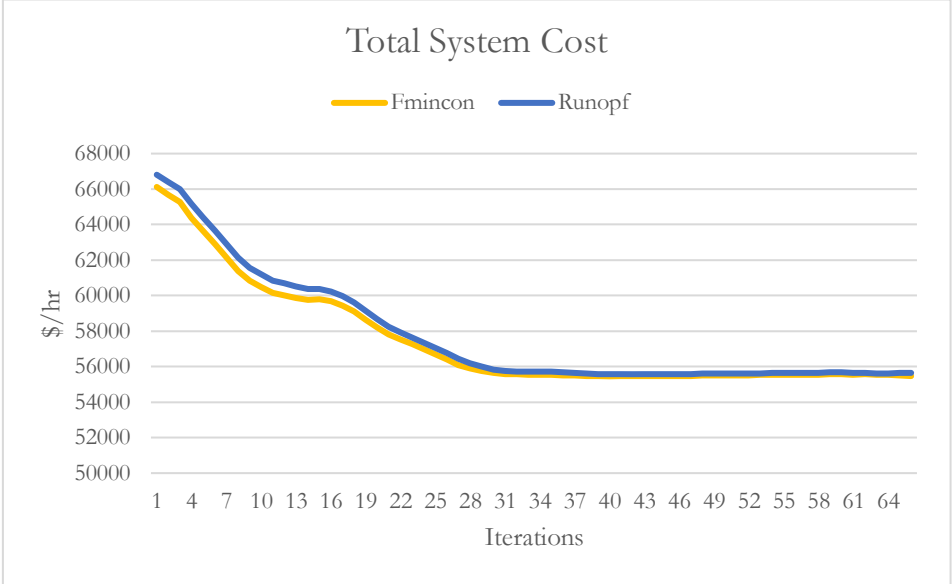

Figure 5.4: Total system operating cost calculated by fmincon and runopf functions for the Autonomous subsystems

This is an indication that our objective function works properly in the adopted power change offers. As the execution progresses the total system cost steadily decreases. Around the 40-th iteration the costs seem to stabilize around a certain value, which is the optimal cost the algorithm tries to reach. The process terminates at the time when the offers have fully converged, which happens at the 64rd iteration. There is a possibility that the optimal cost may be found before the offers converge. The algorithm stores the iterations with the best results and saves them into separate system case files.

5.2.2. Comparison and Evaluation

In the following table, a comparison is made between the power production data of the initial system with the integrated AC interconnections, the proposed optimization algorithm, and the autonomous systems without the interconnections:

Integrated System				
System	**1**	**2**	**3**	**Total**
Generation (MW)	60	205.97	633.81	899.78
Load (MW)	150	430	300	880
Cost ($/hr)	-	-	-	**58523.75**
Autonomous Systems				
Generation (MW)	151.99	436.85	303.32	892.16
Load (MW)	150	430	300	880
Cost ($/hr)	16268.92	34110.51	16979.32	**67358.75**
Optimized System with HVDC Interconnections				
Generation (MW)	60.6	170.8	657.2	886.51
Load (MW)	58	167	655	880
Cost ($/hr)	8944.77	14109.87	32444.55	**55499.19**

Table 5.16: Comparison between the three power system instances (Integrated/Autonomous/Optimized)

By comparing the operation data of the **Autonomous Systems**, calculated by performing optimal power flow analysis to the three autonomous systems, with the data of the **Optimized Cases**, given as output by the algorithm, we can see that their total real power generation is almost the same. Moreover, the total power demand of their respective system cases is exactly equal. This indicates that the sum of the 'dummy' loads, attached by the algorithm to simulate the DC links between the subsystems, is equal to zero. Therefore, the calculated interconnections are established correctly, without disturbing the power demand.

However, the power demand distribution has changed drastically, also affecting the power production of each system accordingly. The optimal DC power flows determined by our optimization algorithm have led to a power production drop on Systems 1 and 2, whereas System 3 has greatly increased its production. By comparing these results with the **Integrated System** with the integrated interconnections, we can see that they are similar. System 1 seems to have reached its prior power generation state with great accuracy. Systems 2 and 3 also tend to simulate their original power productions, although they seem to deviate by some megawatts.

It is evident that the algorithm tries to minimize the overall system's cost by moving the majority of the power demand from the more costly Systems 1 and 2 to the relatively less expensive System 3. Indeed, the resulting interconnected system cases (Optimized Cases) give us a total cost reduction of **21,3%** compared to that of the examined Input Cases. Furthermore, the resulting cost is also **5,2 %** less than the cost of the initial Model Case with the integrated interconnections, determined by performing optimal power flow analysis. This improvement can be attributed to the optimized power generations of Systems 2 and 3.

Apparently, the optimization algorithm we implemented not only manages to give us a highly accurate solution, but has also brought the systems to a new optimal state of operation. The utilization of the calculated DC interconnections offers a significant improvement in the total operating cost compared to that which occurs in the absence of the DC lines. At the same time, the resulting cost is also better than the one calculated by the optimal power flow function of Matpower. Therefore, we can safely assume the proper functionality of our optimization algorithm.

A comparison between the general information of each system case follows below. At this point it is appropriate to make a reference to the terminology used in the names that appear on the following charts:

INTEGRATED: the integrated system with the initial interconnections, optimized by the 'runopf' function of Matpower.

AUTONOMOUS: the three autonomous system cases. The subsystems originate from the removal of the interconnection from the initial system.

OPTIMIZED: the three optimized HVDC systems, embedding the new optimal DC interconnections the algorithm gives as output.

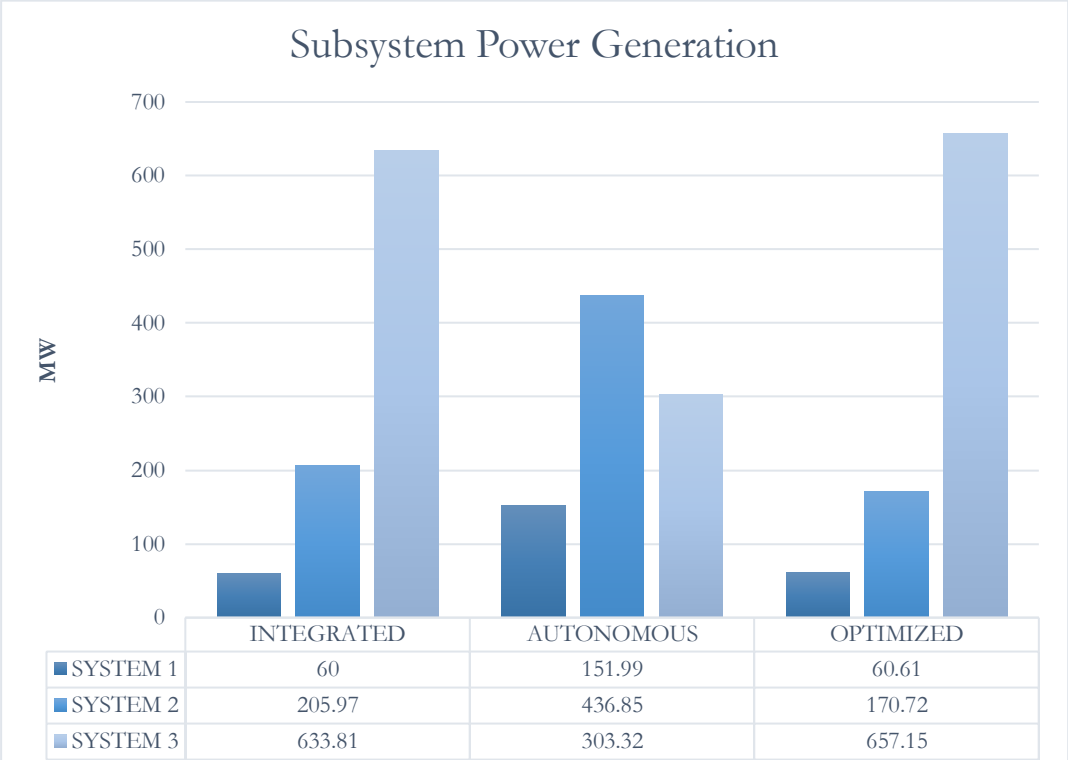

Figure 5.5: Power generation of the Autonomous and Optimized system cases, compared to that of the initial Integrated system

The chart demonstrates the power production distribution of the different system models for each one of their respective subsystems. We can see that the production of the resulting optimized system is almost at the same level with that of the initial integrated system.

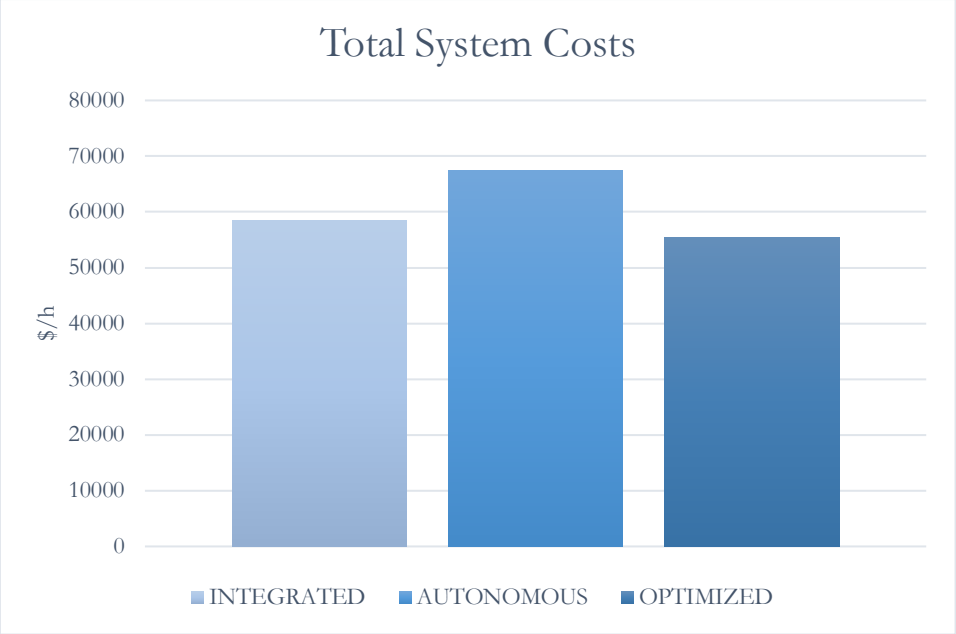

Figure 5.6: Total System Cost comparison between the three power system instances

Above we see a comparison between the total system costs of each examined model. It is clear that the output system optimized by the proposed method gives us a total cost even lower than the integrated system.

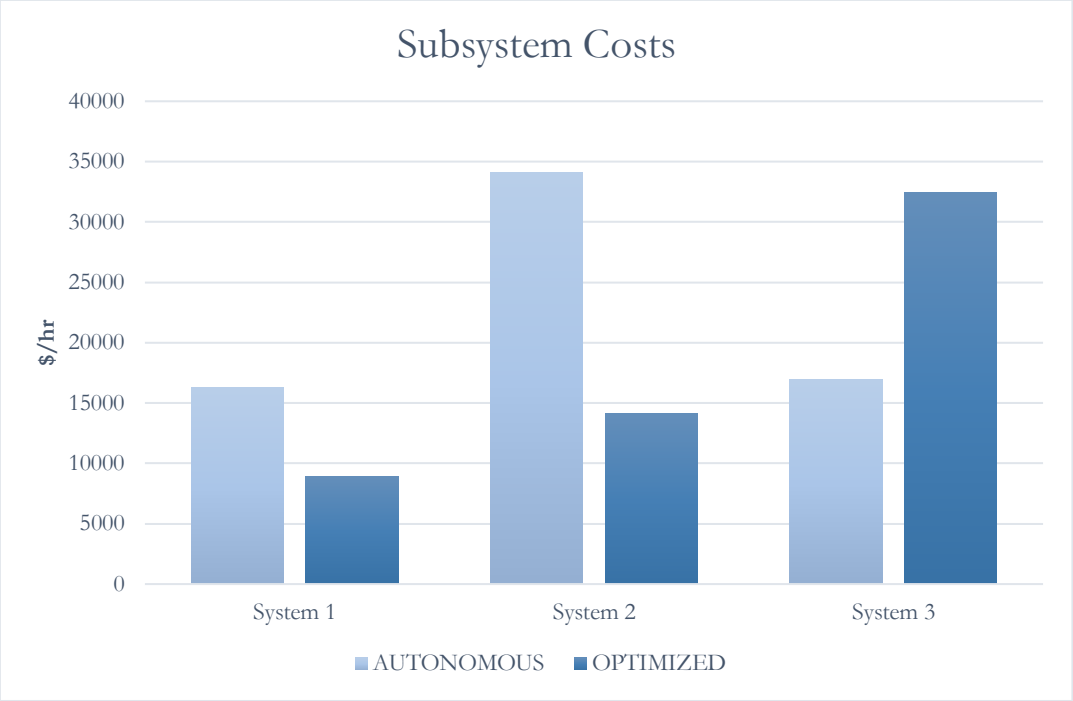

Figure 5.7: Cost comparison of the Autonomous and Optimized power system cases before and after the optimization

Next, we have a chart that compares the operating costs of each subsystem before and after the optimization. Systems 1 and 2 become less expensive as they receive additional power from System 3, which increases its production and therefore, its specific cost.

5.3. Large Power System Case Study

The next step of the evaluation is about the optimization of a large electric power system. HVDC technology distinguishes for its efficiency in long-distance transmission of large power amounts, between systems of considerable scale. Therefore, it is vital to test our optimization algorithm's capabilities in a similar situation.

The model we are about to examine sticks to the topology we introduced earlier: three individual AC subsystems interconnected with an equal number of DC lines, whose transmitted power is going to be calculated by our algorithm, in a way that will allow the systems to operate optimally. This time the systems we chose have a much larger power output and thus, significantly higher operating costs. This example will demonstrate the impact of the optimization algorithm when dealing with more realistic scenarios. The following tables contain general information about the systems to be given as input to the algorithm:

System	1	2	3	Total
Buses	89	118	200	407
Generators	12	54	49	115
Loads	35	99	108	242
Shunts	44	14	4	62
Branches	210	186	245	641
Transformers	32	9	66	107

Table 5.17: Large electric power system case study characteristics

System	Generation		Load		Losses		Cost
	P(MW)	Q(Mvar)	P(MW)	Q(Mvar)	P(MW)	Q(Mvar)	$/hr
1	5852.3	2936.1	5727.9	1374.9	118.72	2133.02	183038.77
2	4282.6	111.1	4242	1438	40.6	215.58	106011.06
3	2248.2	409.9	2228.7	635.1	19.49	310.58	44288.60
Total	**12383.1**	**3457.1**	**12198.6**	**3448.0**	**178.81**	**2659.18**	**333338.43**

Table 5.18: OPF results summary of the large power system case study

It is rather obvious that the particular systems we are examining are rather more complex than the previous ones. They have almost 400 buses in total that maintain a much larger power production, whereas operating at a cost five times higher than before. While this cannot be regarded as a remarkably large electric system, it is sufficiently large for the purposes of this simulation. The systems have escalating operating costs, with System 1 being the most expensive, while System 3 has a fairly low cost compared to the size of its production.

Below the results we obtained using the 'runopf' function on the previously mentioned system cases are shown. Due to the great volume of data produced, only the contents of the system summary of each system are shown:

System 1:

```
Objective Function Value = 183038.77 $/hr
================================================================================
|     System Summary                                                           |
================================================================================

How many?                How much?              P (MW)            Q (MVAr)
---------------------    -------------------  -------------  -----------------
Buses              89    Total Gen Capacity    9921.2       -1582.5 to 4520.1
Generators         12    On-line Capacity      9921.2       -1582.5 to 4520.1
Committed Gens     12    Generation (actual)   5852.3            2936.1
Loads              35    Load                  5727.9            1374.9
  Fixed            35      Fixed               5727.9            1374.9
  Dispatchable      0      Dispatchable          -0.0 of -0.0      -0.0
Shunts             44    Shunt (inj)           -5.7               571.8
Branches          210    Losses (I^2 * Z)      118.72            2133.02
Transformers       32    Branch Charging (inj)   -                 0.0
Inter-ties          0    Total Inter-tie Flow    0.0               0.0
Areas               1

                         Minimum                      Maximum
                -------------------------  --------------------------------
Voltage Magnitude   0.984 p.u. @ bus 6833      1.100 p.u. @ bus 2449
Voltage Angle     -10.81 deg   @ bus 8964      32.33 deg   @ bus 8581
P Losses (I^2*R)             -                14.29 MW    @ line 5416-7637
Q Losses (I^2*X)             -               238.47 MVAr  @ line 7637-8581
Lambda P          -92.24 $/MWh @ bus 8581     104.20 $/MWh @ bus 3493
Lambda Q          -13.91 $/MWh @ bus 5587      25.04 $/MWh @ bus 8581
```

System 2:

```
Objective Function Value = 106011.06 $/hr
================================================================================
|     System Summary                                                           |
================================================================================

How many?                How much?              P (MW)            Q (MVAr)
---------------------    -------------------  -------------  -----------------
Buses             118    Total Gen Capacity    9966.2       -7345.0 to 11777.0
Generators         54    On-line Capacity      9966.2       -7345.0 to 11777.0
Committed Gens     54    Generation (actual)   4282.6            111.1
Loads              99    Load                  4242.0            1438.0
  Fixed            99      Fixed               4242.0            1438.0
  Dispatchable      0      Dispatchable          -0.0 of -0.0      -0.0
Shunts             14    Shunt (inj)           -0.0               95.9
Branches          186    Losses (I^2 * Z)      40.60             215.58
Transformers        9    Branch Charging (inj)   -               1446.6
Inter-ties          0    Total Inter-tie Flow    0.0               0.0
Areas               1

                         Minimum                      Maximum
                -------------------------  --------------------------------
Voltage Magnitude   1.010 p.u. @ bus 81        1.060 p.u. @ bus 89
Voltage Angle     17.75 deg   @ bus 42        37.89 deg   @ bus 10
P Losses (I^2*R)             -                2.39 MW    @ line 37-40
Q Losses (I^2*X)             -               15.68 MVAr  @ line 9-10
Lambda P          29.87 $/MWh @ bus 87        33.68 $/MWh @ bus 41
Lambda Q          -0.11 $/MWh @ bus 17         0.32 $/MWh @ bus 95
```

System 3:

```
Objective Function Value = 44288.60 $/hr
================================================================================
|     System Summary                                                           |
================================================================================

How many?                How much?              P (MW)            Q (MVAr)
---------------------    --------------------  -------------  -----------------
Buses             200    Total Gen Capacity    3543.0         -420.3 to 1436.1
Generators         49    On-line Capacity      3160.9         -377.9 to 1241.7
Committed Gens     38    Generation (actual)   2248.2              409.9
Loads             108    Load                  2228.7              635.1
  Fixed           108      Fixed               2228.7              635.1
  Dispatchable      0      Dispatchable          -0.0 of -0.0        -0.0
Shunts              4    Shunt (inj)            -0.0               227.0
Branches          245    Losses (I^2 * Z)       19.49              310.58
Transformers       66    Branch Charging (inj)    -                308.8
Inter-ties          0    Total Inter-tie Flow     0.0                0.0
Areas               1

                         Minimum                      Maximum
                -------------------------  --------------------------------
Voltage Magnitude   1.052 p.u. @ bus 148      1.100 p.u. @ bus 65
Voltage Angle     -36.61 deg   @ bus 175      -18.98 deg   @ bus 65
P Losses (I^2*R)             -                0.69 MW    @ line 199-25
Q Losses (I^2*X)             -               19.53 MVAr  @ line 105-102
Lambda P           20.75 $/MWh @ bus 65       21.95 $/MWh @ bus 175
Lambda Q           -0.05 $/MWh @ bus 15        0.16 $/MWh @ bus 148
```

Apart from the power system cases we just described; it is necessary to define the interconnections we wish to be created in order to begin the process of the optimization. The next table contains all the data needed for their initialization:

ID	From System	To System	From bus	To bus	R	X	b	rateA
1	3	1	1	89	0.03	0.15	0.01	400
2	1	2	9239	1	0.04	0.12	0.03	400
3	3	2	199	116	0.08	0.14	0.05	500

Table 5.19: Characteristics of the DC interconnections that are about to be implemented

As we mentioned before, the topology we have here is similar to the one we tested before. This happens also for the DC flows we are going to calculate, which are declared with the same layout as before for reasons of consistency. The algorithm will be examined for four different scenarios of various inputs starting change power offers: ±10, ±20, ±30, ±40 MW, and with a convergence step equal to 1 MW. The maximum number of iterations is set to 200 in order to allow for sufficient execution time.

5.3.1. Optimization Results

All the data mentioned above are given as input to our optimization algorithm, which determines the following optimal DC power flows:

Starting Offer (MW)	Interconnection ID			Total
	1	2	3	
±10	259.747	178.253	3.253	441.253
±20	257.781	193.218	25.218	476.218
±30	255.971	184.028	54.028	494.028
±40	265.867	245.132	11.132	522.132

Table 5.20: Comparison of fmincon resulting DC interconnections for different power generation change offers

Higher starting power generation change offers allow the systems to push towards bigger changes in their power production, and therefore result in increased 'dummy' loads for the interconnections.

A summary the results obtained by the 'runopf' function, are shown in the next table:

Starting Offer	Iter.	System	Generation		Load		Cost
			P(MW)	Q(Mvar)	P(MW)	Q(Mvar)	$/hr
±10	96	1	5410.8	2895.6	5289.9	1374.9	164676.64
		2	4464.3	146	4417	1438	111647.7
		3	2517.1	489.8	2491.7	635.1	50641.85
		Total	**12392.2**	**3531.4**	**12198.6**	**3448**	**326966.19**
±20	53	1	5398	2898.1	5276.9	1374.9	164187.22
		2	4458.6	151.5	4410	1438	111473.82
		3	2537.3	495.5	2511.7	635.1	51180.82
		Total	**12393.9**	**3545.1**	**12198.6**	**3448**	**326841.86**
±30	25	1	5408.9	2897.3	5287.9	1374.9	164613.7
		2	4419.9	148.3	4372	1438	110271.58
		3	2564.9	505.8	2538.7	635.1	51944.88
		Total	**12393.7**	**3551.4**	**12198.6**	**3448**	**326830.16**
±40	18	1	5338.5	2902.9	5216.9	1374.9	161880.24
		2	4529.6	173.8	4476	1438	113703.92
		3	2532.1	504.8	2505.7	635.1	51144.43
		Total	**12393.7**	**3581.5**	**12198.6**	**3448**	**326728.59**

Table 5.21: Comparison of the optimized power system cases for different power generation change offers

We can see that the results of the algorithm for the different starting sets of power generation change rather similar. Total generation and load are almost identical in all situation. Slight changes can be noticed in the production distribution between the three systems, which slightly varies. Also, the total system operating cost shows a small decrease as the size of starting power generation change offers increases, as presented in the figure 5.8:

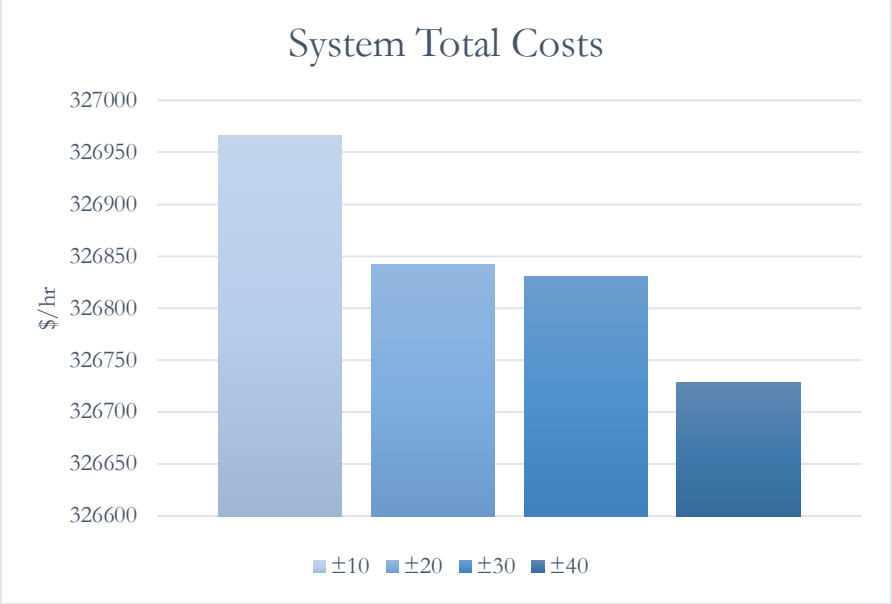

Figure 5.8: Total system cost comparison for different power generation change offers

Thus, we can consider as the optimal operating state obtained in case of $\Delta P = \pm 40$ MW.

Next, we compare the three autonomous systems, with the optimized cases that include the newly calculated interconnections:

Autonomous Systems				
Data	**System 1**	**System 2**	**System 3**	**Total**
Generation (MW)	5852.3	4282.6	2248.2	12383.1
Load (MW)	5727.9	4242	2228.7	12198.6
Cost ($/hr)	183038.77	106011.06	44288.60	**333338.43**
Optimized Systems with HVDC Interconnections				
Generation (MW)	5338.5	4529.6	2532.1	12393.7
Load (MW)	5216.9	4476	2505.7	12198.6
Cost ($/hr)	161880.24	111647.7	50641.85	**326728.59**
Cost Deviation	**-12%**	**5%**	**14%**	**-2%**

Table 5.22: Comparison of the resulting Optimized systems (±40MW) with their respective Autonomous systems

We can see that there is a significant deviation between the individual operating costs. System 1 has decreased its cost in expense of systems 2 and 3, which have increased their power generation to transfer energy through the interconnections. This redistribution of the power production has an impact on the total cost of the system, which has decreased by 2%, compared to that of the three autonomous systems.

The next diagram gives a visual representation of the changes of the power generations of the subsystems at the end of the optimization process. This will give us a clearer understanding about the impact that the three DC interconnections can have to the overall system performance:

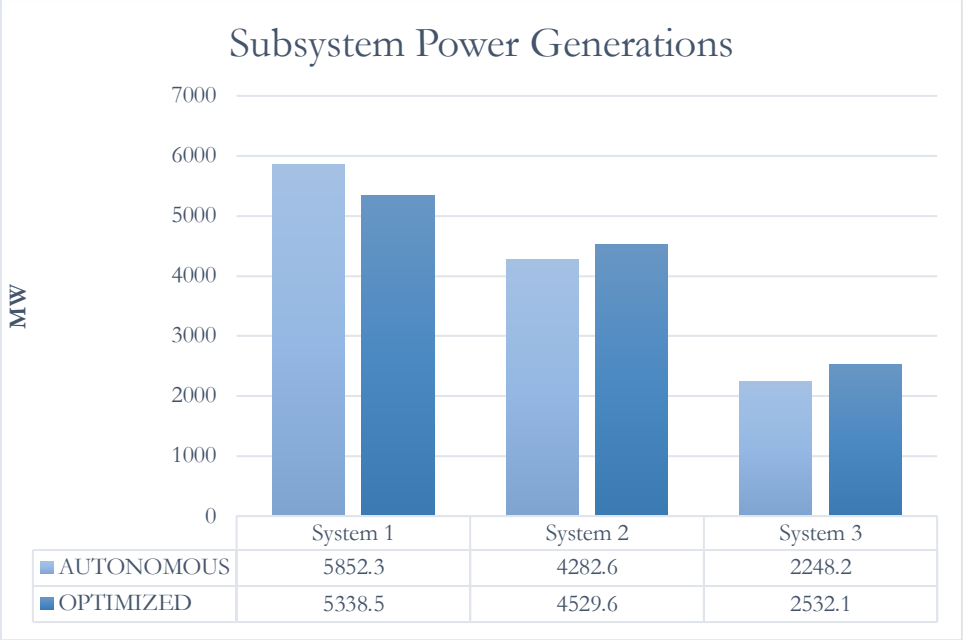

Figure 5.9: Power generation comparison of the Autonomous and Optimized system case instances

The figures below (5.10-5.13) show the total system costs determined by **fmincon** and **runopf** respectively, at each successfully executed iteration of the algorithm. Each figure is associated to a different set of power generation change offers, from ±10 to ±40 MW.

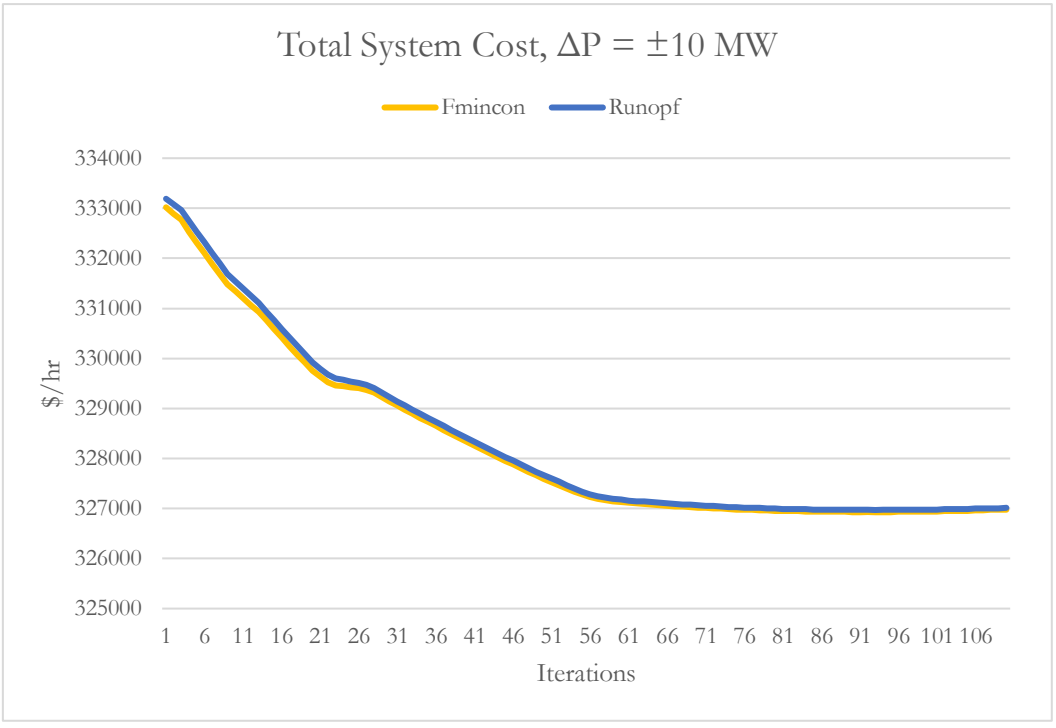

Figure 5.10: Total system operating costs calculated by fmincon and runopf for the Autonomous subsystems, for power generation change offers of ±40MW

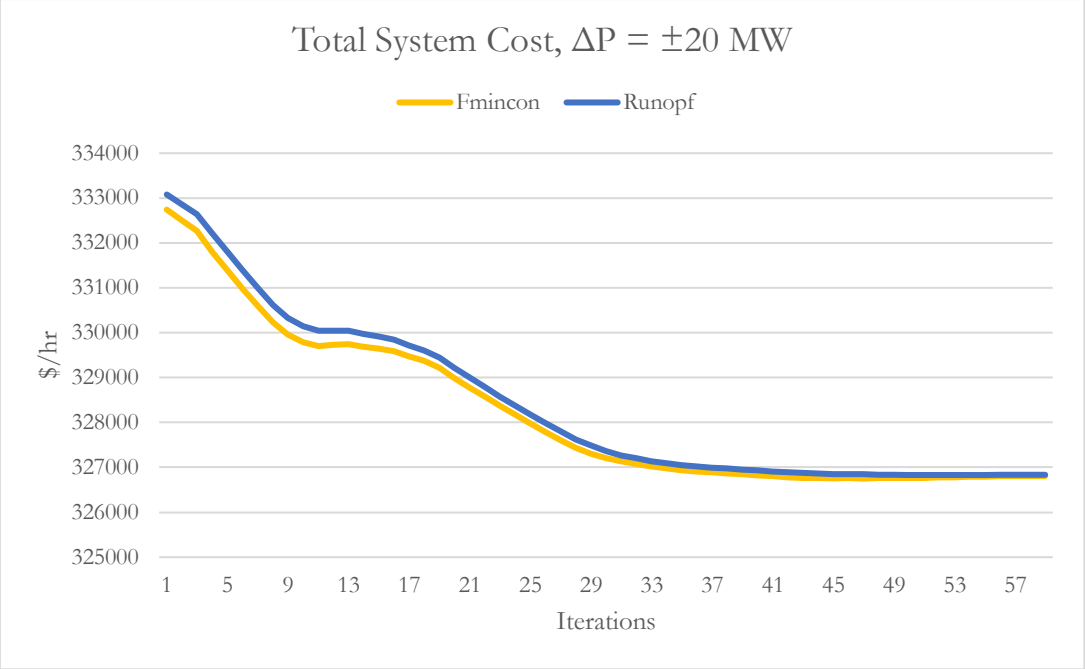

Figure 5.11: Total system operating costs calculated by fmincon and runopf for the Autonomous subsystems, for power generation change offers of ±20MW

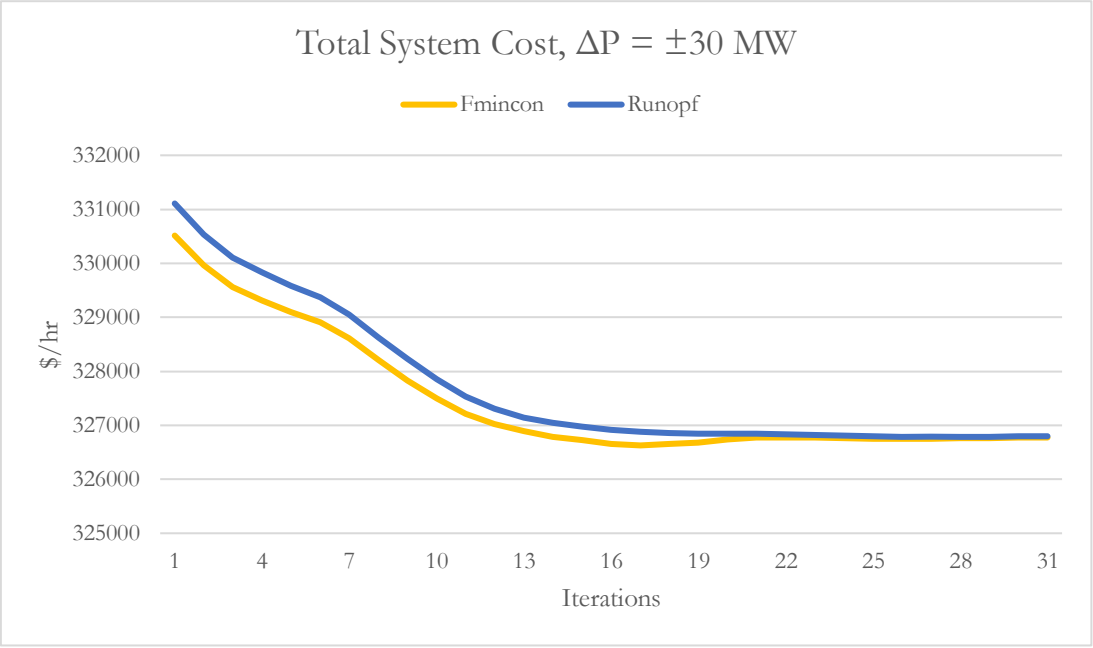

Figure 5.12: Total system operating costs calculated by fmincon and runopf for the Autonomous subsystems, for power generation change offers of ±30MW

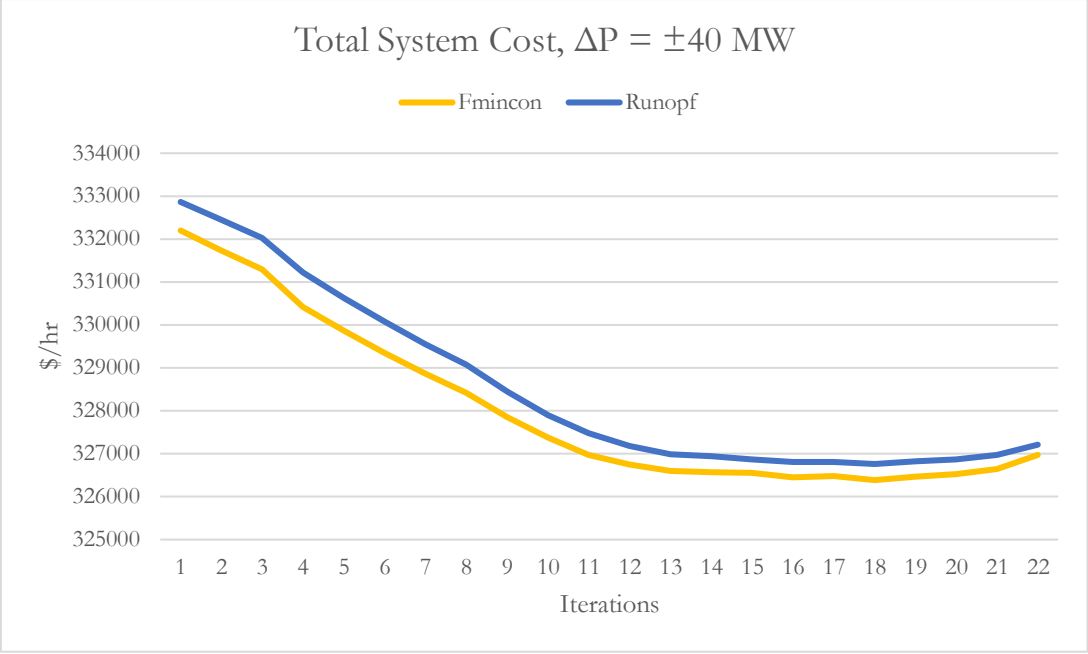

Figure 5.13: Total system operating costs calculated by fmincon and runopf for the Autonomous subsystems, for power generation change offers of ±40MW

We notice that the increase of the initial power generation change offers has an impact on how quickly and smoothly the two curves converge. Lower power offers of ±10 MW give us almost identical cost curves that follow a linear decrease. Higher offers of 20 and 30 MW provide curves with larger gap at the beginning, which does seem to close relatively faster for the former. In these three figures, the cost curves stabilize after a certain point of the execution process, having reached the optimal operation state of the system. However, the power generation change offers of ±40 MW give us cost curves that do not converge fully. Moreover, after 20 iterations the cost shows an upward trend. This is because larger offers tend to push the systems to the optimal state faster, before the gap between the offers has sufficiently closed. The execution is terminated as soon as fmincon starts to produce results that lead to total cost increase. The set of interconnections that give us the optimal solution has already been stored in the process and is applied afterwards to create the new optimal system cases with the minimum global operating cost.

The next four figures (5.14-5.17) demonstrate the fmincon's resulting 'dummy' loads, that iteratively form the final DC interconnection:

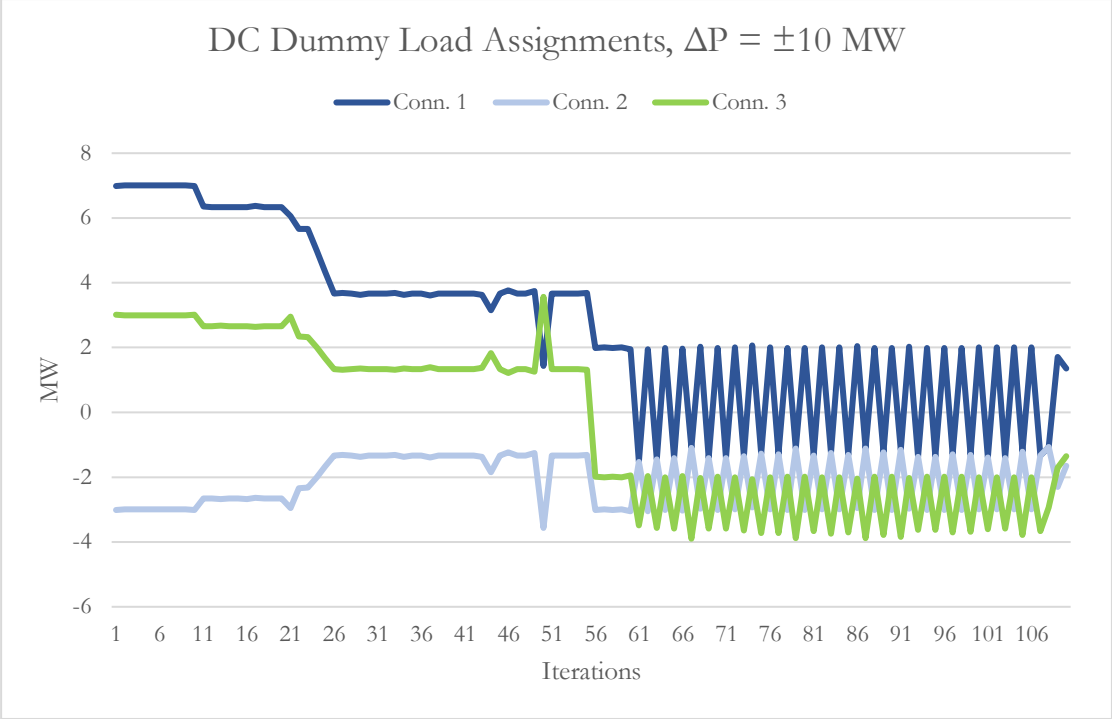

Figure 5.14: Fmincon resulting DC 'dummy' loads for power generation change offers of ±10MW

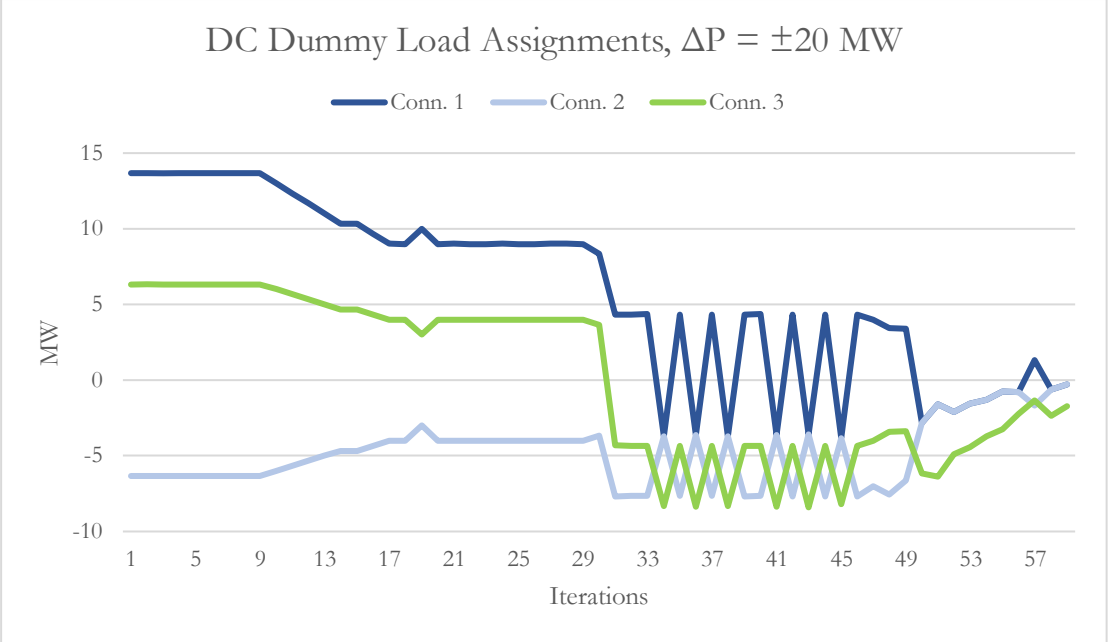

Figure 5.15: Fmincon resulting DC 'dummy' loads for power generation change offers of ±20MW

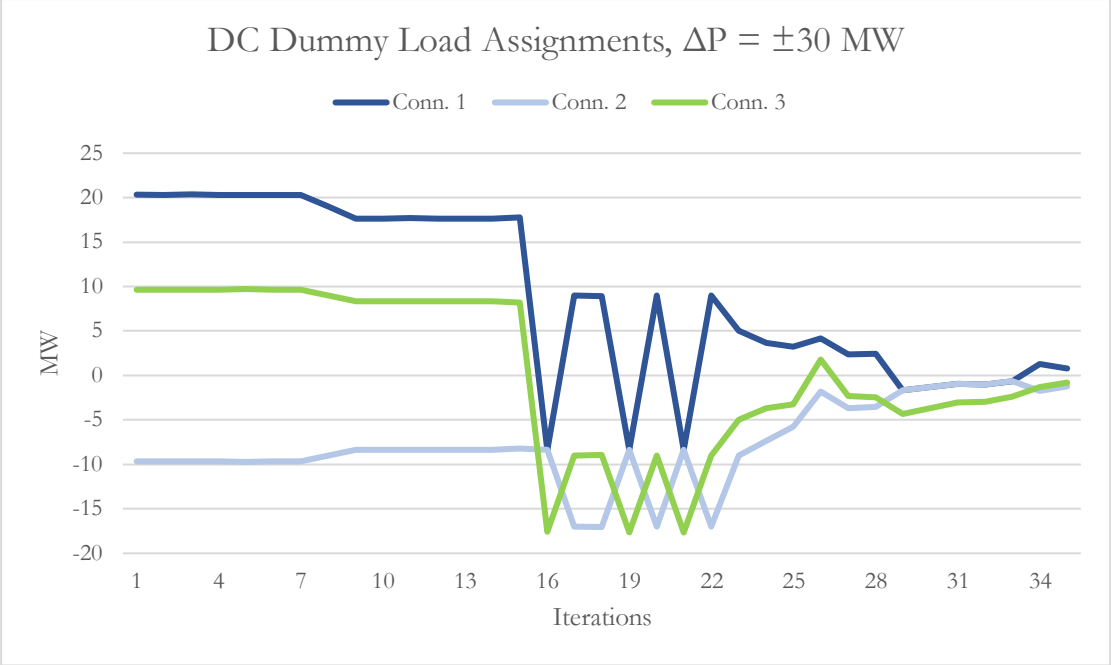

Figure 5.16: Fmincon resulting DC 'dummy' loads for power generation change offers of ±30MW

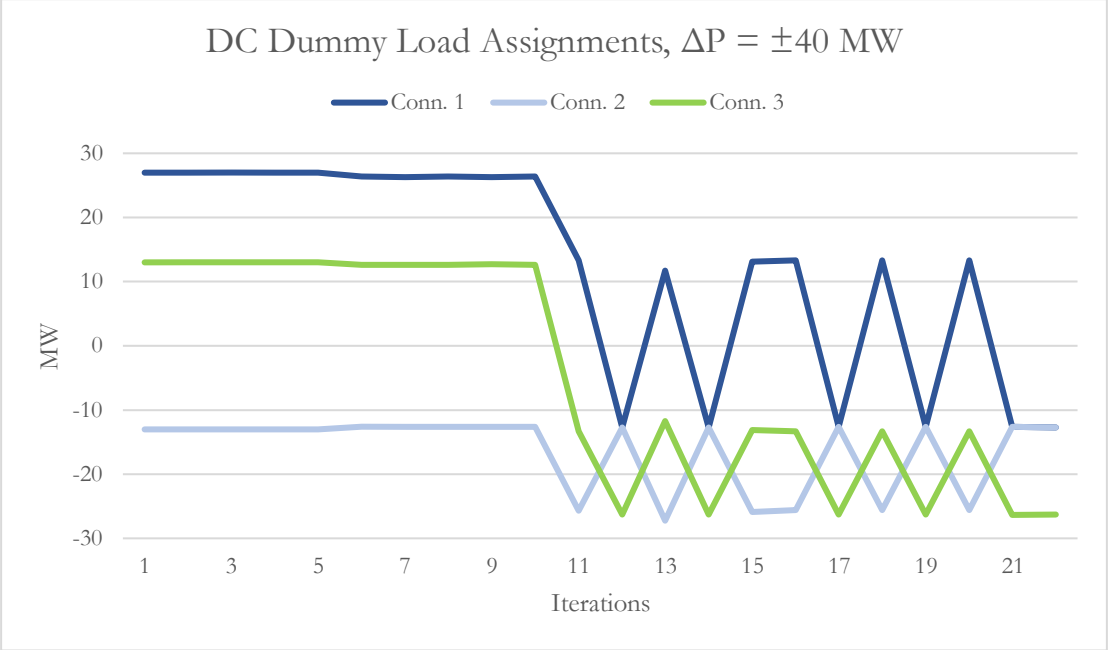

Figure 5.17: Fmincon resulting DC 'dummy' loads for power generation change offers of ±40MW

It is clear that for larger, the results of fmincon converge in less iterations. Lower starting offers lead to more iterations and consequently, larger execution times. Furthermore, the corresponding 'dummy' loads converge more smoothly and show less oscillations. Offer sets of ±20 and ±30 MW generally give us satisfying results, whereas the ±40 MW offers, despite performing better, their associated 'dummy' loads don't converge as excepted.

Figures 5.18-5.21 show us how the systems behave as the algorithm progresses and the results of fmincon are applied for the establishments of the DC power flows. The resulting 'dummy' loads cause the alternation of every subsystem's power generation in order to adapt to the new demand conditions:

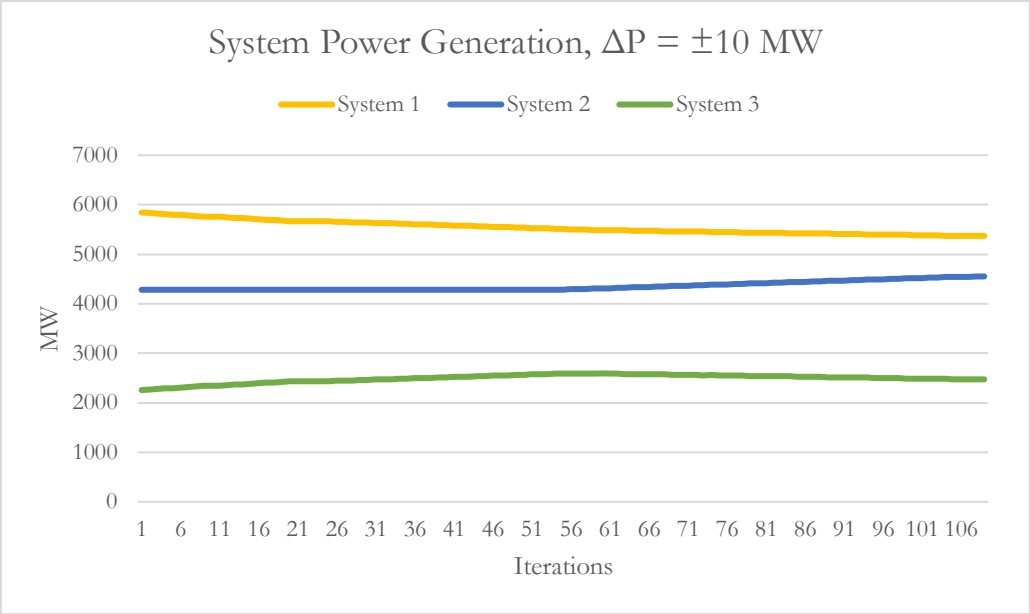

Figure 5.18: Real Power Production of the Autonomous subsystems during the execution process for power generation change offers of ±10MW

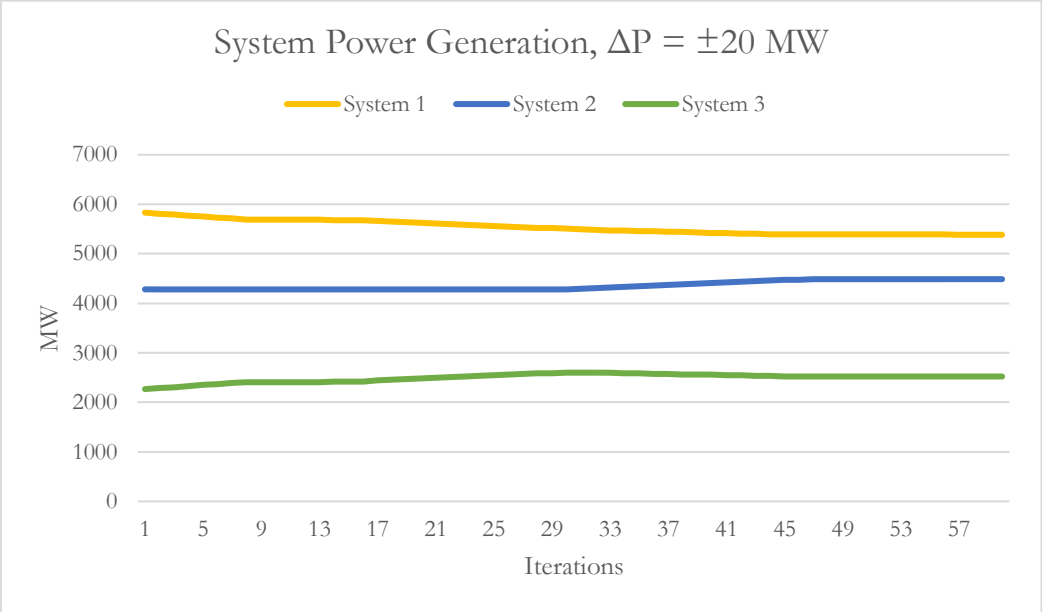

Figure 5.19: Real Power Production of the Autonomous subsystems during the execution process for power generation change offers of ±20MW

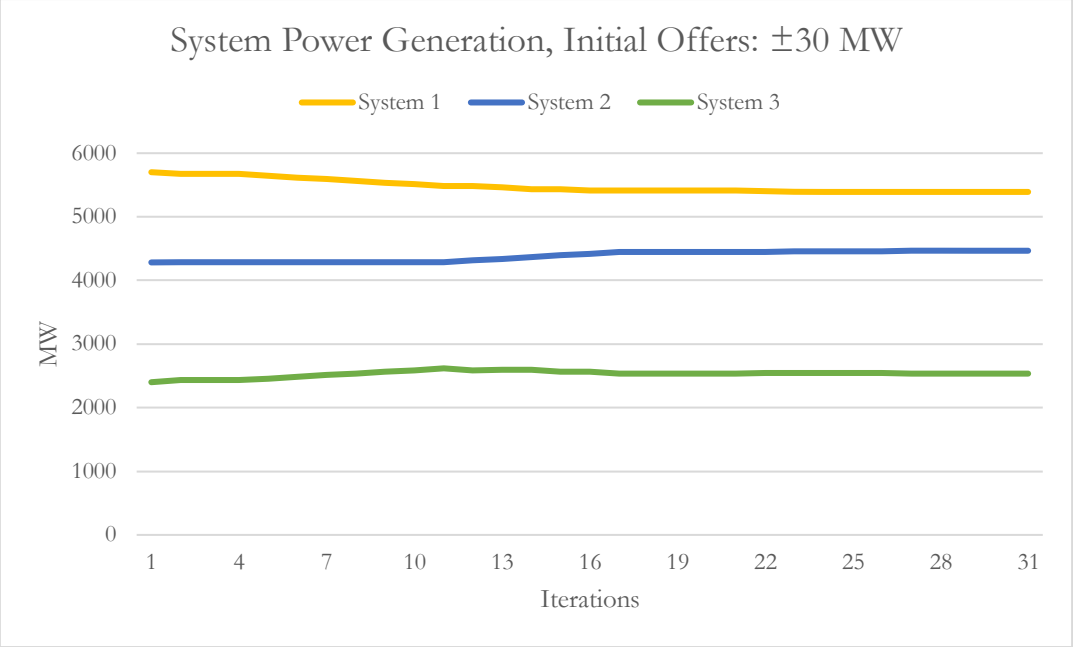

Figure 5.20: Real Power Production of the Autonomous subsystems during the execution process for power generation change offers of ±30MW

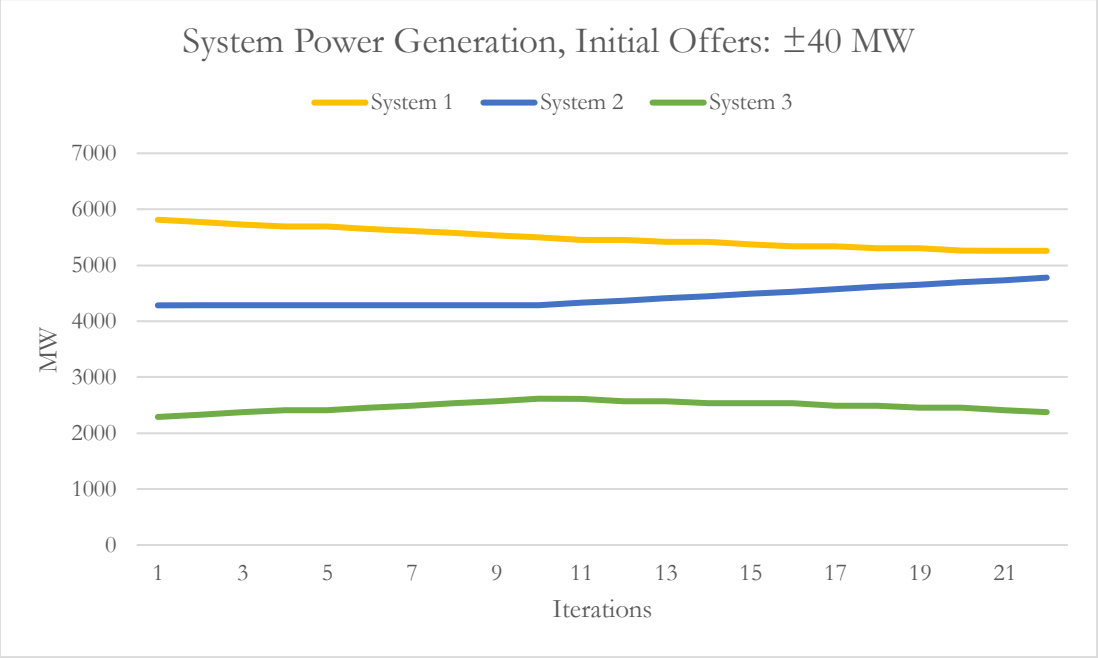

Figure 5.21: Real Power Production of the Autonomous subsystems during the execution process for power generation change offers of ±40MW

System power productions also tend to stabilize faster for larger initial power generation change offers. Yet, the last figure (5.21) shows that the system production hasn't really stabilized by the end of the process. Again, this is clearly an issue caused by the incomplete convergence shown for the power offers of ±40 MW.

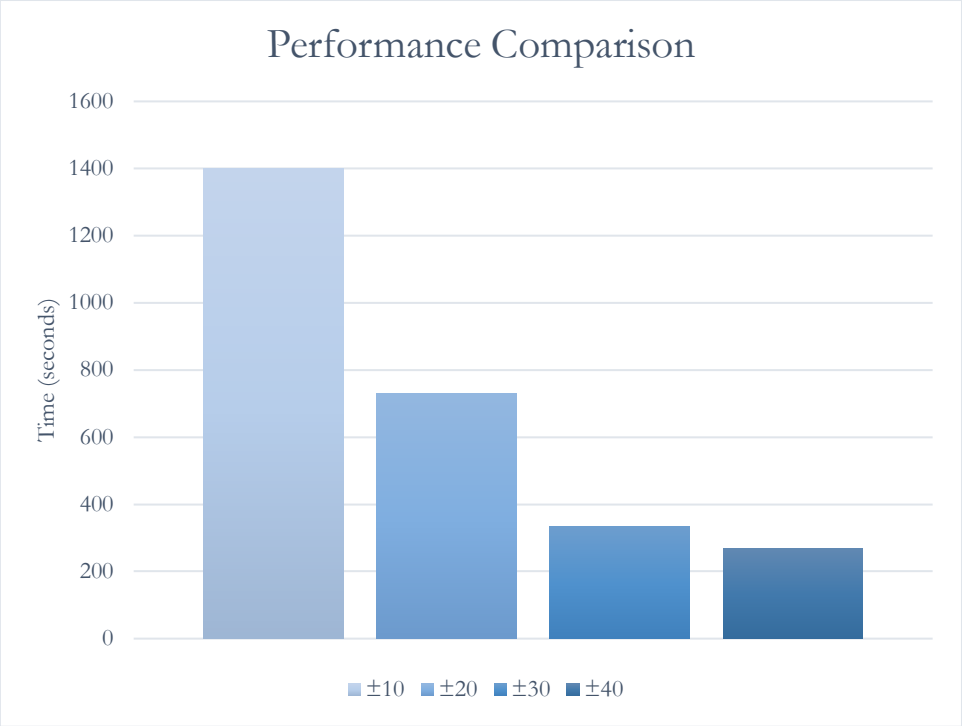

Figure 5.22: Execution time (in seconds) for various initial power generation change offers

It is again verified that the initial power generation change offers given as input to the algorithm directly affects the execution time. For power offers of 30 and 40 MW the total execution time tends to stabilize around 250 seconds (less than 5 minutes). Offers of ±10 MW increase the total execution time dramatically, and need more than 20 minutes to converge. Therefore, power offer of that size can be considered inefficient, especially for larger system input, and is advised be avoided for practical reasons. Also, the results provided by the offers of ±20 MW are rather mediocre. The offer set of ±30 MW seems to be the optimal choice for both experimental and practical reasons. It gives satisfactory results, combined with acceptable execution times.

Chapter 6: Conclusion

6.1. Summary

This thesis focused on the benefits of HVDC technology for the optimization of large electrical grids consisting of interconnected subsystems. It was based on the concept of a transactive network where the participating electric power systems are negotiating by making power offers while being unaware of others power utility and demand. The final purpose of the whole procedure is to detect the optimal operating state by determining the power transactions on the DC interconnections that will minimize the global system cost.

To achieve this, we extended the optimal power flow functionality with the integration of linear interpolation into the core of our algorithm, that is, the objective function we implemented using the fmincon function of Matpower. The evaluation of our implementation was made in three phases: the first was the examination of a small-sized reference model, already interconnected and optimized using Matpower's optimal power flow feature. The second was its division into three subsystems, the OPF results of which were compared with our reference model, in order to validate our algorithm's functionality. Finally, we further examined the performance of our method with a more realistic large power system, from which we extracted additional information about its behaviour.

The algorithm demonstrated great consistency in both case studies. In the first, it managed to approach the results of the OPF reference model with significant accuracy while it improved the global operating cost of the system. Moreover, we tested two different methods regarding the distribution of power generation change offers to the actual dummy loads of the interconnected power systems. The method of proportionally distributing a power offer between the DC interconnected buses proved more appealing than dividing the offer's amount evenly throughout the whole system. During the examination of the large power system case study, we investigated the impact of modifying the step size of the algorithm (size of power offer). Power offers of ± 10 MW led to accurate results but the method proved rather slow to converge due to the increased number of iterations required. Offers of ± 20 and ± 30 MW gave successively better total operating costs and showed smoother convergence in fewer iterations. Power offers of ± 40 MW had the advantage of reaching a slightly better operating cost much faster, but failed to converge properly due to the interruption of the execution caused by potential cost increase.

In general, all power offer sizes gave similar results in terms of minimizing the total system cost. Therefore, we can conclude that for the examined case study, power offers around ± 30 MW can give us reliable results and smooth performance in less iterations. Consequently, we are able to adjust the algorithm's starting point based on the tradeoff between the execution speed and the quality of the results.

6.2. Future Work

Since our work is focused on the optimization of interconnected electric power systems, various future work extensions can be considered.

An attempt to enhance the algorithm's accuracy could be the improvement of the objective function, by adopting a non-linear approach instead of the method of linear interpolation. Such methods are polynomial or spline interpolation, which could give us a more accurate approximation of the total system cost by taking advantage of more known operating states (offers).

An additional improvement that may contribute to the method's accuracy is the consideration of unit shut-down and start-up capability in the OPF formulation. Furthermore, the proposed method could be suitably extended to incorporate AC interconnections, and can also be exploited in unit commitment problems for short-term operation planning, after appropriate modifications and enhancements.

Moreover, instead of solely relying on the operation cost, other criteria such as the cost of RES generation shedding, the minimization of the expected load loss, bilateral contracts, system stability etc., can also be taken into account for more detailed and realistic approximations.

Bibliography

ABB . (2018). *The Gotland HVDC link*. Retrieved from ABB: https://new.abb.com/systems/hvdc/references/the-gotland-hvdc-link

ABB . (n.d.). *Jinping - Sunan: The most powerful transmission line in the world.* Retrieved from ABB Corporation Web site: https://new.abb.com/systems/hvdc/references/jinping---sunan

ABB. (2016, March 10). ABB wins $140 million order to boost integration of renewables in Europe. Zurich, Switzerland.

ABB. (n.d.). *New Zealand Encourages further development of renewable generation like wind and hydro*. Retrieved from ABB Web site: https://new.abb.com/systems/hvdc/references/new-zealand

ABB. (n.d.). *Why HVDC: Economic and environmental advantages*. Retrieved from ABB Corporation Web site: https://new.abb.com/systems/hvdc/why-hvdc/economic-and-environmental-advantages

Agelidis, V. G., Demetriades, G. D., & Flourentzou, N. (2006, 12). Recent Advances in High-Voltage Direct-Current Power Transmission Systems. *2006 IEEE International Conference on Industrial Technology*, (pp. 206-213). doi:10.1109/ICIT.2006.372391

An, T., Tang, G., & Wang, W. (2017). Research and application on multi-terminal and DC grids based on VSC-HVDC technology in China. *High Voltage, 2*, 1-10.

Ardelean, M., & Minnebo, P. (n.d.). HVDC submarine power cables in the world.

Baliga, B. J. (2010). *Fundamentals of power semiconductor devices.* Springer Science & Business Media.

Breuer, W., Hartmann, V., Povh, D., Retzmann, D., & Teltsch, E. (2004). Application of HVDC for large power system interconnections. *Int Council on Large Elec t Sys, Paris, France*.

Buigues, G., Valverde, V., Etxegarai, A., Eguia, P., & Torres, E. (2017, 4). Present and future multiterminal HVDC systems: current status and forthcoming. *Renewable Energy and Power Quality Journal, 1*, 83-88. doi:10.24084/repqj15.223

Callavik, M., Lundberg, P., & Hansson, O. (2015). NORDLINK Pioneering VSC-HVDC interconnector between Norway and Germany. *ABB White Paper*.

C-EPRI Electric Power Engineering Co., Ltd . (n.d.). *Project Reference: Jinping-Sunan ±800kV UHVDC Transmission Project*. Retrieved from C-EPRI Corporation Web site: http://www.cepri.com.cn/products/details_84_407.html

CIGRE. (2012, April). Voltage Source Converter (VSC) HVDC for Power Transmission - Economic Aspects and Comparison with other AC and DC Technologies. *Working Group B4.46*. Cigre.

Coleman, T. F., & Li, Y. (1996). An interior trust region approach for nonlinear minimization subject to bounds. *SIAM Journal on optimization, 6*, 418-445.

Devi, L., Ch, S. B., & Nagaraju, S. (2012, 1). Design modeling of the converter valves in VSC-HVDC transmission systems based on transmission voltage. *Scholarly Journal of Engineering Research*.

E.W.E.A., van Hulle, F., & others. (2010, November). Powering europe: wind energy and the electricity grid. Nov.

Electrical 4U. (2019, June 8). *Insulated Gate Bipolar Transistor | IGBT*. Retrieved from Electrical 4U Web site: https://www.electrical4u.com/insulated-gate-bipolar-transistor-igbt/

Electrical Power Engineering. (n.d.). *The mercury-arc valve*. Retrieved from Electrical Power Engineering Web site: https://electricalpowerengineering.nl/High-Voltage-Direct-Current-Transmission/The-mercury-arc-valve

Electrical4U. (2019, January 27). *High Voltage Direct Current Transmission | HVDC Transmission*. Retrieved from Electrical4U Web site.

Electronics Tutorials. (n.d.). *Power Electronics: Insulated Gate Bipolar Transistor*. Retrieved from Electronics Tutorials: https://www.electronics-tutorials.ws/power/insulated-gate-bipolar-transistor.html

ELPROCUS. (n.d.). *Freewheeling or Flyback Diode Working and Their Functions*. Retrieved from ELPROCUS Web site: https://www.elprocus.com/freewheeling-or-flyback-diode-circuit-working-functions/

Eremia, M., Liu, C., & Edris, A. (2016). CSC–HVDC Transmission. In *Advanced Solutions in Power Systems: HVDC, FACTS, and Artificial Intelligence* (pp. 35-124). IEEE. doi:10.1002/9781119175391.ch3

Eremia, M., Liu, C.-C., & Edris, A.-A. (2016). *Advanced solutions in power systems: HVDC, FACTS, and Artificial Intelligence*. John Wiley & Sons.

feng, Bertling Tjernberg, L., Tuan, L., Mannikoff, A., & anders. (2012, 9). An Overview Introduction of VSC-HVDC: State-of-art and Potential Applications in Electric Power Systems.

Flourentzou, N., Agelidis, V. G., & Demetriades, G. D. (2009, 3). VSC-Based HVDC Power Transmission Systems: An Overview. *IEEE Transactions on Power Electronics, 24*, 592-602. doi:10.1109/TPEL.2008.2008441

Gordon, P. (2019, July 17). *Europe: Renewables overtake fossil fuels in first half of 2019*. Retrieved from Smart Energy International Web site: https://www.smart-energy.com/renewable-energy/europe-renewables-overtake-fossil-fuels-in-first-half-of-2019/

Grady, M. (2006). Understanding power system harmonics. *Dostępny w WWW: http://users. ece. utexas. edu/˜ grady/HarmonicsNotesGradyJune2006print. pdf*.

Grant, J. (2017, 11). Review of HVDC technology, applications and future prospects.

Guarnieri, M. (2013). The alternating evolution of DC power transmission [Historical]. *IEEE Industrial Electronics Magazine, 7*, 60-63.

Haglöf, L. (2004). The history of HVDC Part 1: The mercury-arc valve era. *HVDC 50 years: Presentation at the Gotland seminar, 6 May*. Visby : ABB.

Hertem, D. V., & Ghandhari, M. (2010). Multi-terminal VSC HVDC for the European supergrid: Obstacles. *Renewable and Sustainable Energy Reviews, 14*, 3156-3163. doi:https://doi.org/10.1016/j.rser.2010.07.068

Hoel, A. (2004, 7 1). *HVDC Systems Gotland: the HVDC pioneer*. Retrieved from Power Engineering International: https://www.powerengineeringint.com/2004/07/01/hvdc-systems-gotland-the-hvdc-pioneer/

Huang, H., Uder, M., Barthelmess, R., & Dorn, J. (2008). Application of high power thyristors in HVDC and FACTS systems. *17th Conference of Electric Power Supply Industry (CEPSI)*, (pp. 1-8).

Jovcic, D., & Ahmed, K. (2015, 9 25). *High Voltage Direct Current Transmission: Converters, Systems and DC Grids*. Wiley-Blackwell. doi:10.1002/9781118846704

Jovcic, D., & Ahmed, K. H. (2015). High Voltage Direct Current Transmission: Converters, Systems and DC Grids.

Khatri, P. (2018, February 8). *Cicuit Digest Web site*. Retrieved from What is Thyristor and How it works?: https://circuitdigest.com/tutorial/what-is-thyristor-how-it-works

Khazaei, J., Idowu, P., Asrari, A., Shafaye, A. B., & Piyasinghe, L. (2018, 9). Review of HVDC control in weak AC grids. *Electric Power Systems Research, 162*, 194-206. doi:10.1016/j.epsr.2018.05.022

Klaka, S. (2015, November 23). *Thyristors – The heart of HVDC* . Retrieved from ABB Web site: https://www.abb-conversations.com/2015/11/thyristors-the-heart-of-hvdc/

Lamm, U. (1964). Mercury-arc valves for high-voltage dc transmission. *Proceedings of the Institution of Electrical Engineers*, *111*, pp. 1747-1753.

Marshelec. (n.d.). *Wikipedia Web site*. Retrieved from [CC BY-SA 3.0 (https://creativecommons.org/licenses/by-sa/3.0)]: https://commons.wikimedia.org/wiki/File:Pole_2_Thyristor_Valve.jpg

MATLAB. (2018). *version 9.4.0. (R2018a)*. Natick, Massachusetts: The MathWorks Inc.

MATPOWER. (n.d.). *About: MATPOWER*. Retrieved from MATPOWER - Free, open-source tools for electric power system simulation and optimization Web site: https://matpower.org/about/

Mohammadi, F. (2018). Power Management Strategy in Multi-Terminal VSC-HVDC System., (p. 1).

Normandin, S. (n.d.). *Resources: Mercury Arc Rectifiers*. Retrieved from Edison Tech Center Organization Web Site: https://edisontechcenter.org/MercArcRectifiers.html

Oulis Rousis, A., & Anaya-Lara, O. (2015, 12). DC Voltage Control for Fault Management in HVDC System. *Energy Procedia, 80*, 237-244. doi:10.1016/j.egypro.2015.11.427

Pan, J., Nuqui, R., Srivastava, K., Jonsson, T., Holmberg, P., & Hafner, Y.-J. (2008, 12). AC grid with embedded VSC-HVDC for secure and efficient power delivery., (pp. 1-6). doi:10.1109/ENERGY.2008.4781042

Peake, O. (2010). The History of High Voltage Direct Current Transmission. *Australian Journal of Multi-Disciplinary Engineering, 8*, 47-55. doi:10.1080/14488388.2010.11464824

Pierri, E., Binder, O., Hemdan, N. G., & Kurrat, M. (2017). Challenges and opportunities for a European HVDC grid. *Renewable and Sustainable Energy Reviews, 70*, 427-456.

Pownuk, A., & Kreinovich, V. (2017). *"Why Linear Interpolation?"*. Departmental Technical Reports (CS). 1098.

Pyakuryal, S. (2013, 3). Harmonic Analysis for a 6-pulse Rectifier. *IOSR Journal of Engineering, 3*, 57-60. doi:10.9790/3021-03325760

Rajpoot S., Rajpoot P., & Gupta K. (2017). Analysis of Hvdc Power Transmission Line with Unique Power Control Room. *IOSR Journal of Dental and Medical Sciences*, 16,28-37.

Rudervall, R., Charpentier, J. P., & Sharma, R. (2000). High voltage direct current (HVDC) transmission systems technology review paper. *Energy week, 2000*, 1-19.

Sanchis, G., Betraoui, B., Anderski, T., Peirano, E., Pestana, R., De Clercq, B., . . . Paun, M. (2014). The Corridors of Power: A Pan-European" Electricity Highway" System for 2050. *IEEE Power and Energy Magazine, 13*, 38-51.

Statnett . (2018). *New subsea interconnector between Norway and Germany.* Retrieved from Statnett Corporation Web site: https://www.statnett.no/en/our-projects/interconnectors/nordlink/

Stomberg, H., Abrahamsson, B., & Saksvik, O. (1996). Modern HVDC thyristor valves. *ICEE 96, Beijing China*.

Tiku, D. (2014, April). *DC Power Transmission: Mercury-Arc to Thyristor HVdc Valves*. Retrieved from IEEE Power & Energy magazine: https://magazine.ieee-pes.org/marchapril-2014/history-12/

TYNDP, E.-E. (2014). *Ten Year Developement Plan 2014*. European Network of Transmission System Operators for Electricity.

Vovos, N., & Γιαννακόπουλος, Γ. (2008, 1). *Ανάλυση Συστημάτων Ηλεκτρικής Ενέργειας*.

Wang, F., Bertling, L., Le, T., Mannikoff, A., & Bergman, A. (2011). An overview introduction of VSC-HVDC: State-of-art and potential applications in electric power systems. *Cigrè International Symposium, Bologna, Italy, Sept. 2011*.

Wang, H., & Redfern, M. A. (2010, 8). The advantages and disadvantages of using HVDC to interconnect AC networks. *45th International Universities Power Engineering Conference UPEC2010*, (pp. 1-5).

Westermann, D., Van Hertem, D., Real, G., Rauhala, T., Meisingset, M., Kurrat, M., . . . others. (2012). *Voltage source converter (VSC) HVDC for power transmission--economic aspects and comparison with other AC and DC technologies.* Cigré; Paris.

Wind Europe. (2017). Wind energy in Europe: Outlook to 2020. September.

Wolf, G. (2017, July 25). *HVDC: A Short History of The Mercury-Arc Valve*. Retrieved from T&D World: https://www.tdworld.com/hvdc/short-history-mercury-arc-valve#menu

Zimmerman, R. D., & Murillo-Sánchez, C. E. (2019, 6). MATPOWER User's Manual. Zenodo. doi:10.5281/zenodo.3251118

Zimmerman, R. D., Murillo-Sanchez, C. E., & Thomas, R. J. (2009, 7). MATPOWER's extensible optimal power flow architecture. *2009 IEEE Power Energy Society General Meeting*, (pp. 1-7). doi:10.1109/PES.2009.5275967

Zimmerman, R. D., Murillo-Sánchez, C. E., & Thomas, R. J. (2011, 2). MATPOWER: Steady-State Operations, Planning, and Analysis Tools for Power Systems Research and Education. *IEEE Transactions on Power Systems, 26*, 12-19. doi:10.1109/TPWRS.2010.2051168